ΕΘΝΙΚΟ ΜΕΤΣΟΒΙΟ ΠΟΛΥΤΕΧΝΕΙΟ
Εργαστήριο Ατμοκινητήρων & Λεβήτων
Τομέας Θερμότητας της Σχολής Μηχανολόγων Μηχανικών

ΔΙΠΛΩΜΑΤΙΚΗ ΕΡΓΑΣΙΑ

Experimental evaluation of work recovery potential in commercial heat pumps using a piston expander prototype.

Του Φοιτητή

Πετσανά Δημήτριου

Επιβλέπων

Καρέλλας Σωτήριος, Αναπληρωτής Καθηγητής,
Σχολή Μηχανολόγων Μηχανικών, ΕΜΠ

Αθήνα, Ιούνιος 2017

Abstract

The goal of this diploma thesis is to investigate the possibility of energy recovery in commercial heat pump units. This can be achieved by replacing the standard throttling valve with a radial piston-type expander in order to minimize the thermodynamic losses during the expansion process. Its purpose is to allow the high pressure liquid to expand in order to produce mechanical work that can be converted into electricity. The produced electrical power can be supplied to the heat pump's compressor, reducing its electricity consumption, thus making the system more energy efficient. The expander that was tested in the NTUA laboratory is based on a commercial hydraulic motor of Italgroup®. It was redesigned for use with refrigerants and accordingly manufactured by the company in the framework of the EXP-HEAT project funded by the European Commission. A dedicated test rig for the experimental evaluation of the integrated expander in a commercial heat pump unit was developed and constructed in the laboratory of Steam Boilers and Thermal Plants of NTUA. As far as the retrofitting process is concerned, the major goal was to maintain the modifications on the commercial heat pump as few as possible. This would indicate that the installment of such an expander could be materialized quite easily and would induce a relatively low cost compared to the benefits that the expander's performance can provide in the long term. An initial experimental campaign was launched before and after the expander was incorporated to the heat pump, in order to evaluate the effect of the retrofitting procedure on the performance of the unit in normal operation (i.e. using the initial throttling valve). The results showed that its performance, operational characteristics and output thermal power remained in the same levels.

The second series of experiments concerned the expander mode operation. The main objective of this part was the evaluation of the performance boost of the standard heat pump. A COP increase of over 2% was achieved under 16.16 bar of liquid refrigerant pressure at the expander inlet. The experimental data provided a certain relationship between the COP value and the inlet pressure which led to the extrapolation of the obtained results for higher operational pressures. An encouraging value of a theoretical 3.8% COP increase under a pressure of 25 bar was calculated. The expander's isentropic efficiency reached a maximum value of 17.1% that could theoretically exceed 24% if the inlet pressure is raised at 25 bar. To conclude with the expander's performance, the produced mechanical power by the expander's shaft reached 140.36 W, while through the extrapolation process of the obtained experimental data, an estimated value of over 250 W at 25 bar could be attained.

Last but not least, after the expander mode operation experiment, certain conclusions were drawn regarding maintenance and reliability issues of the expander prototype. An inspection of the expander's interior after several operating hours provided valuable clues on the optimization of its performance that are discussed in the final chapters of the thesis. Finally, the topic of automation is discussed in the direction of developing a fully automated product, as a retrofit kit that could be widely adopted by the heating and refrigeration market.

Περίληψη

Ο στόχος αυτής της διπλωματικής εργασίας είναι να ερευνηθεί η πιθανότητα ανάκτησης ενέργειας σε εμπορικές αντλίες θερμότητας. Αυτό μπορεί να επιτευχθεί αντικαθιστώντας τη συμβατική εκτονωτική βαλβίδα με έναν ακτινικό εμβολοφόρο εκτονωτή, προκειμένου να περιοριστούν οι θερμοδυναμικές απώλειες κατά τη διαδικασία της εκτόνωσης. Ο σκοπός του είναι να επιτρέψει στο υγρό υπό υψηλή πίεση να εκτονωθεί έτσι ώστε να παραχθεί μηχανικό έργο που μπορεί να μετατραπεί σε ηλεκτρισμό. Η παραγόμενη ηλεκτρική ισχύς μπορεί να τροφοδοτήσει το συμπιεστή της αντλίας θερμότητας, μειώνοντας την ηλεκτρική κατανάλωση του και έτσι κάνοντας το σύστημα ενεργειακά αποδοτικότερο. Ο εκτονωτής που δοκιμάστηκε στο εργαστήριο του ΕΜΠ βασίζεται σε έναν εμπορικό υδραυλικό κινητήρα της εταιρείας Italgroup®. Επανασχεδιάστηκε για χρήση με φρέον και αντίστοιχα κατασκευάστηκε από την εταιρεία στο πλαίσιο του προγράμματος EXP-HEAT, το οποίο χρηματοδοτήθηκε από την Ευρωπαϊκή Ένωση. Μια ειδική διάταξη για την πειραματική αξιολόγηση του ενσωματωμένου στην αντλιά θερμότητας εκτονωτή αναπτύχθηκε και κατασκευάστηκε στο Εργαστήριο Ατμοκινητήρων και Λεβήτων του ΕΜΠ. Όσον αφορά την ενσωμάτωση του εκτονωτή, ο στόχος ήταν να διατηρηθούν οι αλλαγές στην εμπορική αντλία στο ελάχιστο. Κάτι τέτοιο θα δήλωνε πως η εγκατάσταση ενός τέτοιου εκτονωτή μπορεί να πραγματοποιηθεί εύκολα και θα επέφερε σχετικά μικρό κόστος σε σχέση με τα πλεονεκτήματα του μακροπρόθεσμα. Μια σειρά πειραμάτων ξεκίνησε πριν και μετά την ενσωμάτωση του εκτονωτή στην αντλία θερμότητας για να διαπιστωθεί αν οι αλλαγές είχαν επίδραση στην κανονική λειτουργία της αντλίας θερμότητας (δηλαδή με τον εκτονωτή να μη συμμετέχει). Τα αποτελέσματα έδειξαν ότι η συμπεριφορά της, τα λειτουργικά χαρακτηριστικά και η παραγόμενη θερμική ισχύς παρέμειναν στα ίδια επίπεδα.

Η δεύτερη σειρά πειραμάτων αφορούσε τη λειτουργία του εκτονωτή. Ο κύριος στόχος αυτού του μέρους ήταν η αξιολόγηση της όποιας αύξησης σε επίδοση της συμβατικής αντλίας θερμότητας. Αύξηση του COP λίγο πάνω από 2% επιτεύχθηκε με πίεση υγρού 16.16 bar στην είσοδο του εκτονωτή. Τα πειραματικά δεδομένα συνιστούν μια συγκεκριμένη σχέση μεταξύ του COP και της πίεσης εισόδου στον εκτονωτή, το οποίο επέτρεψε την εκτίμηση των τιμών του COP για μεγαλύτερες πιέσεις. Μια αρκετά ενθαρρυντική τιμή για αύξηση του COP κατά 3.8% υπολογίστηκε για πίεση εισόδου 25 bar. Ο ισεντροπικός βαθμός απόδοσης του συμπιεστή έφτασε τη μέγιστη τιμή του 17.1% ενώ θα μπορούσε να ξεπεράσει το 24% αν η πίεση εισόδου αυηξηθεί. Κλείνοντας με την επίδοση του εκτονωτή, η παραγόμενη μηχανική ισχύς από την

άτρακτο του έφτασε τα 140.36 W, ενώ σύφωνα με εκτίμηση απο τη συσχέτιση των πειραματικών δεδομένων, η ισχύς αυτή θα μπορούσε να ξεπεράσει τα 250 W υπό 25 bar πίεσης εισόδου.

Τέλος, μετά το πείραμα της λειτουργίας του εκτονωτή, εξήχθηκαν συμπεράσματα σχετικά με ζητήματα αξιοπιστίας και συντήρησης του πρότυπου εκτονωτή. Ένας έλεγχος του εσωτερικού του εκτονωτή μετά από κάποιες ώρες λειτουργίας έδωσε πολύτιμα στοιχεία σχετικά με τη βελτιστοποίηση της λειτουργίας του, τα οποία αναλύονται στα τελευταία κεφάλαια της εργασίας. Κλείνοντας, το θέμα της αυτοματοποίησης αναλύεται σχετικά με την ανάπτυξη ενός εντελώς αυτοματοποιημένου προϊόντος στη μορφή ενός εργαλείου ενσωμάτωσης που μπορεί να υιοθετηθεί από την αγορά των τομέων θέρμανσης και κλιματισμού.

Ευχαριστίες

Θα ήθελα να ευχαριστήσω ιδιαίτερα τον επιβλέποντα αναπληρωτή καθηγητή Σωτήριο Καρέλλα για τη δυνατότητα που μου προσέφερε να ασχοληθώ με ένα τόσο ενδιαφέρον θέμα, αλλά και για την εμπιστοσύνη που μου έδειξε καθ'όλη τη διάρκεια των πειραμάτων και εκπόνησης της εργασίας. Επίσης θα ήθελα να ευχαριστήσω τον Άρη Λεονταρίτη για την πολύτιμη βοήθεια και συμπαράσταση του σε ζητήματα που τέθηκαν όλον αυτόν τον καιρό, χωρίς την οποία η ολοκλήρωση της συγκεκριμένης διπλωματικής εργασίας θα είχε αποβεί δύσκολη έως ακατόρθωτη. Τέλος, θα ήθελα να ευχαριστήσω τους Κωνσταντίνο Αγγελή, Ευθύμιο Δημητριάδη και Αλέξανδρο Γεραμπίνη για την πολύτιμη τεχνική υποστήριξη που προσέφεραν αλλά και τους υποψήφιους διδάκτορες Δημήτρη Γριμέκη και Κωνσταντίνο Μπραϊμάκη για το χρόνο που διέθεσαν σε απορίες μου.

Table of Contents

Table of Figures

1 Introduction

Space heating is a topic of major interest nowadays and a lot of research has been conducted on heating and air-conditioning applications that aim to replace the conventional ones that are being utilized so far. Natural fuels such as coal, lignite, biomass, oil or natural gas are the main energy resources that are used to power heating equipment like combustors and boilers in residences, factories and public state buildings. However, the planet's limited energy resources are constantly decreasing due to the ever increasing demands that come as a result of overpopulation.

Therefore, the need to investigate alternative ways of heating is crucial. Vapor compression cycles (VCC) is a technology that has rapidly evolved in the past decades and is now being adopted by the majority of heating and air-conditioning applications. VCCs are thermodynamic cycles that take advantage of the properties of the different existing refrigerants in order to produce thermal power. As far as space heating is concerned, the diversion of the chemical and thermodynamic properties of refrigerants allows VCCs to operate under various conditions where the conventional fuels mentioned above fail to achieve the desired result. Consequently, any equipment that is designed to exploit the refrigerant's potential would automatically become a great competitor among the traditional heating machines that are being used so far. A heat pump is an innovative solution that uses refrigerants and has been established as the most efficient way to meet thermal demands. Its vapor compression cycle is designed to transfer heat from a colder to a hotter environment with the contribution of mechanical work. This inevitable work is provided by a compressor that increases the refrigerant's pressure. Further analysis of the heat pump's cycle is provided in the next chapters. Useful work can be obtained from the high pressure fluid if expanded properly. This work can be provided to the compressor in order to lower its power consumption and eventually leading to further energy saving.

The goal of this diploma thesis is to investigate the possibility of energy recovery in heat pumps using a dedicated hydraulic piston-type expander that is connected to a generator for electricity production. The commercial standard heat pump will be tested at various operating point in order to gain a complete view of its functioning. The expander will then be retrofitted to the heat pump and certain experiments will be made to measure the useful power delivered by the expander, its torque and rotational speed as well as to find out whether the heat pump continues to operate normally and of course according to the manufacturer's standards. Finally, focusing especially on any improvements to the heat pump's COP, it will be determined if a

dedicated expander can become a valuable asset to a heat pump, making it more efficient even less energy demanding.

1.1 Recent Advances in VCCs

Vapor compression cycles are in fact reverse Rankine thermodynamic cycles. The environmental air, an independent water circuit or even the earth's temperature can function as the heat source that will evaporate the working refrigerant. A compressor rotating at variable speeds provides the mechanical work required to increase the vapor's pressure and inevitably its temperature. The vapor then fully condenses, thus rejects its heat to a heat sink which can be a residential building with certain thermal needs. An expansion valve –in the majority of applications– decreases the liquid's pressure and the cycle repeats itself. A typical Vapor Compression Cycle is described in the following figures:

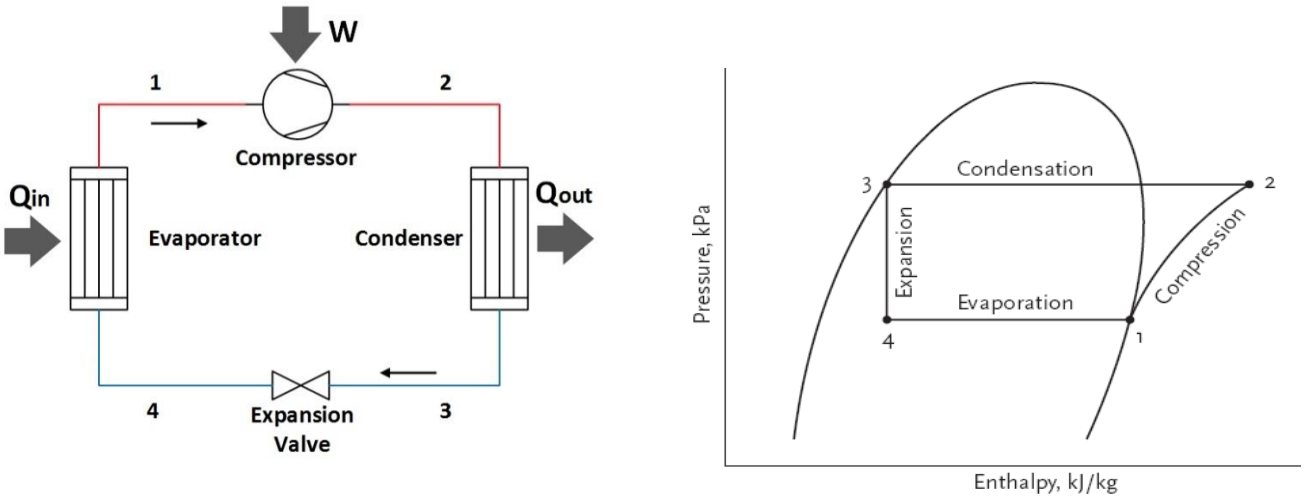

Figure 1 – Standard Vapor Compression Cycle drawing.

The efficiency of a Vapor Compression Cycle is described by the Coefficient of Performance (COP) factor, which is defined as the useful thermal or cooling power delivered, divided by the mechanical work provided to the compressor. In a heating application the useful output power matches the enthalpy difference (h2-h3) of the refrigerant's condensation curve as shown in Figure 1, whereas in a cooling one, the enthalpy difference (h1-h4) of the evaporation curve represents the delivered power. Further thermodynamic analysis of the COP and the VCC is given in the next chapters, where the examined heat pump is being put to the test. At this point, after a qualitative overview of international literature and reports on the specific topic, certain advances in Vapor Compression Cycles will be mentioned in order to highlight their impact on the COP value and in general, the cycle's efficiency.

The concept of these technologies is to maximize the condensation or the evaporation of the refrigerant according to the thermal needs of the application (heating or cooling). Apart from that, the compressor's work must be minimized in order to provide less power to the system and save energy. Focus has been given on three main categories of VCC innovations.

1.1.1 Subcooling Cycles

The first field of interest are the subcooling cycles that aim to increase the condensation curve's enthalpy difference (h_2-h_3) by transferring point 3 (Figure 1) to the left, towards the subcooled liquid region as shown in Figure 2.

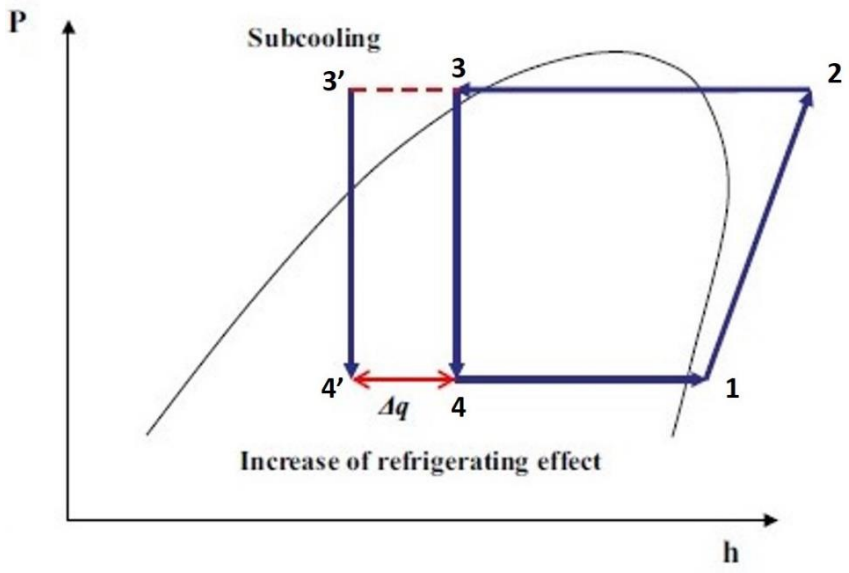

Figure 2 – The impact of the subcooling operation on the standard VCC. Δq stands for the increased condensation which leads to higher thermal outputs. Graph from [1].

A subcooling cycle can be accomplished with the use of a suction line heat exchanger (SLHX) or internal heat exchanger (IHX). The heat exchanger's purpose is to cool down the refrigerant that exits the condenser. This ensures that no remaining vapor will enter the expansion valve since all of the refrigerant is at liquid state, therefore any equipment damage related to that will be avoided. To perform this operation, colder vapor from the evaporator's outlet is led to the other side of the heat exchanger. As a result, a slightly superheated vapor enters the compressor.

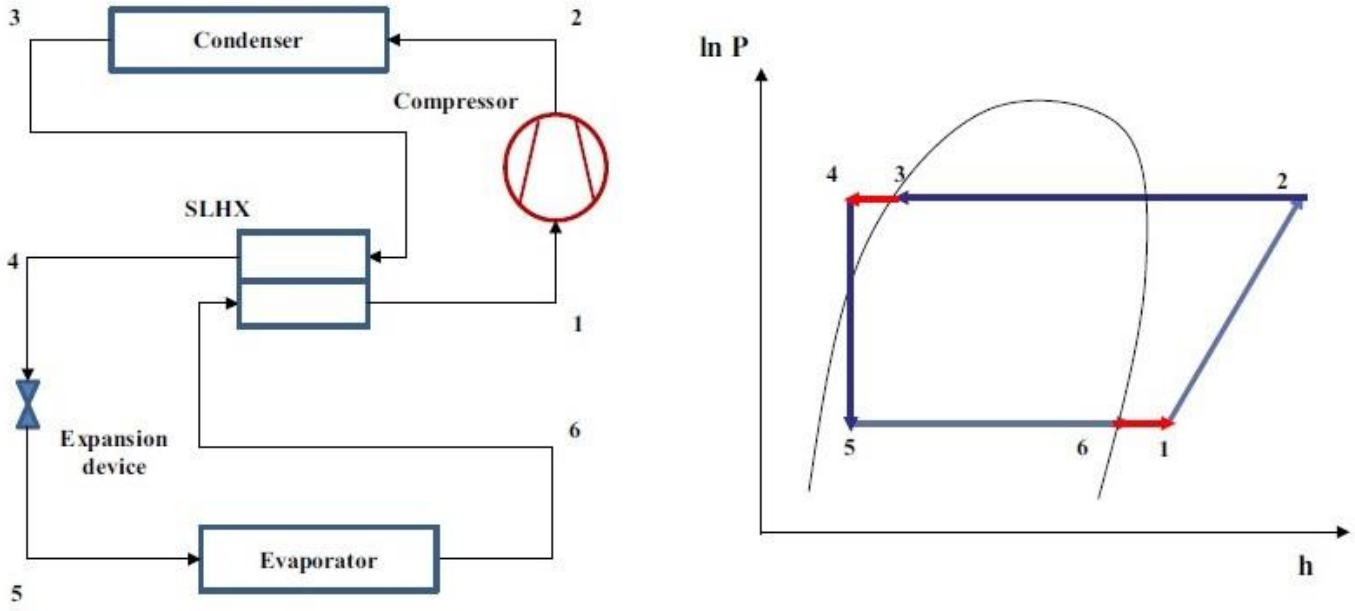

Figure 3 – Typical SLHX application and P-h diagram of the refrigerant. Graph from [1].

However, the warmer vapor has now an increased density that affects the volumetric efficiency of the compressor, given that the majority of air conditioning and heating applications use scroll type compressors. This is a disadvantage that should be considered and carefully balanced with the SLHX's benefits. Apart from that, experimental data from many international researches indicate that the exchanger's performance is greatly affected by the refrigerant's properties. As a result, the SLHX can be practically useless in some applications (especially the ones using R-22, R-32 or R-17 as their working medium) and beneficial to others (R-134a, R-407C, R-404A) leading in serious COP improvement.

Another alternative to the subcooling cycle is the use of a mechanical subcooler. Specifically, the use of a heat exchanger is once again inevitable but in this case, the subcooling operation is accomplished in a separate system, as shown in Figure 4.

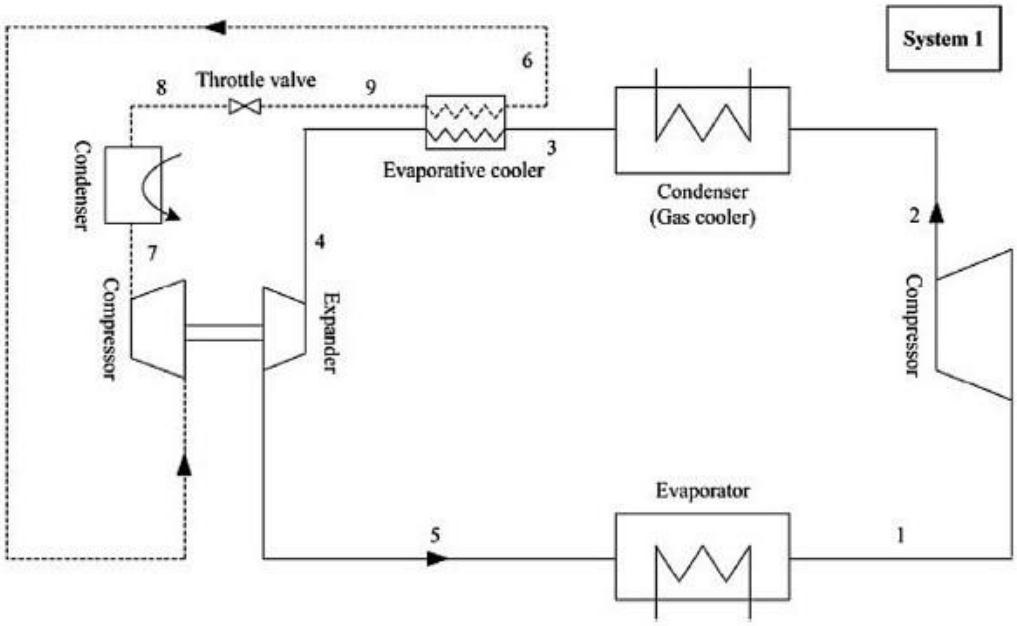

Figure 4 – The mechanical subcooler's operation is defined by points 6,7,8,9. The rest of the points represent the standard VCC. The links between the two systems are the evaporative cooler end the expander. Graph from [14].

The concept of this method to recover the expansion losses by replacing the typical throttling valve with an expander. The work produced by the expander supplies the compressor of the subcooling system, which also performs a Vapor Compression Cycle with a different refrigerant than the one of the main system. Its goal is to provide a colder liquid to the heat exchanger so that the main refrigerant will be further cooled down because of the heat transfer taking place, increasing the condenser's capacity. This specific method has been tested and the results indicate that an increase of the COP value by 10%-20% can be achieved. This value strongly depends on the type of refrigerants used in the two systems and the overall design quality of the expander and the other components. The complexity of this application and its higher cost, however, creates thoughts on its utilization.

To conclude with the subcooling cycles, some applications take advantage of thermoelectric elements based on physics principles and specifically the Peltier effect. Electricity is being directly converted to temperature difference which is the key for heat transfer and the subcooling process. The main disadvantage of these devices is their low efficiency conversion rate. As a result, the COP value increase cannot be guaranteed and once again strongly depends on the system's quality design.

1.1.2 Compressor replacement with ejector concept

Ejectors are the second main application that aims to improve the VCC in general. Its functioning is based on fluid mechanics principles. A VCC using an ejector is depicted in Figure 5, which also explains its operation.

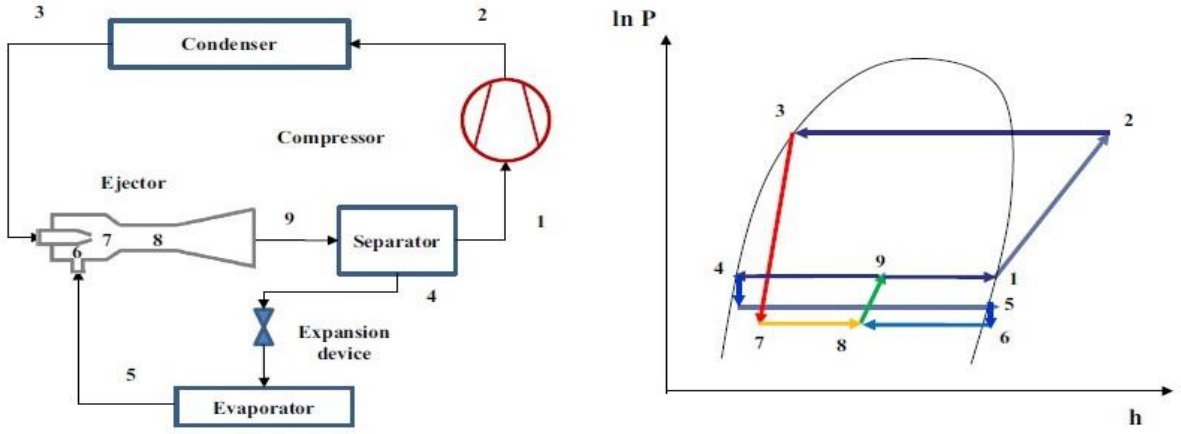

Figure 5 – Schematic diagram of an ejector in a VCC and its respective P-h diagram. Graphs from [1].

The ejector is similar to a Bernoulli pipe and consists of a small nozzle in its entry, a mixing chamber and a diffuser at the end. High pressure liquid (cycle point 3) enters the nozzle which creates a significant pressure drop (cycle point 7). This pressure difference forces vapor from the condenser's exit to flow into the ejector (cycle point 6). The two currents are then mixed (cycle point 8) and pressure recovery is achieved at the diffuser section. In that way, kinetic energy is transformed into a pressure increase (cycle point 9). The vapor that enters the compressor is now at higher pressure than expected, meaning that the compressor requires less power in order to perform the rest of the compression. As a result, the cycle's COP value tends to increase. A separator is required so that vapor is led to the compressor and the remaining liquid back to the evaporator. The separator's efficiency and proper functioning is of great importance, since any liquid that enters the compressor can create serious damages and rapidly decrease the cycle's efficiency. Therefore, the separator must block all droplets, ensuring that only vapor flows into the compressor. Additionally, the ejector cycle is greatly affected by the temperatures of the heat source and the heat sink as well as the refrigerant that is being used. Taking all those parameters into account, a COP increase by more than 16% is quite feasible.

1.1.3 Multi-stage Cycles

Multi-staged cycles have been greatly applied in many heat pump units during recent years. Their goal is to deal with the high temperature difference between condensation and evaporation, especially when the heat pump is operating at a high load. This can destabilize the unit's operation, affecting its reliability and efficiency. In order to avoid this, the compression process is divided into two parts. The first stages of the compressor increase the pressure of the mass flow that exits the evaporator. The rest of the refrigerant is injected in the compressor's later stages at a liquid, vapor or two-phase state. Figure 6 depicts a two-stage compression with the assistance of an intermediate subcooler that injects vapor into the compressor.

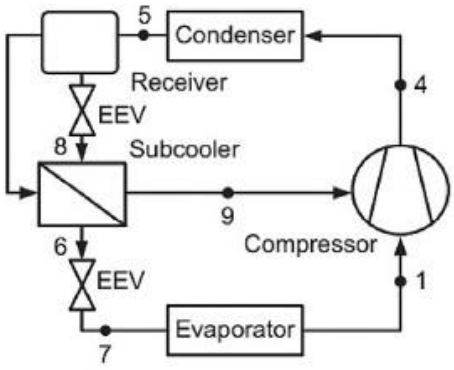

Figure 6 – Two-stage compression using vapor injection. Graph from [15].

The liquid refrigerant that leaves the condenser flows through an expansion valve that decreases its pressure, causing it to reach a two-phase state (point 8). Then, a phase separator is used to ensure that any remaining liquid will be lead to the evaporator and the vapor to the compressor. The subcooler (is depicted with the same shape as the phase separator in Figure 6) reduces the vapor's temperature so that it will cool down the already compressed refrigerant at the point that the injection will take place. It is crucial for the expansion valve (point 8) to maintain the intermediate pressure at a specific level so that the vapor can easily enter the compressor, as well as to control the mass flow that will be injected. The main benefit of this two stage compression is the decreased temperature of the refrigerant vapor that exits the compressor. In other applications, the phase separation is accomplished in a flash tank that contains two-phase refrigerant. Experiments with a variety of refrigerant have indicated a possible improvement of the COP value by 10%-15%.

Depending on the application, the budget required to cover operational and retrofitting costs, combined rigs that take advantage of the above mentioned VCC improvements have been

adopted. Other ideas have been abandoned due to their complexity and the minor improvement that is correlated to that.

1.1.4 Expansion Loss Recovery

Another main category of VCC improvements concern power recovery from the expansion process. The standard VCC uses a throttling or an expansion valve to decrease the working medium's pressure. This is considered to be an isenthalpic process but the inevitable increase of the refrigerant's entropy implies thermodynamic losses that decrease the cycle's efficiency. Certain devices have been designed in order to recover those losses at the highest rate possible, maintaining the working medium's entropy increase relatively small.

Expanders can prove to be valuable assets for air conditioning and heating applications that perform Vapor Compression Cycles. Their goal is to extract mechanical work which will then be directly transferred to the compressor or converted into electricity that will supply it, reducing the required power for the compression process. A typical drawing and a P-h diagram of an expander installed in a VCC application can be seen in Figure 7 – Schematic diagram of an expander installed in a VCC. P-h diagram from [1]. The red curve approaches an isentropic process.

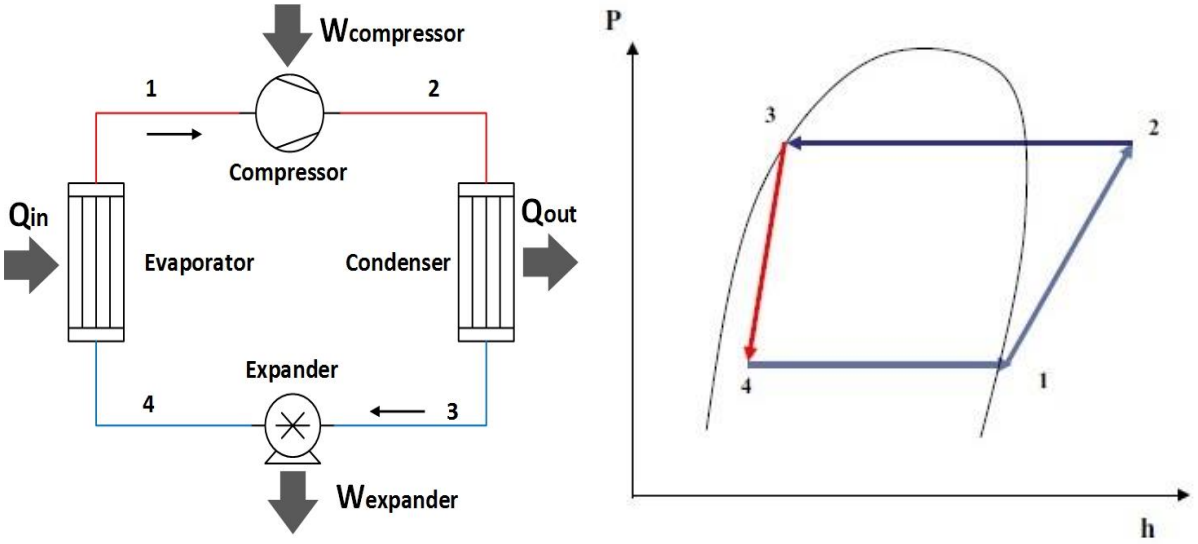

Figure 7 – Schematic diagram of an expander installed in a VCC. P-h diagram from [1]. The red curve approaches an isentropic process.

The existing expanders can be divided in two main categories. The first one is consisted of positive displacement equipment that mainly includes piston type and swash plate machines. The second one comprises compressors that operate in reverse. Any type of scroll or screw compressor can

function as an expander with the suitable modifications. Special attention must be paid so as to ensure the machine's proper operation especially when the expander's shaft is directly connected to the compressor. Figure 8 shows the expander's different connections to the system.

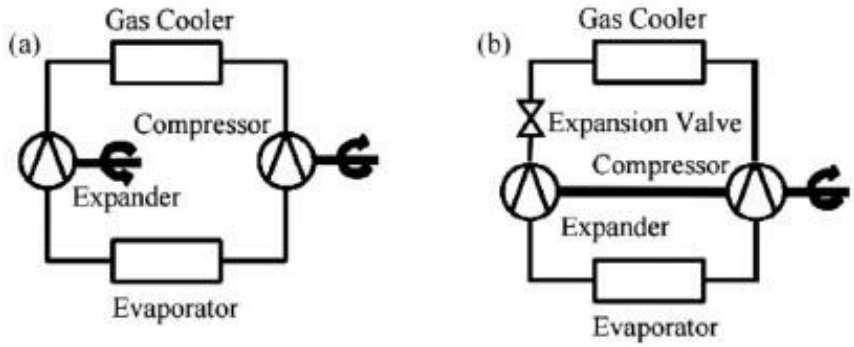

Figure 8 – Basic expander arrangements. Gas cooler refers to the VCC's condenser. Graphs from [16].

In case (a) the useful work extracted by the expander can be converted into electricity by connecting the expander to a generator, though a gear box to control the rotational speed or an electrical inverter for the produced current is required in the majority of applications. In (b) case, the two components are connected to the same shaft and the work is directly transferred to the compressor, assisting the rotation. The expansion valve is a control option so that the expander's power output can be adjusted. The expander method has great potential and experiments suggest that a great increase of the COP value by even more than 40% is quite possible.

1.2 Research on positive displacement expanders

As presented above, in the space heating sector, research has been conducted on several ideas that can improve the performance of a standard heat pump, leading to significant financial and environmental benefits. The option of recovering work from the high pressure, under which most refrigerants operate in heat pumps, makes the idea of integrating an expansion machine very intriguing. The involvement of expansion processes with two-phase refrigerants makes positive displacement expansion machines as the most promising technology for this kind of applications.

Different types of expanders have been developed over the past decade. Their common goal is to exploit the high pressure of the refrigerant, leading to energy recovery and eventually reduced electricity consumption of heat pump units. In general, the research that has been carried out in this field of interest, involves expanders that are actually compressors, which have

been modified in order to operate in reverse. A variety of expanders has been tested in several different applications, according to the refrigerant that is used and the high pressure of the circuit. Hewitt et al. [2-4] has studied and tested a turbine coupled on the same shaft with a rotary compressor. Some problems in the experiments were encountered, such as leakage of refrigerant from the turbine to the compressor via the shaft and intense heat transfer between the expander and the compressor sides. Even though turbochargers are used by the current state-of-the-art heat pumps, the above mentioned leakage problem as well as rotational speed issues of the two components (compressor/expander) must be resolved. Gear boxes can prove to be a solution, yet they increase the cost and the complexity of the unit. The efficiency of this concept at part loads is relatively low and does not exceed 50% even at full load operation.

A major category of expander applications contains experiments done on positive displacement machines. Stosic et al. [5-9] developed a screw expander able to produce power in an organic trilateral cycle used to recover energy from waste heat available in industrial process. The same expander was tested in a refrigeration cycle with carbon dioxide as its working fluid. A twin screw expander with one pair of rotors has been developed in order to replace the standard throttling device. This type of expander recovers power from the two-phase expansion process and directly recompresses a portion of the vapor formed during the expansion. The overall expansion-compression efficiency reaches a maximum value of 55%. The relatively high volume expansion ratio that characterizes refrigerants in heating and air-conditioning applications is a disadvantage for screw expanders and generally positive displacement machines. Therefore, Meng Wang et al. [10] presented a novel vane-type expander with two internal expansion stages for an R-410A system. The COP increase was found to range from 6%-22%, according to operating conditions such as condensation and evaporation temperature.

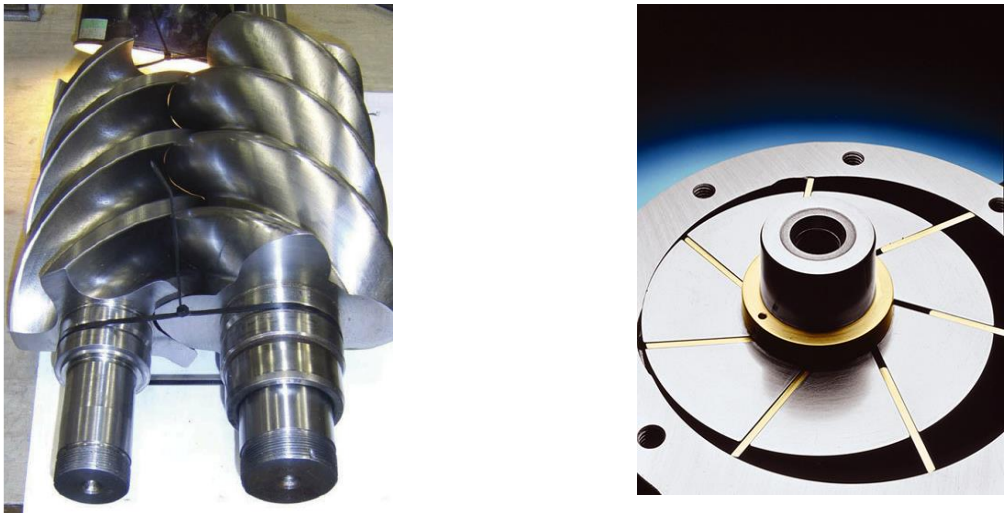

Figure 9 – Screw expander (left) and vane type expander (right).

All these works witness that there is a strong interest in the scientific community for the energy recovery, since significant work is lost in the throttling process in VCC units. However, most of the research has been carried out on several different technologies (screw, vane or rotary expanders), but very few experiments have been conducted for hydraulic piston and reciprocating type expanders, which seem instead the most feasible technology for small-scale applications.

1.3 Literature review: simulation and experimental analyses of piston-type expanders for heating and refrigeration applications.

Li Zhao et al. [11] performed a simulation analysis of a two-rolling piston expander that aims to replace the throttling valve in a heat pump unit. The expander is made of two sets of a single piston expander that contains a cylinder, a rolling piston, a sliding valve and an eccentric wheel. As the refrigerant fills the cylinder's chamber and expands, the eccentric wheel begins to rotate. After certain degrees of rotation, the outlet port is revealed and the working fluid that exits the first piston flows into the second, through a connecting pipe. The process is repeated and the rotation of the two wheels provides useful work. The simulation results suggest that this type of expander can overcome the high expansion ratio of the low pressure refrigerants, though the friction losses are a major factor that affects the expander's efficiency. Specifically, friction losses account for 78.5% of the total losses. The expander reached its peak performance with a 43.7% isentropic efficiency. If the friction losses are minimized following a series of suggested improvements, a theoretical value of 72% could be achieved.

An experimental study on a radial piston-type expander for a CO_2 refrigeration system was conducted by Mitsuhiro Fukuta et al. [12]. The expander has four cylinders and pistons arranged radially, and controls supply and discharge of refrigerant by a reciprocating motion of an adjacent piston. The results suggest that this novel type expander could fit well in a small scale refrigeration cycle. As far as performance is concerned, a value of 40% overall efficiency is achieved. The expander's overall efficiency is defined as the ratio of the measured power that is recovered to the power that is theoretically obtainable with the theoretical mass flow rate by this expander. Friction losses are once again a crucial factor to the expander's efficiency and must be reduced in order to improve the overall performance.

Giovanni Ferrara et al. [13] conducted an experimental research on another piston expander suitable for refrigeration systems, with CO_2 as its working fluid. The initial prototype was a hydraulic motor, which was converted into an expander with certain modifications. The results were pretty encouraging, as an isentropic efficiency of 19% was reached during the experiment. It is also possible for this value to overcome 41% if the friction losses and the leakages of the machine's different components are dealt properly. In terms of thermodynamic performance, there is large margin for COP increase. The expander was tested in inverse CO_2 cooling cycles and provided a COP increase by 7.4%, while the theoretical value could exceed 20.5% with a reasonable reduction of the mechanical losses. As a result, the tested expander could replace the throttling valve in a heat pump system in a very effective way. This prototype expander, originally manufactured and developed in Italy, is the experimental subject of this diploma thesis.

2 Thesis concept and objectives within the EXP-HEAT project

The main concept of the Exp-Heat project was to replace the throttle/expansion valve used in common vapour-compression units with a hydraulic piston-type expander in order to investigate the possibility of energy recovery (Figure 10). Its purpose is to recover energy from the high-pressure liquid (condensed) refrigerant with the use of the expander and provide it to the compressor, reducing its electricity consumption.

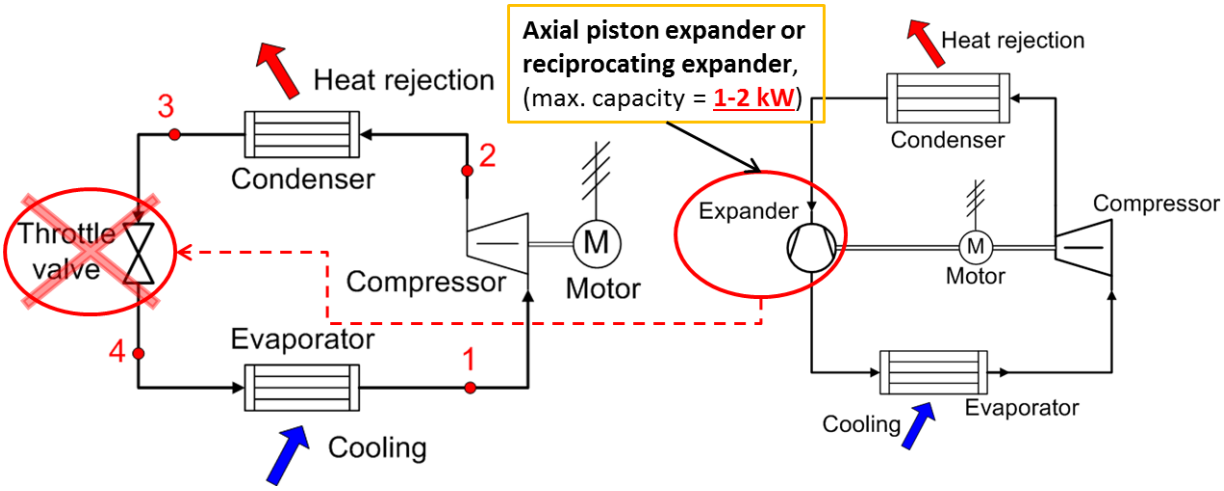

Figure 10 – The concept of replacing the standard heat pump's throttling valve with a piston type expander for energy recovery.

Within the project activities, a dedicated expander was developed by the Italian manufacturer Italgroup®, a company that specializes in hydraulic piston motors. The prototype's performance was tested by University of Florence in stand-alone operation in a hot gas cycle (i.e. not integrated in a heat pump unit) and the results were pretty encouraging, as it will be shown next.

The experimental evaluation of the performance of the final expander prototype, integrated in a commercial heat pump unit is the research topic of the thesis. In this context, the dedicated expander was retrofitted in an existing commercial heat pump in order to boost its performance.

During the retrofitting process, a minimum number of modifications and adjustments to the heat pump unit will be pursued, so that the installation of an expander to a commercial heat pump will be as easy as possible. The normal operation of the unit along with the thermal power that the manufacturer promises must be ensured, even after the retrofitting. Most importantly, no replacement of any basic components such as the compressor, the evaporator and condenser

heat exchangers, safety and control systems was ensured. The first stage of the experiments aimed at the evaluation of the heat pump's operation without the contribution of the expander, to determine whether the retrofitting has affected the unit's normal operation (i.e. using the original throttling valve). The second stage of the experiment involved the expander mode operation. The retrofitted unit is installed and will be examined in the NTUA laboratory, in a dedicated test-rig that has been constructed for its experimental evaluation, focusing more on its testing at various operating conditions, and on the components' coupling rather than pure performance. Special effort will further be given on the operation optimization, while ensuring the minimum modifications to the control of the unit.

Finally, the maintenance of the expander is also a point of interest. Any operational issue that will be encountered will be dealt by suggesting the most feasible solution that will not affect the structure of the expander as it has been developed by its manufacturers. Finally, an estimation whether some automation regarding the expander's operation will be presented.

The expander is expected to be beneficial as far as energy saving is concerned. In a heat pump unit, the specific component could achieve a 2%-5% COP increase. In terms of electricity production, a power of 200W-500W is expected under an isentropic efficiency that ranges from 10%-30% depending on the conditions at the different operating points. Although the produced power may seem low, it must be mentioned that this expander was developed for small scale heating applications. Specifically, 500W stands for about 12% of the power that the heat pump's compressor requires to deliver its nominal thermal power at an ambient temperature of 7^{o}C and a medium condensation temperature. Taking that into account, the expander could have a major contribution to a unit that operates for many hours (e.g. a Nordic country during winter) leading to reduced operating costs and overall system energy saving.

2.1 The developed expander prototype

The purpose of this chapter is the presentation of assessment of the expander redesign (Figure 11 - version 2.0- retrofitted to the installed heat pump), highlighting the main incurred modifications in order to achieve a significant improvement of the performance compared to the previous prototype (Figure 11 - version 1.2).

The initial expander was based on a single displacement motor of Italgroup®. The tests carried out with R134a, and with CO2 by the University of Florence, showed the main issues that negatively affected the performance of the original hydraulic expander with limited

modifications (v 1.1) and its modified version (v 1.2). The redesign was focused on solving part of the issues that arose.

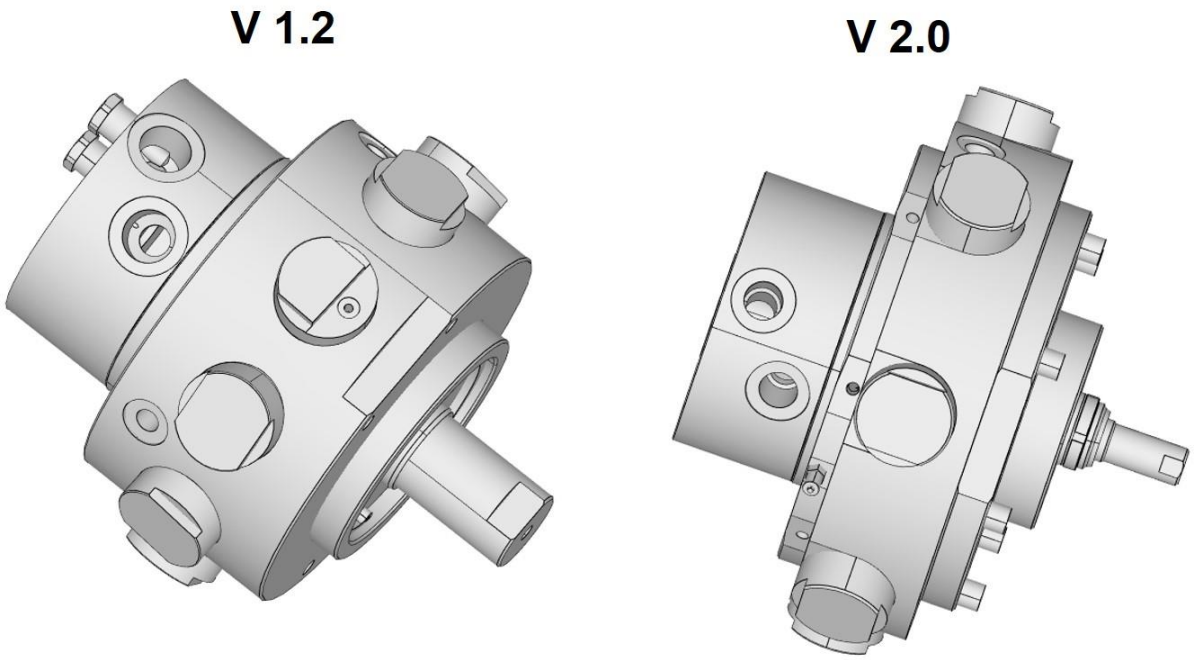

Figure 11 – The prototype expander manufactured by Italgroup® (left) and the redesigned model that will be tested in the NTUA laboratory (right).

The implementation of a more effective lubrication system of the expander was one of the main objectives for the expander development. It opened the way to the first important upgrade of the v 1.2: oil inlet holes and ducts to connect the outer surface of the case to the inner of the expander were done. In order to evaluate the performance improvement, a new dedicated test rig was designed and manufactured. The tests were carried out with R404a and R410a, which are HFC refrigerants with significantly different properties compared to R134a. Such refrigerants are ecofriendly and will be widely adopted in heating and refrigeration applications according to EU directives, tending to gradually replace R134a. Therefore, the simulation of the expander's performance was performed under the concept of the suitable refrigerants for future applications.

The achieved results are presented and discussed, with special focus on the comparison to the features and performance achieved with the previous versions of the expander (1.1 and 1.2).

2.1.1 Final Redesign of the Expander

The tests performed on the v 1.1 and v1.2 with R134a and CO2 as working fluids showed an interesting potential of the expander when used in a vapor compression cycle in substitution of a throttling valve in the former and a remarkable potential in the latter. The results obtained from the indicated cycles showed that the indicated isentropic efficiency reaches very interesting values, leading to a considerable COP improvement of the inverse cycle where the expander runs. In fact, by considering the indicated power that neglects the influence of the mechanical losses, the achieved isentropic efficiency was almost 24% with R134a and 60% with CO2. However, the measured useful shaft power output of the expander highlighted that the performance was negatively affected by the following issues:

- the required volumetric expansion ratio of the fluids that, in case of R134a, is significantly higher than the built-in volumetric ratio and, consequently, allowed low expansion work.
- the leakages through the components inside the expander, that reduced the expander efficiency.
- the unavoidable mechanical losses inside the expander, that decreased the power produced by the machine.

Whereas the first issue influences the behavior if the fluid inside the cylinder, the second and third affect the performance by increasing the elaborated mass flow rate and reducing the power produced by the expander. These loss sources are related to the original application of the tested machine, which belongs to hydraulic purpose instead of refrigerants. The oil has totally different properties, in particular higher viscosity and very high levels of pressure (i.e. up to 300 bar). Specifically, the contribution of each component to the friction torque at different rotational speeds was evaluated and showed that the bearings and the frontal seal are the components mostly affecting the total friction torque.

For these reasons, a new version of the expander (2.0) was designed and manufactured, still maintaining the original concept of the machine but with modifications specially focused to address the main issues that have been mentioned above. First of all, the redesign is focused on the reduction of the mechanical losses and the increase of the volumetric ratio, in order to make the expander more suitable for use with HFCs, specifically those with higher expansion ratios and largely used in industrial heat pumps like R410a and R404a.

By considering to work with HFC refrigerants having lower required volumetric expansion ratios than R134a (for instance, R410a or R404a), in the new design it was assessed to increase the built-in volumetric ratio of the expander from 2.4 to a 6 ÷ 7, in order to achieve a better fluid volumetric behavior inside the cylinders. With this goal, the eccentricity of the shaft was increased in order to enhance the stroke of the piston and the volumetric expansion ratio. This modification led to the increase of radial case size and, consequently, the length of the intake duct, that is part of the dead volume. As a compromise, the stroke was increased from 16 to 32 mm. In order to limit the increase of the radial dimension due to the increase of the eccentricity, the number of the pistons was reduced from nine to seven. The obtained displacement of the expander was enhanced from 102 to 150 cm^3, whereas the expansion ratio was more than doubled, also considering that the axial size of the case was reduced.

In addition to the improvement of the thermodynamic behavior of the cylinders, these changes led also to the reduction of the mechanical losses. In particular, the reduction of number of pistons leads to a reduced number of interacting surfaces in the expander. Thus, the related friction losses due to the contact between the pistons and the cylinder walls are reduced.

Moreover, it must be considered that the shaft and the bearings in the original version of the machine were sized to stand loads up to 300 bar. By considering the pressure of the current application, the size of these components was reduced to stand loads up to 80 bar. The reduction of the loads, together with the need of reducing the length of the intake duct, led to another interesting simplification of the design: in addition to the bearing on the eccentric shaft, the two tapered bearings were removed, whereas only a double row angular contact ball bearing was used at the right end of the axis to stand both axial and radial loads. Due to the removal of a bearing, the axial size of the expander and, consequently the intake duct, could be reduced, leading to decrease of the dead volume. Finally, by considering that the diameter of the shaft at the outlet of the expander was decreased from 40 mm to 18 mm, the diameter of the frontal seal was reduced, thus leading to furtherly lower frictional losses.

Regarding the distributor, the rotating plate and the case were modified in order to invert the inlet with the outlet. In this way, whereas in the previous version the fluid passed through the holes in the plates radially, in the modified design the fluid enters the plates axially: in this way, the concentrated pressure losses during the suction phase, that causes a reduction of the peak pressure inside the cylinder and of the expander efficiency, are appreciably reduced. It follows that the increase of pressure losses during the discharge phase are much smaller in

comparison to the pressure losses in the suction phase, as observed from the experimental results.

2.1.2 The lubrication system

One of the most important issues addressed in the redesign of the expander is related to the lubrication. In the previous version, the lubrication of the components inside the expander was assured by putting an amount of oil in the bottom drain chamber to be spread by the eccentric rotating shaft and by injecting a small amount of oil in the cycle working fluid upstream the expander. In the modified expander, it was expected to inject oil in two different parts of the machine. In particular, a duct in the shaft from the outlet of the expander to the internal part of the case is present to lubricate the bearings and the pistons. Moreover, a modification is applied to lubricate the plates through a duct from the external part of the case to the distributor, in order to reduce both the friction losses between the rotating and the stationary plates and the leakages through these components.

2.1.3 Experimental Results of stand-alone expander operation

In the dedicated test rig that would simulate the operation of a heat pump, with high pressure liquid suitable for the expansion process, the modified expander was tested experimentally in order to evaluate any effective improvement of the performance. The tests were carried out with both R404a and R410a. The thermodynamic conditions are listed in Table 1. The pressure levels reached during the tests were kept relatively low so that the mass flow rate elaborated by the expander does not exceed the design values. Otherwise, at higher pressure levels the mass flow rate increases and the condenser cannot condense completely the fluid leading to obtain a fluid with a quality higher than 0 at the inlet of the expander, meaning that the refrigerant is at a two-phase state.

Table 1. Experimental thermodynamic conditions with R404a and R410a.

Parameter	R404a	R410a
Suction temperature (°C)	**40**	**36**
Suction pressure (bar)	**18.3**	**22**
Discharge temperature (°C)	**2**	**8**
Discharge pressure (bar)	**6.5**	**10.25**

These tests show the improvement obtained after the redesign of the expander and by using a fluid with a lower required volumetric expansion ratio. Figure 12 and Figure 13 report the isentropic efficiency and the indicated isentropic efficiency obtained with R404a and R410a respectively. The peak values of the isentropic efficiency measured at the shaft that reaches and exceeds 20% during the experimental tests (i.e. in case of R410a, it reaches a value up to 26%) demonstrate that a strong improvement is reached in comparison to the tests with the previous tested HFC refrigerant (i.e. R134a), where the efficiency reached at maximum 9%. In addition, the values of the indicated isentropic efficiency, which reaches over 40-50%, show a proper thermodynamic behavior of the fluid inside the cylinders due to both the increase of the built-in volumetric expansion ratio, as well as the decrease of the required volumetric ratio of the fluid. However, the indicated isentropic efficiency shows also that the mechanical losses still have a great impact on the performance and further improvement can be achieved. It must be considered that the isentropic efficiency depends strongly on the thermodynamic conditions at the inlet and outlet of the expander. In particular, higher pressure levels lead to greater performance. For this reason, it is reasonable to think that the performance of the expander should improve when used in a VCC unit at a higher pressure difference between the condenser and the evaporator, especially working with R410a.

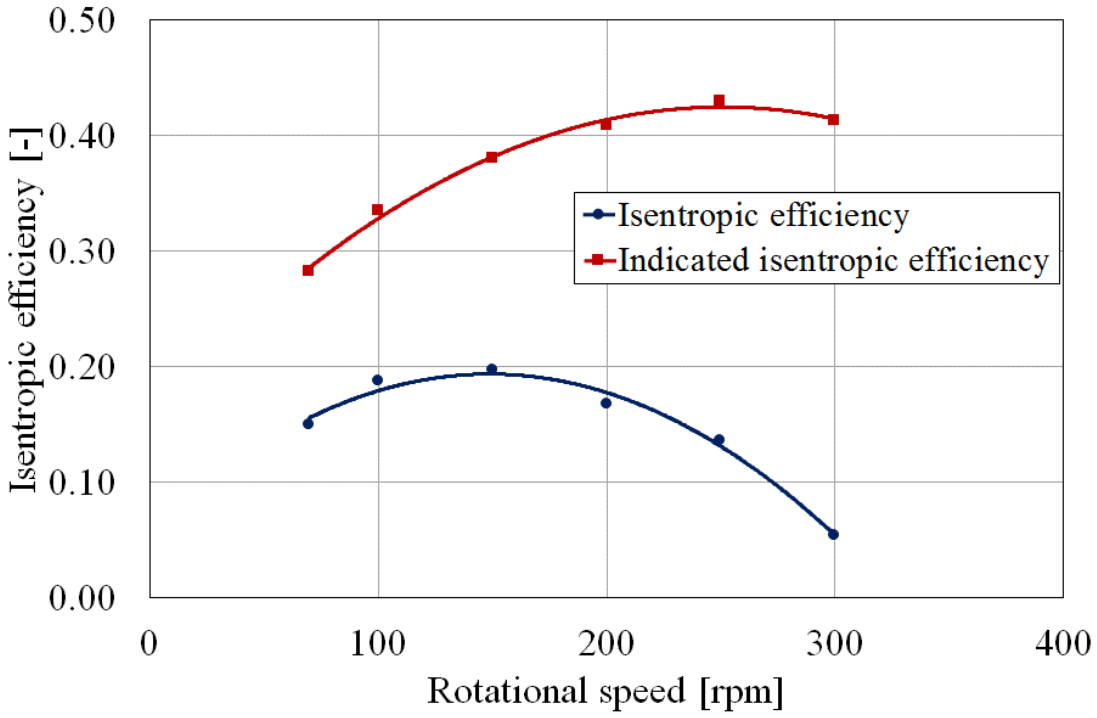

Figure 12 - Measured and indicated isentropic efficiencies as function of rotational speed with R404a.

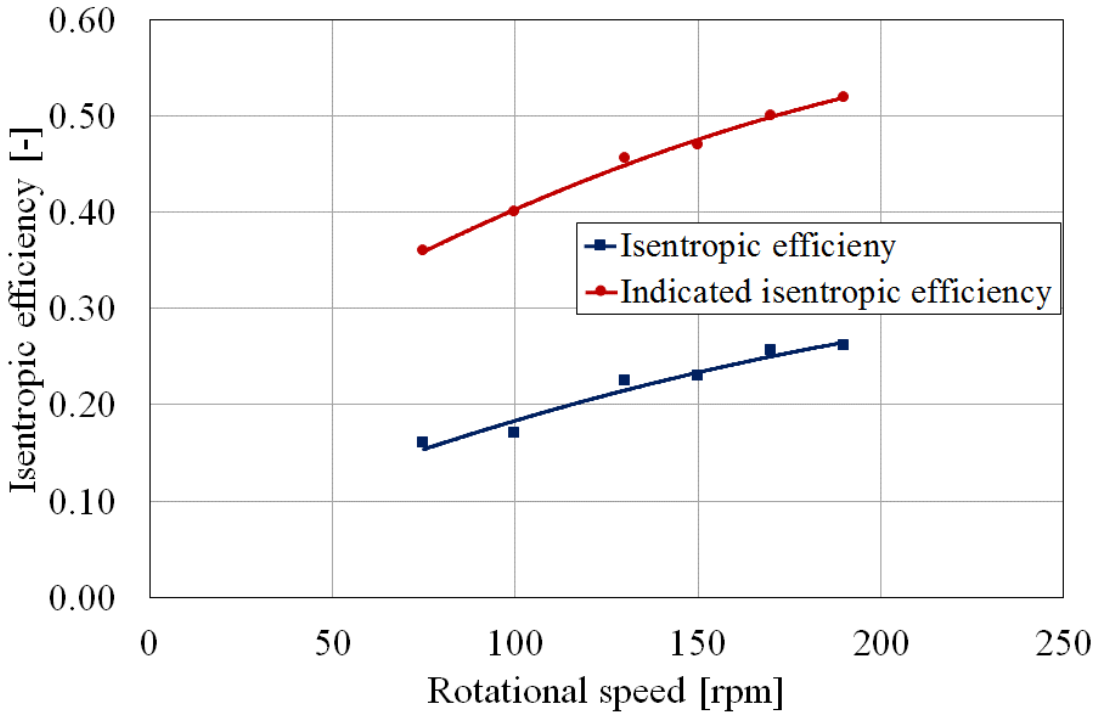

Figure 13 - Measured and indicated isentropic efficiencies as function of rotational speed with R410a.

3 Installed commercial heat pump

An ON/OFF heating only commercial unit was selected for the retrofitting of the expander. The ON/OFF unit is more suitable for retrofitting the expander compared to an inverter driven unit as it does not require any changes to the control unit, keeping the retrofitting costs low.

3.1 Model and Manufacturer

The installed heat pump is NIBE's model F2300. NIBE Energy Systems is the largest manufacturer of domestic heating products in the Nordic Countries and a market leader in Northern Europe in the electric water heater and heat pump segments.

The F2300 is an Air / Water Heat Pump, which means that it uses environmental air to achieve evaporation of the working fluid (absorption of ambient heat), and water – usually from a closed circuit – in order to deliver the heat generated from the pump. A hermetic scroll type compressor is utilized for the necessary pressure rise of the working medium vapour. Further analysis of the heat pump's operating circle is given in the next chapter. The F2300 comes out with two models, the F2300-14 and the F2300-20, each one referring to the nominal thermal output of the heat pump (14 and 20 kWth).

Both models are CE marked, meaning that the product meets all demands and regulations based on relevant EU directives. It also fulfils IP24, a regulation that ensures that the heat pump is impenetrable by objects with a diameter larger than or equivalent to 12,5 mm and protected against water droplets from all directions, allowing the heat pump to operate in any weather conditions. The material has a long service life and is designed to withstand the harsh Nordic conditions.

Last, it is labelled as an Energy Efficiency Class of A++ product, the second highest rank according to EU directives dealing with energy consumption, emissions, sound levels and other environmental issues.

3.2 Working Fluid

The heat pump's working fluid is R407c. The specific fluid is a zeotropic cooling hydrofluorocarbon mixture that consists of: 23% difluoromethane (R32), 25% pentafluoroethane (R125) and 52% 1,1,1,2 tetrafluoroethane (R134a). R32 provides the heat capacity, R125

decreases flammability and R134a reduces pressure. It is really suitable for air-conditioning and medium temperature applications such as heat pumps, even though a drop in its cooling efficiency must be taken into account at low temperatures. Its critical temperature is 86.2 °C.

It is a non-toxic mixture with an ODP (Ozone Depletion Potential) equal to zero. The ODP is a measure used to describe the effect of a certain substance on the ozone layer of the planet and is defined as the ratio of global loss of ozone due to given substance over the global loss of ozone due to CFC-11 (reference substance) of the same mass. Furthermore, the heat pump's working fluid has a GWP (Global Warming Potential) equal to 1774. As described before, the GWP is a measure similar to the ODP and describes the heat trapped by a gas in the atmosphere compared to the amount trapped by the same mass of carbon dioxide which is the reference substance with a GWP equal to 1. The mixture's value may be seemingly high but it is lower than that of many other refrigerants. In addition to that, the GWP factor values can change depending on the time horizon the certain substance is expected to be present in the atmosphere. Overall, the R407c is considered as an environmentally friendly fluid which makes it a frontrunner at refrigeration and heating applications, replacing other gases such as the R22 which is more harmful to the environment.

As far as the lubrication of the heat pump or another application, polyolester (POE) oil is considered as the best match for this type of refrigerant. POE oil is widely adapted by heating or refrigerating applications that use scroll type compressors, such as the specific heat pump. It allows the oil and the working gas to mix well so that a sufficient oil return to the compressor is possible, ensuring its efficient function.

3.3 Technical Data

The heat pump's innovative scroll compressor allows operation at temperatures down to -25°C. It has a wide working area, delivering hot water flow temperatures of 65°C at an ambient temperature of -10°C and 63°C at an ambient of -25°C. The F2300 also includes defrosting technology and has intelligent control systems connected to indoor modules and thermostats to provide flexibility during operation. A table of the heat pump's technical characteristics at different operating points is presented below:

Table 2. NIBE F3200/20 Technical Characteristiscs

Ambient Temperature (°C)	Hot Water Output Temperature (°C)	Delivered Power (kW)	Supplied Power (kW)	COP
15	55	23.6	6.43	3.68
7	35	19.6	4.22	4.63
2	45	17.9	5.11	3.49
-7	45	14.6	4.92	2.96
-7	55	15.2	5.95	2.55
-15	55	12.7	5.69	2.23

This table refers to the heat pump's heating medium operation at nominal flow. The conditions of this operating point are specified as following:

Table 3. NIBE F3200/20 representing operation point

Minimum/Maximum Pressure	**MPa**	**0.05 / 3**
Nominal Flow	**l/s**	**0.48**
Internal Pressure Drop at Nominal Flow	**kPa**	**4.5**

As mentioned before the heat pump has a defrosting operation to prevent icing during the condensation. This has an impact on the heat pump's performance that must be taken into account. Therefore, the following table presents the technical characteristics of the heat pump during the heating medium at nominal flow including defrosting:

Table 4. NIBE F3200/20 Technical Characteristiscs including the defrosting process

Ambient Temperature (°C)	Hot Water Output Temperature (°C)	Delivered Power (kW)	Supplied Power (kW)	COP
10	35	20.85	4.47	4.66
7	35	17.7	4.37	4.04
7	45	18.3	5.38	3.41
7	55	19.04	6.55	2.91
2	35	15.46	4.38	3.53
2	45	15.95	5.28	3.02
-7	35	12.83	4.32	2.97
-7	45	13.28	5.15	2.58
-15	35	10.37	4.2	2.47
-15	45	10.73	4.97	2.16

Other useful data:

Table 5. NIBE F3200/20 other useful data

Fan		
Air Flow (Low / High)	m^3/h	3700 / 6000
Minimum/Maximum Temperature	°C	-25 / 40
Rated Voltage	400 V / 3NAC / 50 Hz	
Maximum Operating Current, Heat Pump	A_{rms}	16
Maximum Operating Current, Compressor	A_{rms}	12.8
Nominal Ouput Fan (low / high)	W	100/224

3.4 Heat Pump Operation

In this section the operation of the heat pump and the respective standard operating cycle as well as the theoretical cycle are presented.

3.4.1 Air/Water Heat Pump Diagram

Figure 14 is a simplified drawing of an air / water heat pump's standard operation. A heat pump is consisted by four major components: the evaporator, the compressor, the condenser and the expansion valve. Therefore, there are also four main cycle points that fully represent the function of the heat pump as described below.

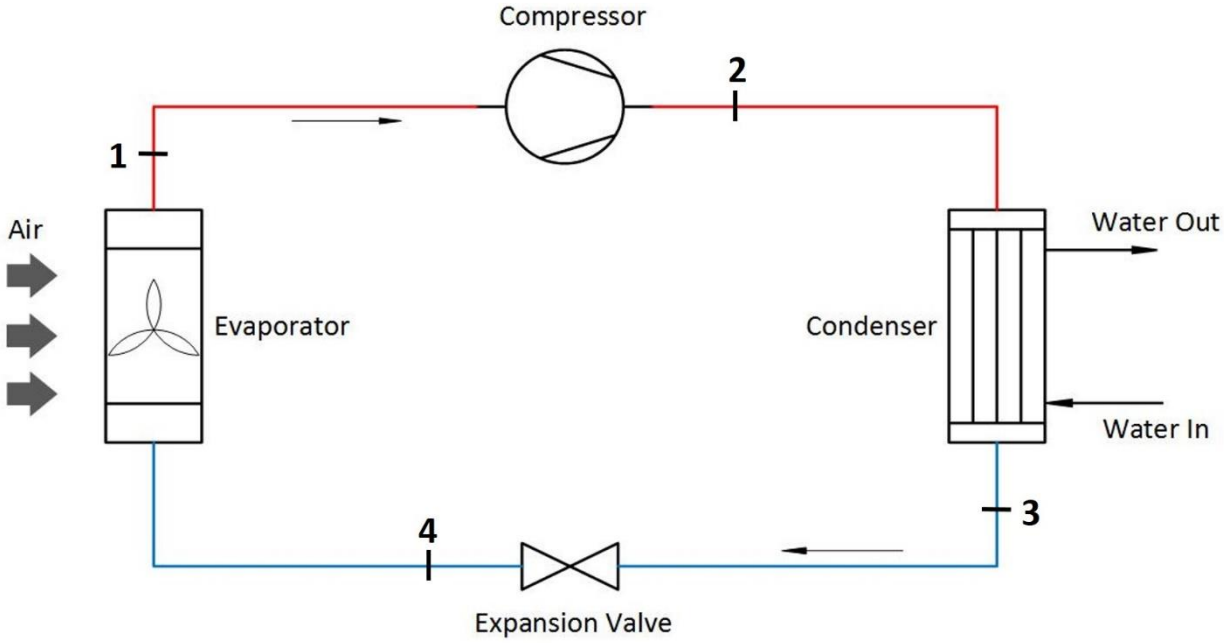

Figure 14-Standard Heat Pump Diagram and Cycle Points. Blue color refers to liquid state and red refers to vapor.

3.4.2 Standard Heat Pump Operating Cycle

A heat pump is a machine that allows heat to transfer from a low temperature source to a high temperature medium, often referred as heat sink. However, heat cannot be automatically transferred from low to high temperatures as it is predestined to do the exact opposite. According to the second law of thermodynamics, this transfer can only be achieved with the use of mechanical work or a higher temperature heat source.

As far as the operation of the heat pump is concerned, the working fluid exits the evaporator at a saturated vapour state under low pressure (Point 1). The saturated vapour then enters the compressor which increases its pressure and exits at a superheated vapour state under high pressure (Point 2). Next, the superheated vapour comes into the condenser. The condenser is actually a heat exchanger and its goal is to abstract the heat generated from the pump and deliver it to the heat transfer fluid. In this specific case, water at a lower temperature also enters the condenser and absorbs the heat that is produced by the condensation of the high pressure refrigerant at higher temperature. As a result, the hot water exits the condenser at a much higher temperature than the one it entered. The superheated vapour has now been fully condensed and exits the condenser at a saturated liquid – high pressure state (Point 3). After that, it comes into the expansion valve which decreases its pressure through its isenthalpic throttling. The working fluid is now in two-phase state (Point 4). Finally, the two-phase mixture enters the evaporator. The properties of the fluid; its low temperature and its two-phase state, allow it to evaporate simply by abstracting heat from the environmental air. Similar to the condenser, the evaporator is also a heat exchanger that uses a fan to create an air stream around the working fluid tubes in order to achieve better heat transfer. As the air delivers its heat, it comes cooler out of the heat exchanger. The refrigerant has now been fully evaporated and slightly superheated, it subsequently enters the compressor and the cycle starts again.

An air/water heat pump application uses the environmental air as its low temperature source, and water as its heat sink. The water may be provided from a closed circuit inside a residence and so the hot water that comes out of the heat pump can deliver heat inside the house. The necessary mechanical work of the cycle is provided by the compressor, which is usually driven by an electric motor.

3.4.3 Standard Cycle P-h Diagram

A P-h diagram of a refrigerant is a representation of its thermodynamic properties. The X-axis stands for specific enthalpy and the Y-axis for pressure. Apart from those two, the diagram

also contains curves for temperature, specific entropy, specific volume and quality of the substance. Each individual cycle point of the heat pump can be marked on a P-h diagram of the pump's working medium. This gives a clear image of the heat pump's function and accurately represents the different processes that take place inside the heat pump. A P-h diagram has the following form:

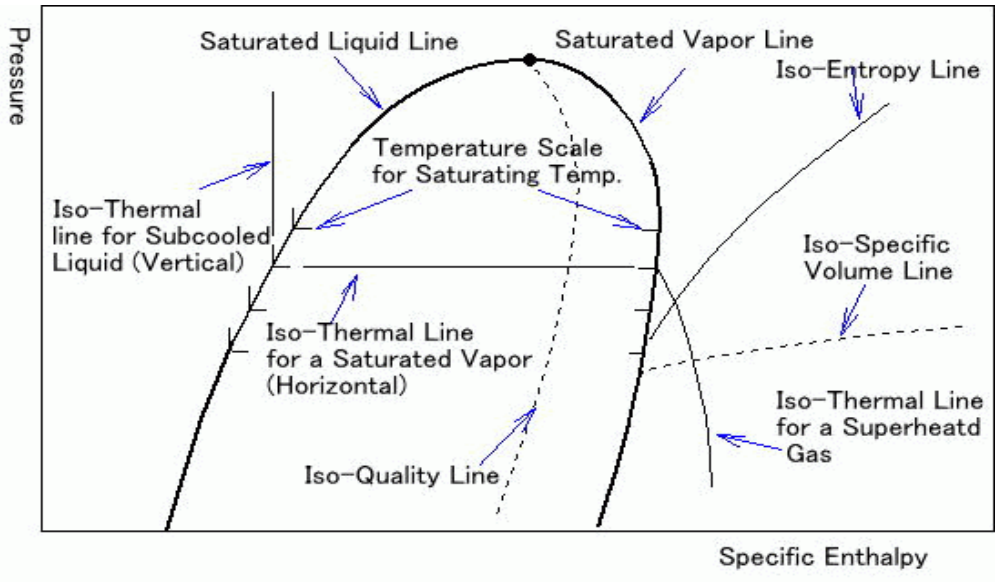

Figure 15-A substance's different property curves on a P-h diagram.

The working fluid of the F2300 is the zeotropic mixture R407c as mentioned before. Using Coolpack, a free refrigeration and heating software developed by IPU, the standard cycle of the heat pump can be represented on the R407c P-h chart (Figure 16). The depicted processes are explained next:

1 → 2: Isentropic compression. Theoretically, in the standard cycle of the heat pump, the entropy of the vapour remains the same during the compression. In reality, an increase of this property is inevitable due to the second law of thermodynamics. Because of that, a factor called the isentropic efficiency of the compressor is expressed as:

$$\eta_{is} = \frac{h_{2is} - h_1}{h_2 - h_1} \quad (3.1)$$

where $h_{2is}$is the theoretical value of the vapor's enthalpy if the compression was 100% isentropic.

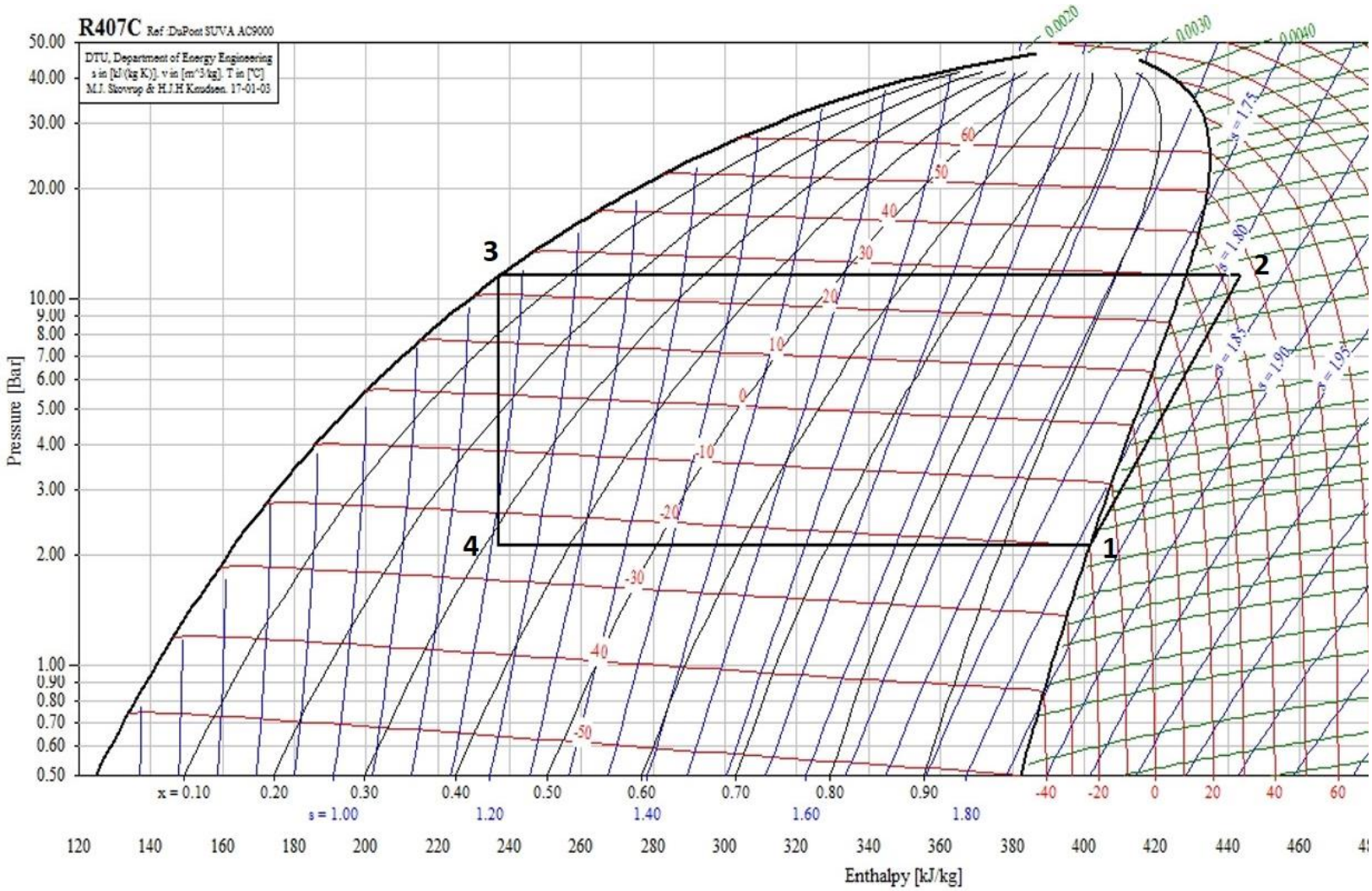

Figure 16-The standard heat pump cycle and its cycle points, assuming no thermodynamic losses.

The theoretical mechanical work that is required for the operation of the heat pump is given by the following equation:

$$\boldsymbol{W = \dot{m} \cdot (h_2 - h_1)} \quad \boldsymbol{(3.2)}$$

where $\dot{\mathbf{m}}$ is the mass of the vapor coming into the compressor.

As the value of the isentropic efficiency $\boldsymbol{\eta_{is}}$ increases, the enthalpy at cycle point 2 decreases ($\mathbf{h_{2is}}$remains stable during the compression from a fixed point at low pressure –point 1– to a higher pressure level). Therefore, less mechanical work is required which leads to lower operational cost of the heat pump, since the compressor is powered by electricity in order to function.

2 → 3: Condensation at a stable pressure. During this process, the water abstracts the heat from the working medium to increase its own temperature. The working mixture's enthalpy decreases as it is cooled inside the condenser. The heat delivered from the fluid to the water is given by the following equation:

$$\boldsymbol{Q = \dot{m} \cdot (h_2 - h_3)} \quad \boldsymbol{(3.3)}$$

Technically, the terms inside the parenthesis of the equation (3.3) should be reversed so Q would get a negative value which is quite reasonable as heat exits the system. Though, for computational purposes, a positive value of Q is adopted throughout the thesis.

3 → 4: The pressure decrease in the expansion valve can be accurately treated as an isenthalpic process, since no work is produced and the valve and pipelines are well insulated to prevent any heat losses.

4 → 1: Evaporation at a stable pressure: As seen in Figure 16, cycle point 4 is in the two-phase area at a low temperature. If the mixture is further heated by the environmental air it will evaporate. The fact that R407c is a zeotropic mixture must be taken into account, as an increase of its temperature is quite noticeable during evaporation. The amount of heat that is delivered to the working fluid in order to evaporate can be calculated using the following equation:

$$\boldsymbol{Q_{evap} = \dot{m} \cdot (h_1 - h_4)} \quad \boldsymbol{(3.4)}$$

As a measure of the heat pump's operating efficiency, the Coefficient of Performance-COP factor is defined. The COP in a heat pump, refrigerating or HVAC system is the ratio of useful heating or cooling provided to the mechanical work required for the respective operation and is

the basic measure to describe the function of such a machine. In the specific application, the heat pump's COP is given by the following equation:

$$\boldsymbol{COP = \frac{Q}{W}} \quad (\mathbf{3.5})$$

Higher COP means higher performance and thus lower operational costs.

3.5 The NIBE-F2300/20 Part Assembly

As it has already been mentioned, the goal of this project is to study the possibility of obtaining useful work from an operating heat pump in a real cycle. Therefore, the inner layout and design of the machine must be carefully examined so that it is clearly understood which components perform the respective operations. The heat pump layout and its components as delivered by the retailer are depicted in the following figures.

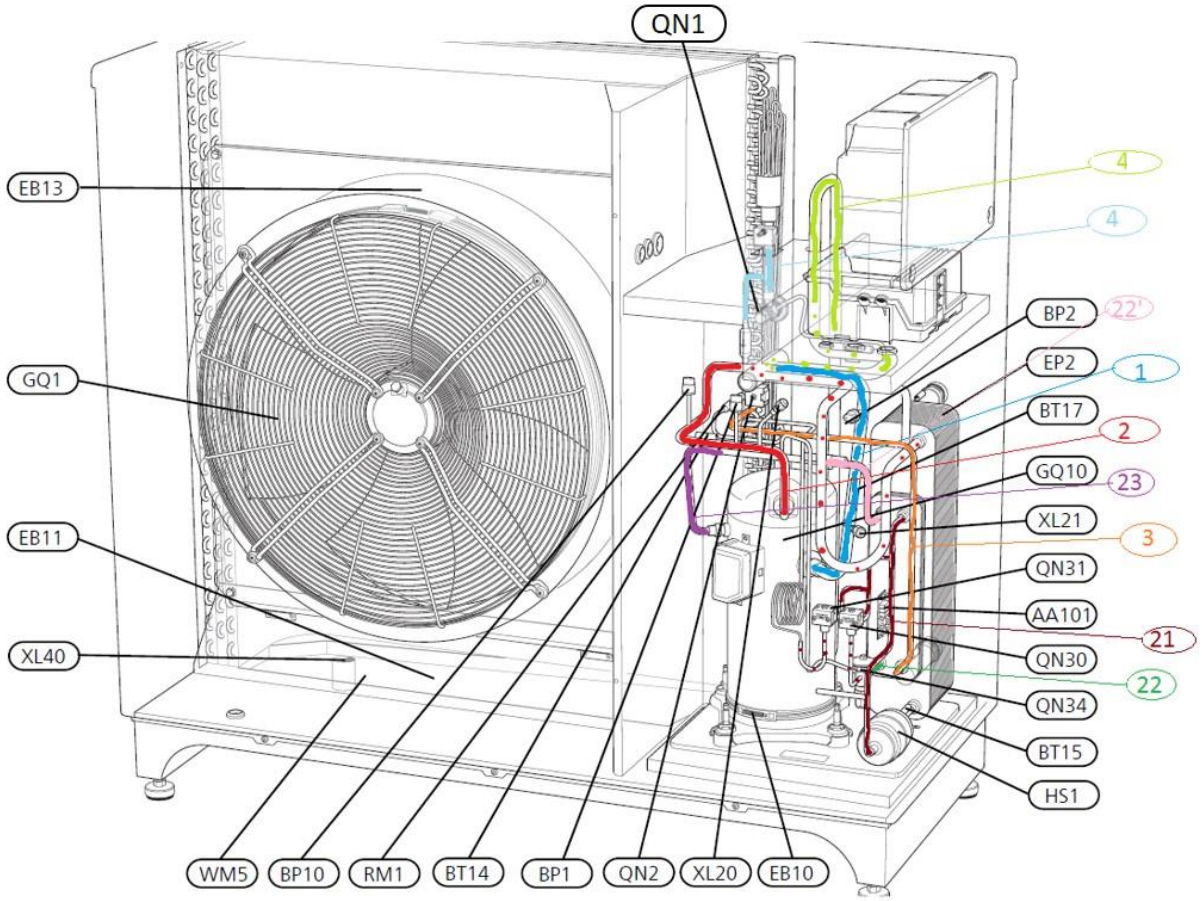

Figure 17-Front view of the heat pump.

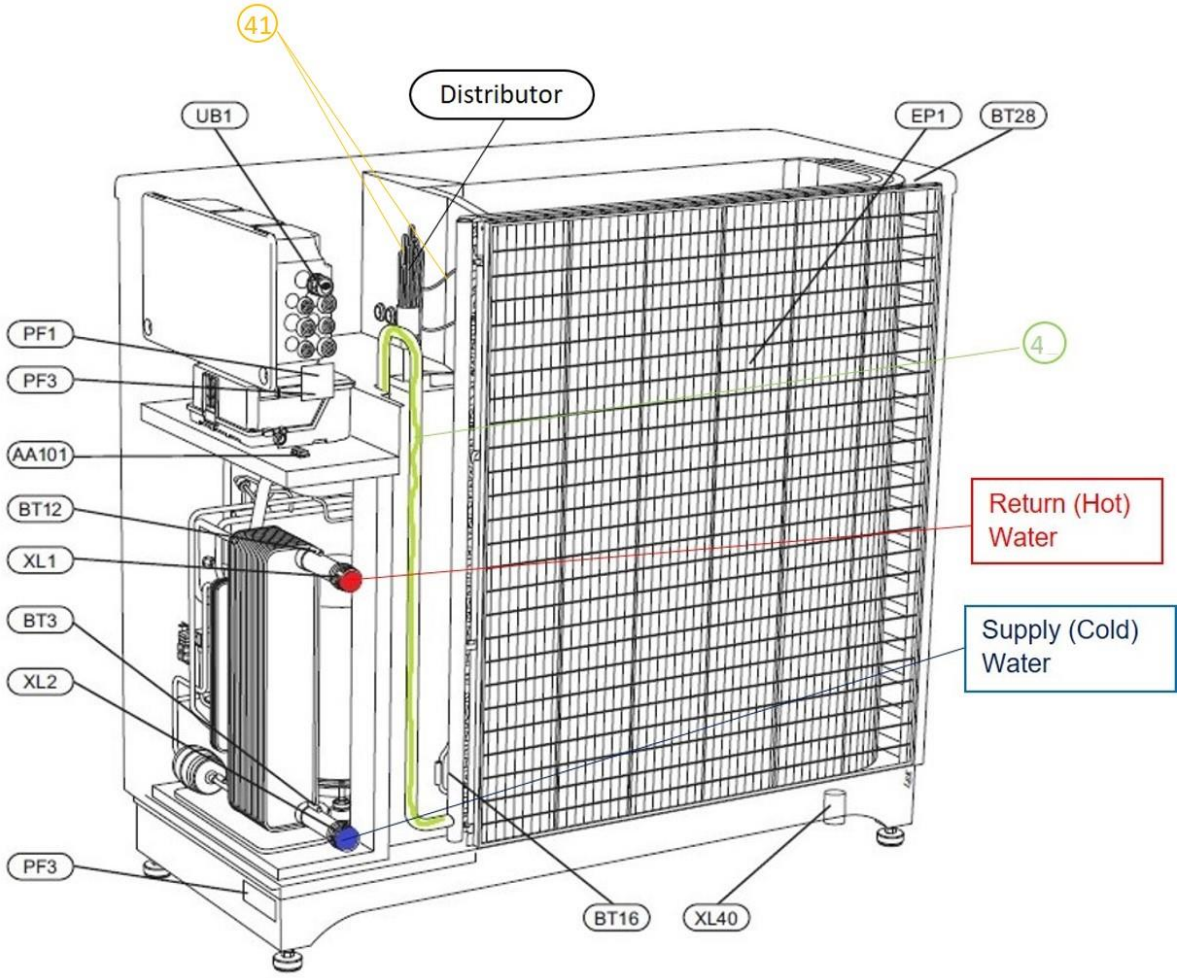

Figure 18-Rear view of the heat pump.

In Figure 19 a schematic diagram of the configuration of the heat pump provided by the manufacturer is provided.

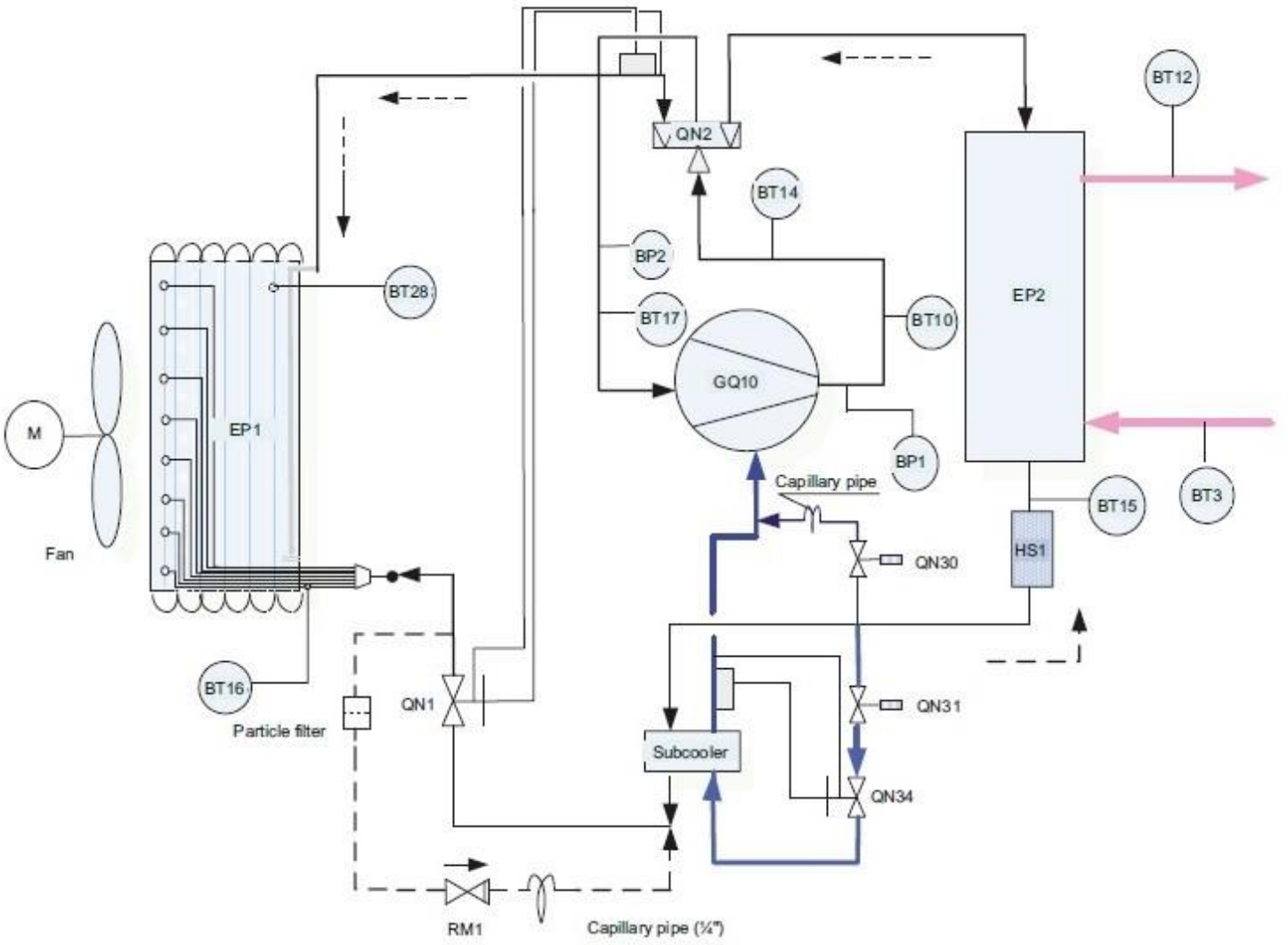

Figure 19-Drawing of the NIBE-F2300/20 with its main components and sensors provided by the manufacturer.

The main components mentioned in the above figures are listed below:

Major Components

GQ10 Compressor (Can be seen on figure 4)

EP1 Evaporator (Can be seen on figure 5)

EP2 Condenser (Can be seen on figure 4)

QN1 Main Expansion Valve (Can be seen on figure 4)

These components are utilized in every heat pump. However, the NIBE-F2300/20 is equipped with a majority of other elements, such as mechanical parts and control systems, each of those aiming to improve the overall performance. A list of the parts that are being used during the operation of the heat pump in addition to other crucial components is presented below:

Pipe Connections

XL1 Connection, return hot water out of the heat pump (G1-1/4'', 35mm pipe diameter)

XL2 Connection, supply cold water into the heat pump (G1-1/4'', 35mm pipe diameter)

Temperature and Pressure Sensors

BP1 High pressure switch (29 bar)
Protects the compressor against pressures that are too high during defrosting

BP2 Low pressure pressostat
Protects the compressor against pressures that are too low

BP10 High pressure switch (32 bar)
Protects the compressor against pressures that are too high during normal operation

BT1 Temperature sensor of the two phase mixture that comes out of the main expansion valve.

BT3 Temperature sensor of the supply water that comes into the heat pump
Stops the compressor at high temperatures

BT12 Temperature sensor of the return water that comes out of the heat pump
Stops the compressor at high temperatures

BT14 Temperature sensor of the superheated vapor that comes out of the compressor.
Stops the compressor at high temperatures.

BT15 Temperature sensor of the subcooled liquid that comes out of the condenser

BT16 Temperature sensor of the two phase mixture after the distributor
Starts and stops defrosting operation according to the working fluid's temperature

BT17 Temperature sensor of the vapour that comes in the compressor

BT28 Ambient temperature sensor
Stops compressor at high and low environmental temperatures and switches fan speed

Cooling components

HS1 Drying filter

QN2 4-Way Valve

QN30 Solenoid Valve for fluid injection

QN31 Solenoid Valve for the subcooling system

QN34 Expansion Valve for the subcooling system
(The heat pump's subcooling system is explained in the next part of the report)

Electrical Components

EB10 Compressor heater
Prevents condensation of the R407c on the crankshaft when the heat pump is off

EB11 Drip tray heater

EB13 Collar heater
Prevents ice formation on the fan blades when the heat pump is off

GQ1 Fan

3.6 The NIBE-F2300/20 Function and Operating Diagram

Although it may seem complex, the heat pump's function is quite simple and efficient. A simplified overview of the function of the F2300/14 can be seen in the schematic diagram presented in

Figure 20, where the cycle points, the mass flow currents and the various measuring sensors have been depicted in order to give a better understanding of the heat pump operation. Different colours represent a certain state of the working fluid throughout the function of the heat pump. A graphic overview of cycle is given in Figure 21, where the cycle processes system and points are depicted on the P-h diagram.

The operation of the pump and its main processes are thoroughly explained next:

- **Point 2:** High-pressure superheated vapour at the compressor outlet (full flow $\dot{m}$) . The superheated vapour passes through the four-way valve QN2 and is led to the condenser.
- **Point 21:** Slightly subcooled liquid under high pressure at the condenser outlet (full flow $\dot{m}$). The abstracted heat is delivered to the hot water circuit. The subcooled liquid is then divided into three currents ($\dot{m}_A$, $\dot{m}_B$, $\dot{m}_C$). The first one is the main flow ($\dot{m}_A$). which is driven into the subcooler, a small heat exchanger that is located in front of the condenser (Figure 17). There the mixture is further cooled down to ensure that there will be no remaining vapour in case the condenser fails to fully condense the mixture, at a heavy load operation for example. The second flow $\dot{m}_B$ is used as the cooling medium for the subcooler and the third flow is mixed with $\dot{m}_B$ and is used to intercool the compression process in the compressor. These two processes are analyzed next.
- **Point 3:** Subcooled high pressure liquid (main flow $\dot{m}_A$) at the subcooler exit. It is subsequently led to the main expansion valve QN1.
- **Point 22:** Two phase intermediate pressure mixture at the secondary expansion valve QN34. After its split at the condenser outlet, the second flow $\dot{m}_B$ is throttled in the expansion valve QN34, where its pressure and temperature are decreased. It is then lead into the subcooler as the cooling medium to cool down the main flow $\dot{m}_A$. The third flow , $\dot{m}_C$, after its split at the condenser outlet passes through a capillary pipe where its pressure and temperature are also decreased. Its state matches point 22.
- **Point 22':** Slightly superheated vapour (flow $\dot{m}_B$) under intermediate pressure at the subcooler cooling medium outlet.

- **Point 23:** Slightly superheated vapor under intermediate pressure after the adiabatic mix of flow $\dot{m}_B$ at state 22' and flow $\dot{m}_C$ at state 22. This current is subsequently injected into the compressor to cool down the vapor at an intermediate point of the compression process, thus making it more efficient. This process is widely used in refrigeration applications and is referred as "vapor injection".
- **Point 4:** Two phase low pressure mixture at the outlet of the main expansion valve QN1 (main flow $\dot{m}_A$). The two-phase mixture is then led to the distributor of the evaporator.
- **Point 41:** Two phase low pressure mixture after the distributor. The distributor is indicated at Figure 18. The small pipes through which the two face mixture is led to the evaporator, cause an additional pressure drop that should be taken into account during calculations.
- **Point 1:** Slightly superheated mixture vapour under low pressure at the outlet of the evaporator (main flow $\dot{m}_A$). It passes through the four-way valve QN2 on its way to the compressor inlet.

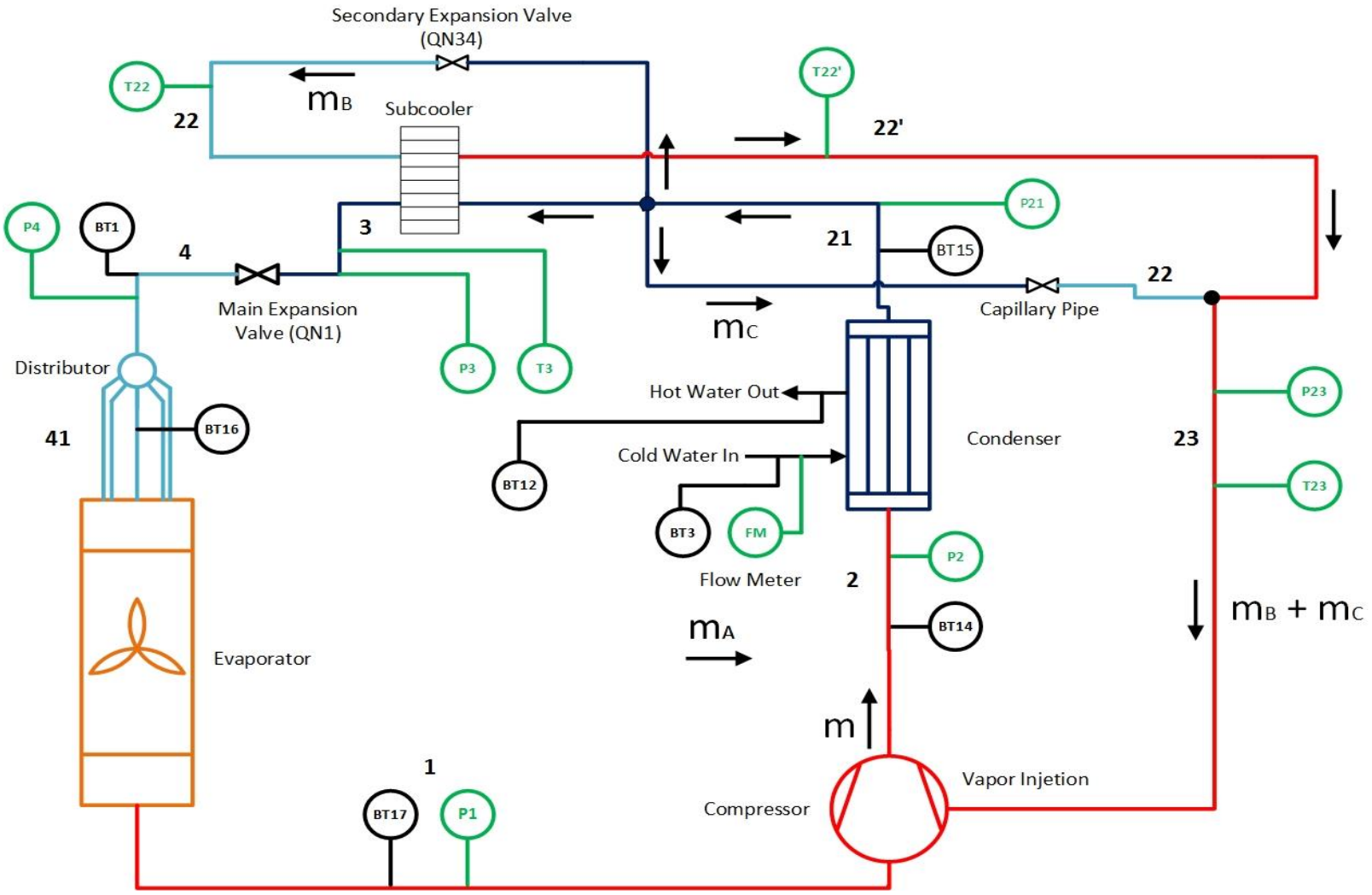

Figure 20-Simplified Drawing of the NIBE-F2300/20 operation. Red color refers to vapor state, blue to liquid state and light blue to a dual-phase state, with most of the mixture being liquid.

As far as the measuring sensors are concerned, they are marked as circles with lines connecting them to their respective position on the heat pump. As produced by the company, the F2300/14 already had temperature sensors at certain positions. These are marked with black color in

Figure 20. Temperature sensor BT1 was originally not used and was placed at the indicated point. Apart from those, some additional sensors have been placed on the heat pump in order to monitor its performance during the experiment. These sensors are marked with green color in

Figure 20. A complete list of the measuring sensors at each cycle point are summarized next:

Table 6. List of measuring sensors

Sensor Number	Measured Property	Cycle Point
P1 (Additional)	Pressure	1
BT17	Temperature	
P2 (Additional)	Pressure	2
BT14	Temperature	
P21 (Additional)	Pressure	21
BT15	Temperature	
T22 (Additional)	Temperature	22
T22' (Additional)	Temperature	22'
P23 (Additional)	Pressure	23
T23 (Additional)	Temperature	
P3 (Additional)	Pressure	3
T3 (Additional)	Temperature	
P4 (Additional)	Pressure	4
BT16	Temperature	
BT3	Temperature	Supply water in
BT1	Temperature	41
BT12	Temperature	Hot water out
FM	Supply Water Flow meter	Supply water closed circuit

3.7 The NIBE-F2300/20 Theoretical P-h Diagram

A P-h diagram representing a heat pump at real working conditions has significant differences with the one that was described in section 3.4.3. In contrast to the standard heat pump cycle, the saturated vapor that exits the evaporator gets slightly superheated, to ensure that no liquid enters the compressor, which can reduce its efficiency and damage its components

(corrosion nature, mixing with the compressor oil, etc.). Apart from that, the specific heat pump applies a subcooling system which greatly alternates the standard cycle. Considering zero pressure losses through the pipelines and the components, the ideal operation of the F2300/14 would be described by the P-h diagram presented in Figure 21.

The purple line represents the subcooling system. A part of the high pressure- subcooled liquid (cycle point 21 - flow $\dot{\mathbf{m}}_{\mathbf{B}}$) is extracted from the total mass flow and expands in the secondary expansion valve QN34 and gets at a two-phase state at a lower pressure and temperature (cycle point 22). Due to the temperature difference between points 21 and 22 heat is transferred from the warmer (flow $\dot{\mathbf{m}}_{\mathbf{A}}$) to the colder current (flow $\dot{\mathbf{m}}_{\mathbf{B}}$). This is how the main stream (flow $\dot{\mathbf{m}}_{\mathbf{A}}$) – the one that will enter the main expansion valve QN1 – is further cooled and lead away from the saturated liquid curve (cycle point 3). The secondary current has absorbed heat and is now in a vapor state (cycle point 22'). A small amount of the total mass flow current is also extracted (flow $\dot{\mathbf{m}}_{\mathbf{C}}$) expands through a capillary pipe and is considered to have the same properties with cycle point 22. This small amount of mass flow is adiabatically mixed with the warm mass flow current that exits the subcooler forming a lower temperature (cycle point 23) vapor that is used for compressor intercooling. Therefore, the compression can be represented as a two stage process. Firstly, the vapor is compressed from point 1 to point 11, which is considered to have the same intermediate pressure with cycle points 22,22' and 23. As the colder vapor enters the compressor, it cools down the superheated vapor, shifting its point to the left at lower temperatures and enthalpies (cycle point 12). The second stage of the compression is the process from point 12 to 2 and the rest of the cycle continues normally.

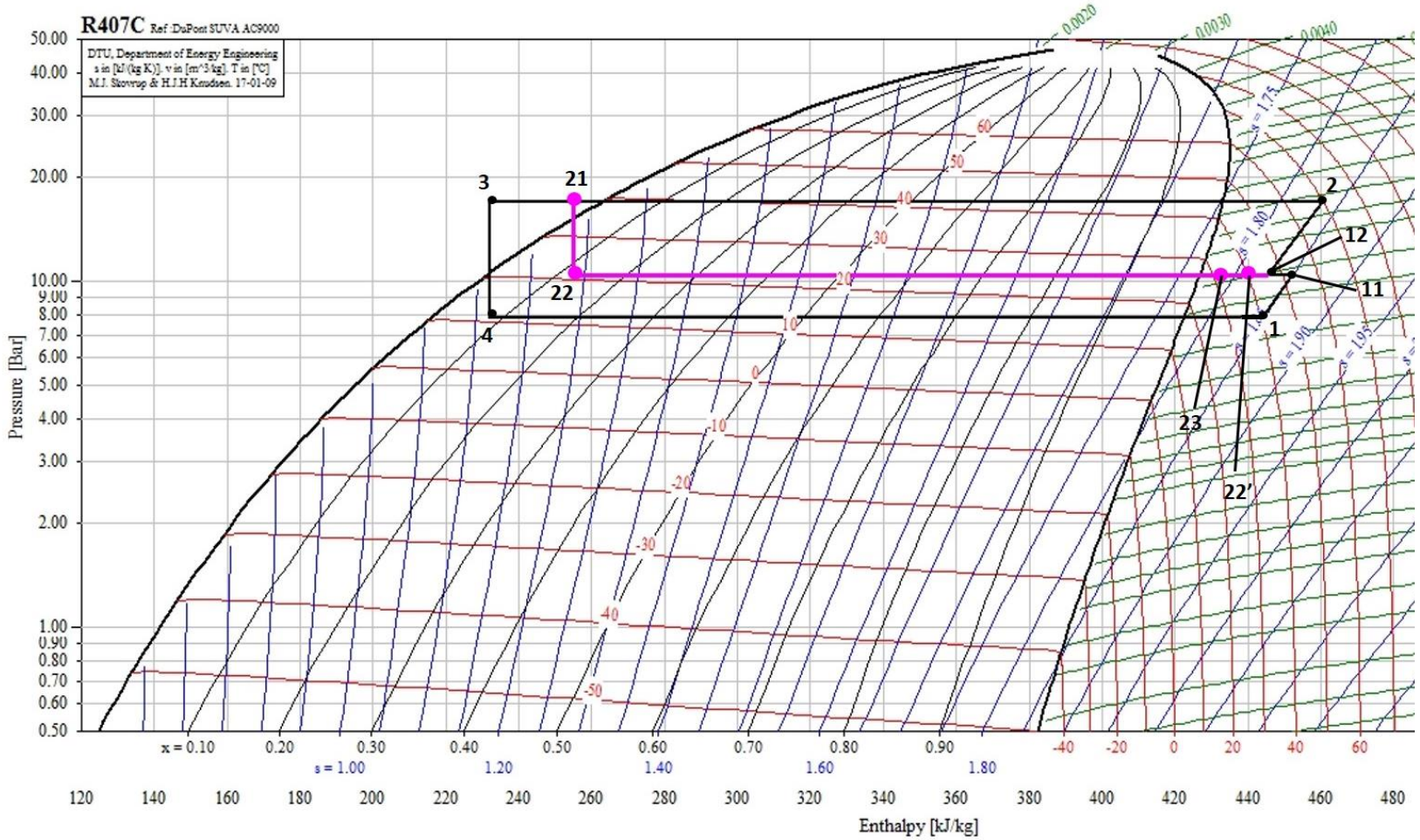

Figure 21 – Expected P-h diagram of the F2300/14 during ideal operation. Pressure losses throughout the cycle are neglected.

4 Experimental Data from a Real F2300/14 Operating Cycle

The real cycle, however, is slightly different compared to the one presented in Figure 21. The alternations that take place are caused by various reasons. The most significant one is the pressure losses throughout the whole system. As the mixture is led through the pipelines to the different heat pump components its pressure drops due to friction losses. Furthermore, there is a pressure drop in the heat exchangers (subcooler, evaporator, condenser) as the mixture flows through their tubes. As described before, there is no work exchange as the liquid expands in a throttling valve. The effective insulation surrounding the valves and the pipes makes the expansion a practically adiabatic process. Therefore, the enthalpy of the mixture remains the same before and after an expansion valve. This assumption is quite accurate, and allows calculating the thermodynamic properties of certain cycle points.

The heat pump is tested at different cold water inlet temperatures. A separate closed circuit which consists of a heat exchanger and a water pump circulates the water in and out of the heat pump absorbing the produced heat. This heat is delivered to another water circuit (secondary water mass flow) through another heat exchanger and the thermal power is used for space heating. The secondary mass flow can be adjusted by a manual valve and this way the cold water supply to the heat pump (cold input water) can be consequently adjusted. The aim of this experiment is to determine how effectively can the heat pump adjust to a heavier load and whether its performance meets the standards that the manufacturer declares.

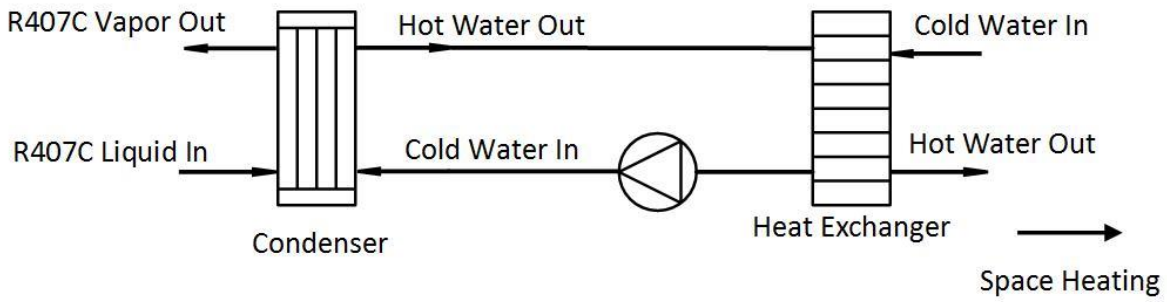

Figure 22-Operation of the heat pump under varying hot water inlet temperature.

As the inlet water temperature increases, the heat pump operates at different cycle points. Once a desired operating point is selected, a stable state of the heat pump around that point must be reached. This process is presented in Figure 23. Note that the temperature difference is practically constant at 10 degrees regardless of the operating point. After that, an average of the

mixture's thermodynamic properties at each cycle point is calculated, exploiting the available data that the sensors provide. Using REFPROP, a software developed by NIST to calculate the thermodynamic properties of a wide variety of commonly used refrigerants, each cycle point can be fully defined.

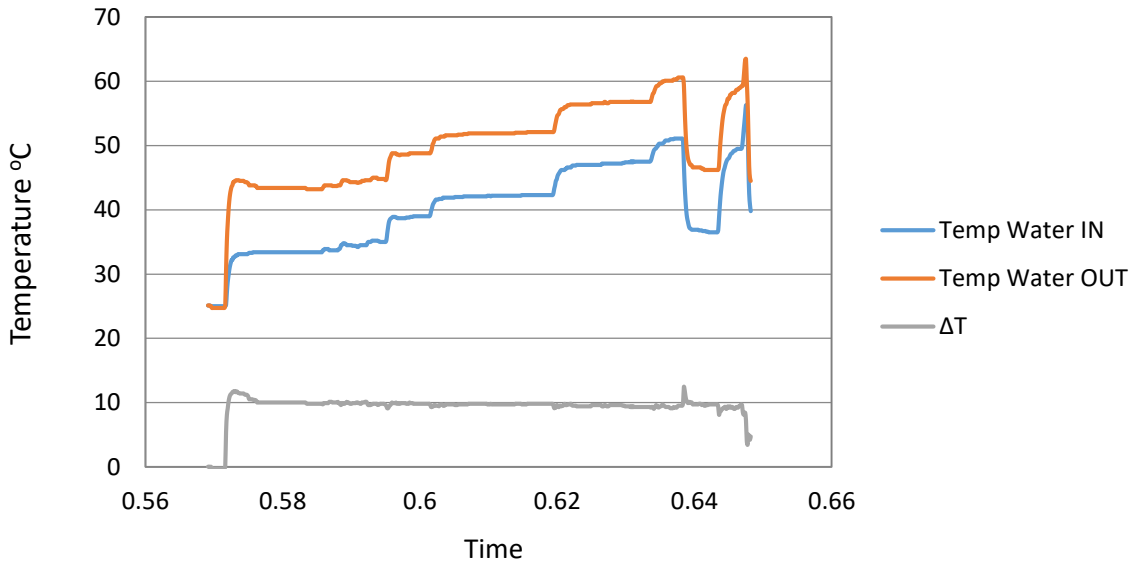

Figure 23 – Operation of the heat pump under varying hot water inlet temperature.

A specific operation point is taken as a showcase example. The calculation process is thoroughly described next:

Cycle Point 1 - Evaporator Out / Compressor In				
Pressure [bar]	**Temperature [°C]**	**Enthalpy (kJ/kg)**	**Entropy (kJ/kgK)**	**Quality**
5.42	**14.88**	**421.53**	**1.805**	**Superheated vapor**

Cells with a grey filling stand for data provided by the sensors located at each cycle point, whereas cells with a green filling are calculated by REFPROP.

Cycle Point 2 - Compressor Out / Condenser In				
Pressure [bar]	**Temperature [°C]**	**Enthalpy (kJ/kg)**	**Entropy (kJ/kgK)**	**Quality**
20.37	**81.7**	**465.33**	**1.833**	**Superheated vapor**

Cycle Point 21 - Condenser Out				
Pressure [bar]	**Temperature [°C]**	**Enthalpy (kJ/kg)**	**Entropy (kJ/kgK)**	**Quality**
20.17	**45.41**	**269.346**	**1.230**	**Subcooled liquid**

The pressure of cycle points 22 and 23 are considered the same. The pressure and temperature are measured at cycle point 23 so they are defined as follows:

Cycle Point 23 - Cooling Current ($\dot{m}_B + \dot{m}_C$) Into the Compressor				
Pressure [bar]	Temperature [°C]	Enthalpy (kJ/kg)	Entropy (kJ/kgK)	Quality
10.17	34.47	430.596	1.783	Superheated vapor

The enthalpy at cycle point 22 is the same as the one at 21, as flow through throttling valves or capillary pipes causes no alteration of this property as it has already been mentioned. For cycle point 22' we consider an additional pressure drop of 200 mbar as the current $\dot{m}_B$ flows through the subcooler. Cycle points 22 and 22' are defined as:

Cycle Point 22 - Secondary Expansion Valve (QN34) and Fluid Injection Valve (QN30) Out				
Pressure [bar]	Temperature [°C]	Enthalpy (kJ/kg)	Entropy (kJ/kgK)	Quality
10.17	20.42	269.346	1.239	0.206

Cycle Point 22' - Subcooler Out, Current $\dot{m}_B$/ Adiabatic Mix with Current $\dot{m}_C$				
Pressure [bar]	Temperature [°C]	Enthalpy (kJ/kg)	Entropy (kJ/kgK)	Quality
9.97	34.3	430.846	1.786	Superheated vapor

Cycle Point 3 - Main Expansion Valve (QN1) In				
Pressure [bar]	Temperature [°C]	Enthalpy (kJ/kg)	Entropy (kJ/kgK)	Quality
19.86	23.79	234.788	1.118	Subcooled liquid

Similarly to points 22 and 21, cycle points 3 and 4 have the same enthalpy, since the only component separating them is the main expansion valve. With pressure and enthalpy as known variables, cycle point 4 is defined as:

Cycle Point 4 – Main Expansion Valve (QN1) Out				
Pressure [bar]	Temperature [°C]	Enthalpy (kJ/kg)	Entropy (kJ/kgK)	Quality
7.34	8.77	234.788	1.124	0.107

Cycle point 41 has the same enthalpy with point 4. Given that the temperature is already known, the additional pressure as well as the rest of the thermodynamic properties can be calculated as follows:

Cycle Point 41 – Distributor Out / Evaporator In				
Pressure [bar]	Temperature [°C]	Enthalpy (kJ/kg)	Entropy (kJ/kgK)	Quality
6.11	3.1	234.788	1.126	0.143

The thermal power delivered by the heat pump can be calculated using the available data for the supply and return water. For the specific operation point, the temperature of the supply and return water, along with other data are presented below:

m_w [lt/min]	Cold Water In [°C]	Cp [kJ/kgK]	ρ_w [kg/m3]	Hot Water Out [°C]	T_{amb} [°C]
35	40.1	4.187	995.65	49.5	17.29

The heat pump's delivered power is calculated as:

$$\boldsymbol{Q_{delivered} = \frac{\dot{m}_w 10^{-3}}{60} \rho C_p (T_{wout} - T_{win})} \quad (4.1)$$

which gives $\mathbf{Q_{delivered} = 22.86\ kW}$

The mass flow of the working fluid that passes through the compressor can be found as:

$$\boldsymbol{\dot{m} = \frac{Q_{delivered}}{h_{21} - h_2}} \quad (4.2)$$

which gives: $\mathbf{\dot{m} = 0.1166\ kg/s}$

The adiabatic mix of the $\mathbf{\dot{m}_B}$ and $\mathbf{\dot{m}_C}$ flows is described by the following equation:

$$\boldsymbol{(\dot{m}_B + \dot{m}_C) h_{23} = \dot{m}_B h_{22'} + \dot{m}_C h_{22}} \quad (4.3)$$

Inside the subcooler, the energy balance is described by the following equation:

$$\boldsymbol{\dot{m}_B (h_{22'} - h_{22}) = (\dot{m} - \dot{m}_B - \dot{m}_C)(h_{21} - h_3)} \quad (4.4)$$

where $\mathbf{\dot{m}}$ has already been calculated above. Solving this linear system (3.3 and 3.4), it is calculated that:

$$\boldsymbol{\dot{m}_B = 0.0204\ kg/s}$$

$$\boldsymbol{\dot{m}_C = 3.16 \cdot 10^{-5} kg/s}$$

It is also taken into consideration that cycle points 11 and 12 have the same pressure as 23. Cycle point 11 can be estimated by considering an isentropic efficiency value during the first stage of the compression. This value will be slightly higher than the isentropic efficiency of the whole compressor, which can be found using the following data:

Cycle Point 2' – Isentropic Compression		
Pressure [bar]	Entropy [kJ/kgK]	Enthalpy [kJ/kg]
20.37	1.805	455.6099687

In the theoretical cycle as described before (because we assume isentropic compression) the points 2 and 2is are exactly the same. The isentropic efficiency states the quality design of the compressor.

The pressure of point 2 is is the same with point 2 and its entropy the same with 1. So, its enthalpy can be found by REFPROP. It is possible to calculate the compressor's efficiency simply by using equation (3.1). The result is:

$$\boldsymbol{\eta_{is} = 77.8\%}$$

Based on that value, an approximation can be made as far as the first stage of the compression is concerned. It is considered that:

$$\boldsymbol{\eta_{is1-11} = 78.15\%}$$

Also REFPROP calculates the enthalpy of 11is:

Cycle Point 11' – Isentropic Compression Before Cooling Current		
Pressure [bar]	**Entropy [kJ/kgK]**	**Enthalpy [kJ/kg]**
10.17	**1.805**	**437.483**

The enthalpy of point 11 is then found by the equation:

$$\boldsymbol{h_{11} = h_1 + \frac{h_{11is} - h_1}{\eta_{is1-11}}} \quad \boldsymbol{(4.5)}$$

which gives:

$$\boldsymbol{h_{11} = 441.944\ kJ/kg}$$

Finally, the adiabatic mix of the cooling vapour that is injected into the stage of the compressor at the exact moment that the mixture that is compressed is at state 11 gives the enthalpy of point 12. The respective equation is as follows:

$$\boldsymbol{(\dot{m}_B + \dot{m}_C)h_{23} + (\dot{m} - \dot{m}_B - \dot{m}_C)h_{11} = \dot{m} \cdot h_{12}} \quad \boldsymbol{(4.6)}$$

which gives $\mathbf{h_{12} = 439.96\ kJ/kg}$

The work provided by the compressor can be found as:

$$\boldsymbol{W_{comp} = \dot{m}(h_2 - h_1)} \quad \boldsymbol{(4.7)}$$

Assuming an electromechanical efficiency of 0.85 the electrical consumption of the heat pump would be

$$\boldsymbol{W_{supplied} = \frac{W_{comp}}{\eta_{elmech}} = \frac{W_{comp}}{0.85}}$$

which gives $\mathbf{W_{supplied} = 5.11kW}$ and **COP=3.8**

This COP value is an estimation value. An energy meter has been installed to measure the exact electric power consumption of the heat pump.

The whole cycle can now be represented on the P-h diagram which is presented in Figure 24. The intercooling of the compression process with vapour injection is presented in Figure 25, which is an enlargement of the P-h diagram of Figure 24.

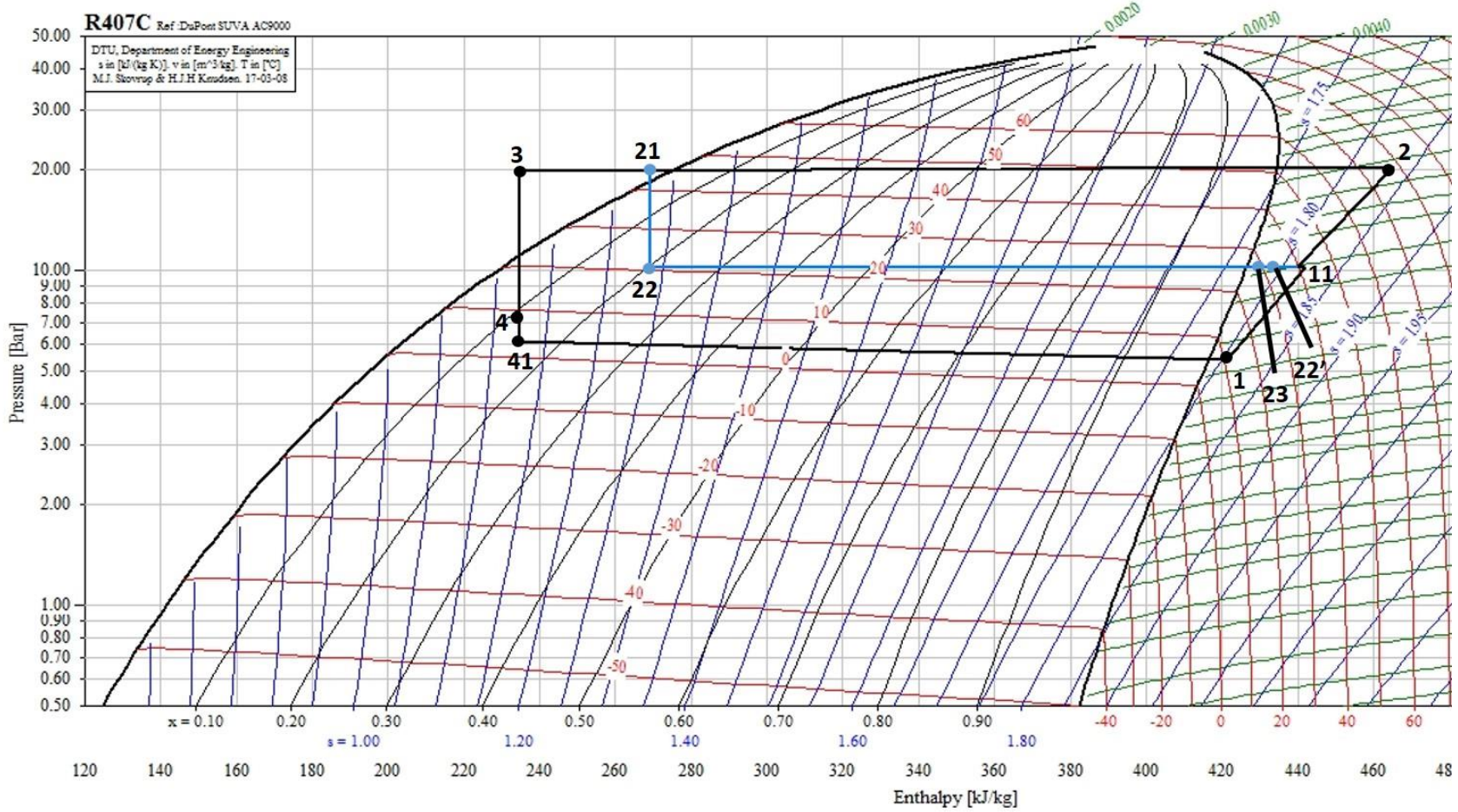

Figure 24 – Real P-h diagram of the specific operation. Blue stands for the subcooling process. In contrast with the theoretical cycle, a major pressure drop (0.7 bar) takes place in the evaporator.

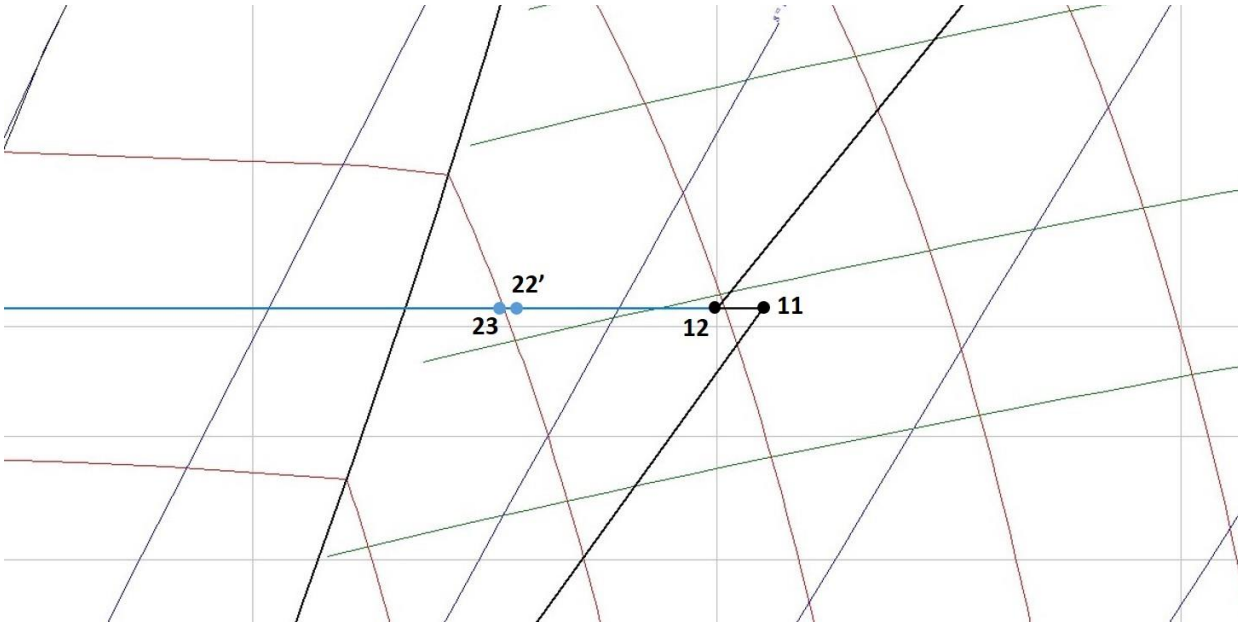

Figure 25 – Focus on the vapour injection cooling of the compressor. The vapor is only cooled by 1 °C, though this is enough to increase compressor efficiency.

The heat pump was tested under various operating conditions and the obtained results are summarized in the following table:

Table 7. Experimental results for normal operation of the heat pump under various conditions

1					
Evaporator Out / Compressor In					
Pressure [MPa]	Pressure [bar]	Temperature [°C]	Enthalpy (kJ/kg)	Entropy (kJ/kgK)	Quality
0.53	5.30	14.91	421.85	1.81	Superheated vapor
0.54	5.36	15.10	421.90	1.81	Superheated vapor
0.54	5.38	14.74	421.50	1.81	Superheated vapor
0.54	5.42	14.87	421.53	1.81	Superheated vapor
0.55	5.45	15.10	421.67	1.81	Superheated vapor
0.55	5.48	15.10	421.60	1.80	Superheated vapor

2					
Compressor Out / Condenser In					
Pressure [MPa]	Pressure [bar]	Temperature [°C]	Enthalpy (kJ/kg)	Entropy (kJ/kgK)	Quality
1.53	15.28	66.30	455.67	1.83	Superheated vapor
1.73	17.29	72.70	459.65	1.83	Superheated vapor
1.85	18.47	76.50	462.16	1.83	Superheated vapor
2.04	20.37	81.70	465.33	1.83	Superheated vapor
2.20	21.97	86.56	468.69	1.84	Superheated vapor
2.35	23.46	90.10	470.80	1.84	Superheated vapor

21					
Condenser Out					
Pressure [MPa]	Pressure [bar]	Temperature [°C]	Enthalpy (kJ/kg)	Entropy (kJ/kgK)	Quality
1.51	15.06	33.11	249.34	1.17	Subcooled liquid
1.71	17.06	38.40	257.79	1.19	Subcooled liquid
1.83	18.25	41.20	262.35	1.21	Subcooled liquid
2.02	20.17	45.41	269.35	1.23	Subcooled liquid
2.18	21.79	49.21	275.83	1.25	Subcooled liquid
2.33	23.28	51.40	279.57	1.26	Subcooled liquid

22					
Cycle Point 22 - Secondary Expansion Valve (QN34) and Fluid Injection Valve (QN30) Out					
Pressure [MPa]	Pressure [bar]	Temperature [°C]	Enthalpy (kJ/kg)	Entropy (kJ/kgK)	Quality
0.86	8.58	14.17	249.34	1.17	0.14
0.93	9.29	17.06	257.79	1.20	0.17
0.97	9.70	18.62	262.35	1.22	0.18
1.02	10.17	20.42	269.35	1.24	0.21
1.03	10.30	21.04	275.83	1.26	0.24
1.08	10.84	22.92	279.57	1.27	0.24

22'					
Subcooler Out, Current $\dot{m}_B$/ Adiabatic Mix with Current $\dot{m}_C$					
Pressure [MPa]	Pressure [bar]	Temperature [°C]	Enthalpy (kJ/kg)	Entropy (kJ/kgK)	Quality
0.86	8.38	25.76	424.98	1.7784	Superheated vapor
0.91	9.09	30.39	428.64	1.7858	Superheated vapor
0.95	9.50	32.13	429.57	1.7853	Superheated vapor
1.00	9.97	34.30	430.85	1.7855	Superheated vapor
1.03	10.30	35.35	431.25	1.7842	Superheated vapor
1.08	10.84	37.63	432.54	1.7843	Superheated vapor

23					
Cooling Current ($\dot{m}_B + \dot{m}_C$) Into the Compressor					
Pressure [MPa]	Pressure [bar]	Temperature [°C]	Enthalpy (kJ/kg)	Entropy (kJ/kgK)	Quality
0.86	8.58	26.08	425.31	1.7795	Superheated vapor
0.93	9.29	30.54	428.36	1.7831	Superheated vapor
0.97	9.70	32.23	429.24	1.7825	Superheated vapor
1.02	10.17	34.47	430.60	1.7831	Superheated vapor
1.05	10.50	35.33	430.81	1.7812	Superheated vapor
1.10	11.04	37.78	432.28	1.7820	Superheated vapor

3					
Main Expansion Valve (QN1) In					
Pressure [MPa]	Pressure [bar]	Temperature [°C]	Enthalpy (kJ/kg)	Entropy (kJ/kgK)	Quality
1.48	14.76	19.75	228.76	1.0990	Subcooled liquid
1.68	16.75	20.66	230.09	1.1029	Subcooled liquid
1.79	17.95	21.99	232.08	1.1093	Subcooled liquid
1.99	19.86	23.79	234.79	1.1179	Subcooled liquid
2.15	21.49	24.90	236.45	1.1230	Subcooled liquid
2.30	22.97	26.86	239.40	1.1324	Subcooled liquid

4					
Main Expansion Valve (QN1) Out / Distributor In					
Pressure [MPa]	Pressure [bar]	Temperature [°C]	Enthalpy (kJ/kg)	Entropy (kJ/kgK)	Quality
0.70	7.03	7.23	228.76	1.1027	0.088
0.71	7.12	7.69	230.09	1.1073	0.092
0.72	7.21	8.14	232.08	1.1143	0.098
0.73	7.34	8.77	234.79	1.1237	0.107
0.74	7.43	9.19	236.45	1.1294	0.113
0.75	7.54	9.76	239.40	1.1397	0.124

41					
Distributor Out (Additional Pressure Drop)					
Pressure [MPa]	Pressure [bar]	Temperature [°C]	Enthalpy (kJ/kg)	Entropy (kJ/kgK)	Quality
0.596	5.955	2.17	228.76	1.1040	0.119
0.605	6.052	2.70	230.09	1.1098	0.124
0.608	6.082	2.90	232.08	1.1164	0.131
0.611	6.108	3.10	234.79	1.1257	0.143
0.621	6.209	3.64	236.45	1.1324	0.148
0.623	6.229	3.81	239.40	1.1419	0.160

Supply Water	Return Water	Water Temperature Difference (Input-Output)
Twin [°C]	Twout [°C]	Twout-Twin [°C]
28.3	37.6	9.3
33.3	42.6	9.3
36.1	45.5	9.4
40.1	49.5	9.4
42.9	52.25	9.35
46.4	55.9	9.5

Delivered Power (kW)	Supplied Power (kW)	COP
22.6157	4.575	4.94
22.6157	5.005	4.52
22.8588	5.34	4.28
22.8588	5.47	4.18
22.7372	5.7	3.99
23.1020	5.97	3.87

Three P-h diagrams of the heat pump at low, medium and high condensation temperature operation are presented below. It is clear that the work consumed by the compressor (h_2 - h_1) increases as the pump operates at higher condensation temperatures. At the same time, the heating power delivered by the pump (h_2 – h_3) decreases, resulting in lower COP values. To conclude with, the cooling of the compressor becomes necessary and therefore is more obvious at high condensation temperatures, contributing to a higher isentropic efficiency.

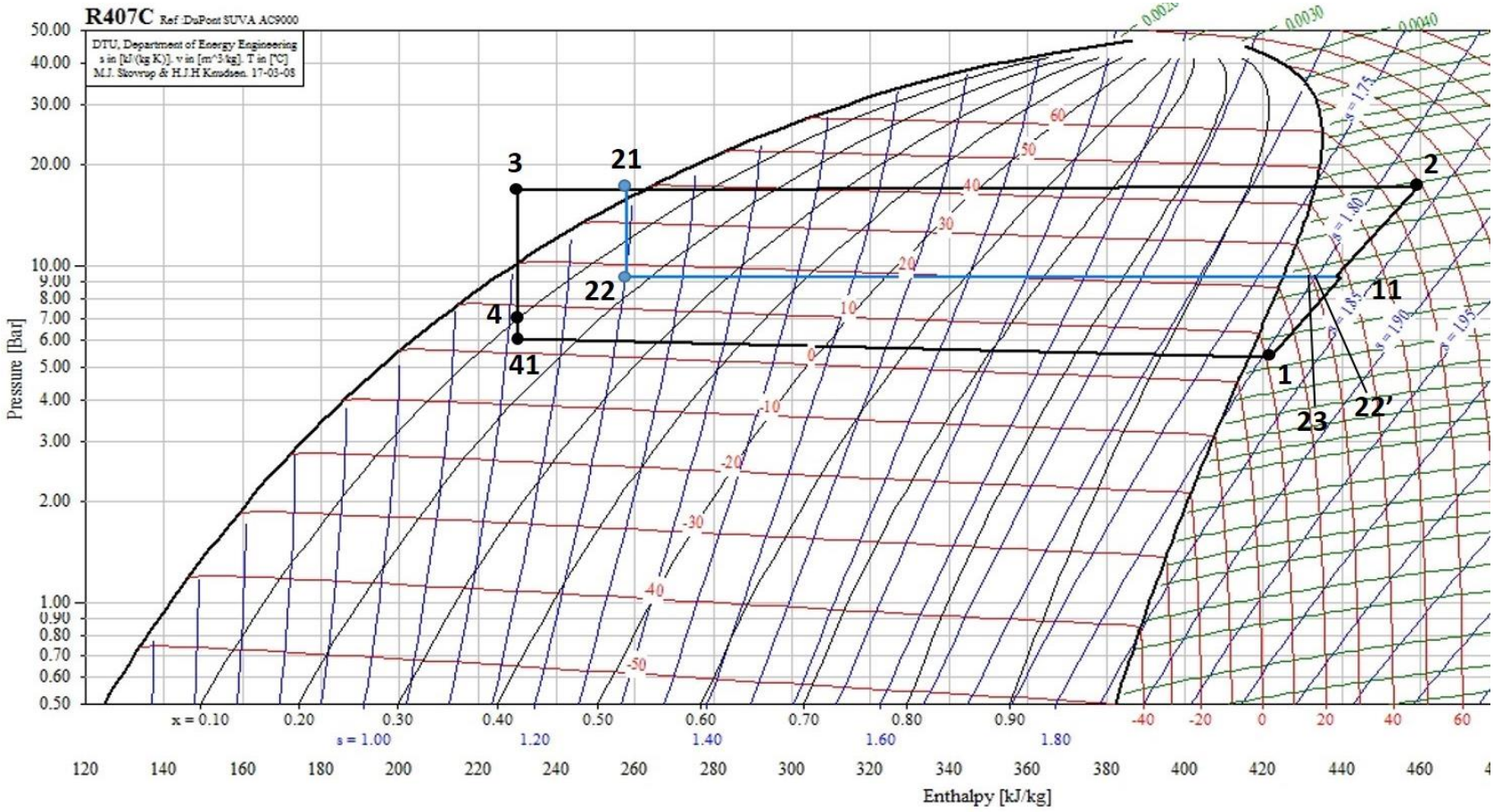

Figure 26 – Standard heat pump operation at low condensation temperature (Hot water output 42.6 °C). Minor amount of work required by the compressor ($h_2 – h_1$) and high heating power delivered by the pump ($h_2 – h_3$) result in a high COP value. The cooling of the compressor is not significant yet and has small effect on the cycle.

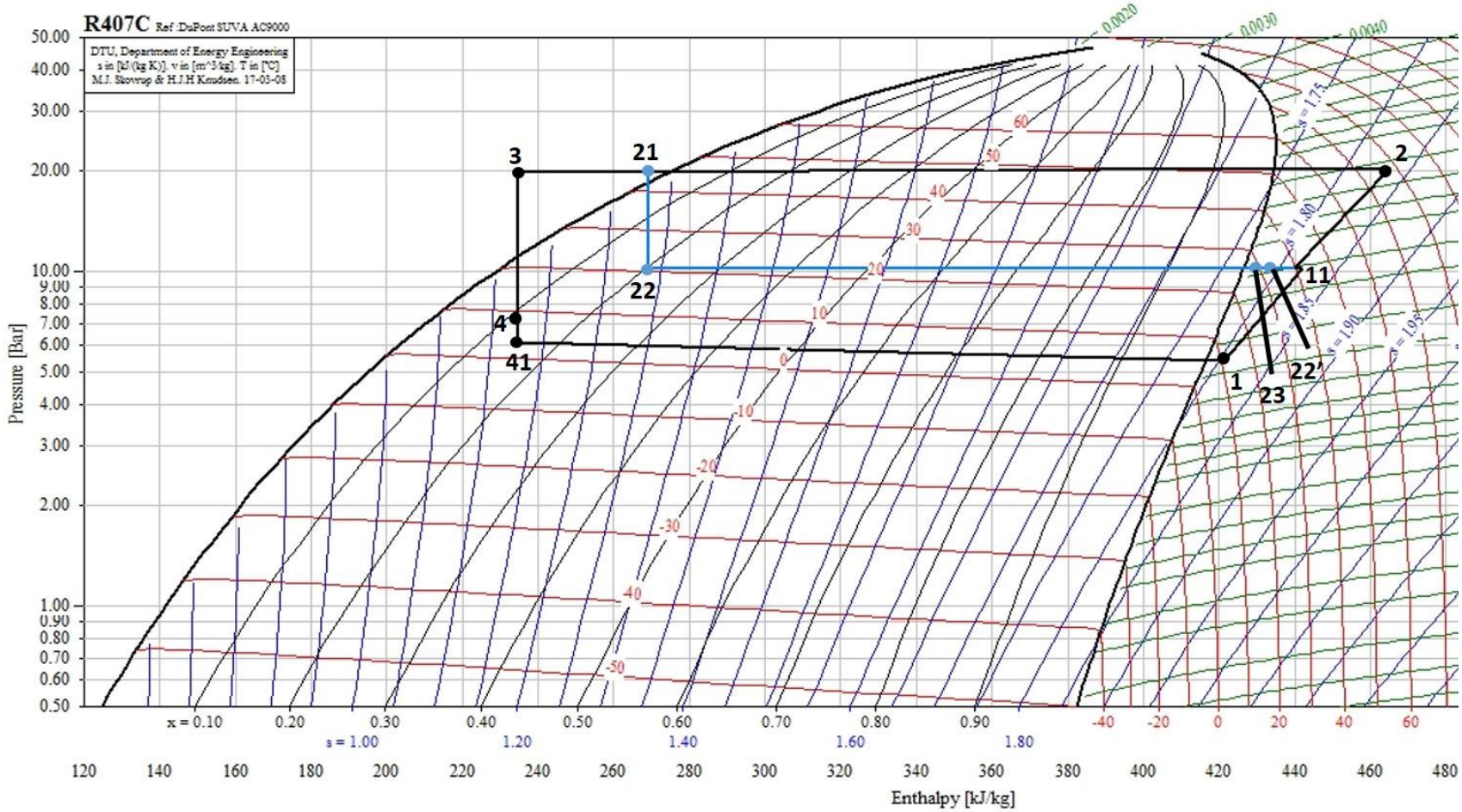

Figure 27 – Standard heat pump operation at medium condensation temperature (Hot water output 49.5 °C). More mechanical work is required by the compressor ($h_2 – h_1$) and the heating power delivered by the pump ($h_2 – h_3$) begins to decrease. The cooling of the compressor becomes necessary and is now more obvious (small but noticeable break on the 1 ➔2 curve).

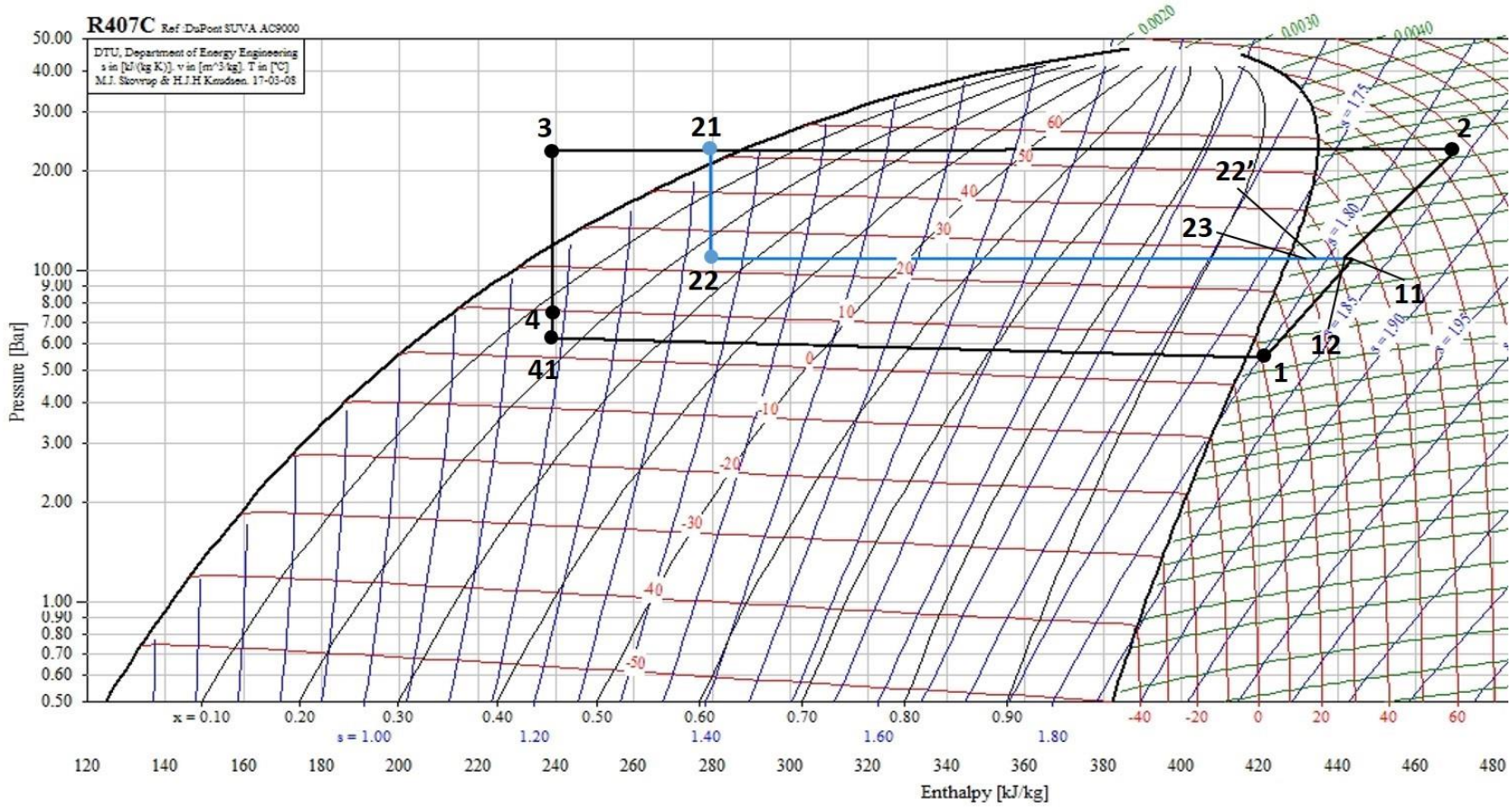

Figure 28 – Standard heat pump operation at high condensation temperature (Hot water output 55.9 °C). The mechanical work required by the compressor ($h_2 – h_1$) further increases as the heating power delivered by the pump ($h_2 – h_3$) decreases and the whole cycle is lead to the supercritical region. As a result, the COP factor gets its lowest value. The cooling of the compressor is now obvious (break on the 1➔2 curve) and contributes to a reduced mechanical work provided to the compressor.

5 The installed heat pump retrofitted with the piston expander prototype

5.1 Experimental test rig overview

The installed heat pump was subsequently retrofitted with the expander prototype coupled to an asynchronous generator. The generator is driven by a regenerative frequency drive (inverter) in order to control its rotational speed. Regarding the measuring sensors, they are marked as circles with lines connecting them to their respective position on the test rig. As delivered by the company, the F2300/20 heat pump unit already had temperature sensors placed at different points. These are marked with black colour in Figure 29 and Figure *31*. Temperature sensor BT1 was originally used to measure the internal room temperature in domestic applications and was placed at the indicated point in order to measure the temperature before the evaporator distributor (point 41). Apart from those, some additional sensors marked with green colour in Figure 29 and Figure 31 have been placed on the test rig in order to monitor its performance during the tests:

- a torque-meter to measure the produced mechanical power of the expander
- two energy-meters to measure the consumed electric power of the heat pump unit and the produced electric power of the generator
- a flow meter of the closed hot water circuit was also installed in order to measure the delivered thermal power of the unit
- an indicator of the superheating degree at the evaporator outlet was installed in order to control the evaporator superheating and prevent the suction of liquid refrigerant by the compressor and the substantial damage that could be caused to it. The indicator works with a temperature and pressure sensor and is programmable. Setting the basic parameters, such as the refrigerant used, the superheating degree is calculated and shown on a small attached screen.

The piping system that leads the refrigerant high pressure mixture to the expander inlet/outlet as well as the respective electromagnetic valves for the remote control of the system can be seen in Figure 29. When the electromagnetic **valve A (by-pass valve)** is open and valves B and C are closed the heat pump works normally. Subsequently, in order to switch to expander mode of operation, the by-pass valve is closed and the expander **liquid inlet valve (B)** and the **expander outlet valve (C)** are simultaneously opened. A **needle valve** has been placed in the expander outlet in order to control the mass flow rate of the heat pump without changing the

expander rotational speed. It is very important to control the mass flow rate as it is directly connected with the superheating degree at the evaporator outlet in order to avoid the presence of liquid at the compressor suction.

As far as the lubrication system is concerned, an oil tank has been installed as it can be seen in Figure 29 and Figure 31. The tank is pressurized by the compressor discharge line with a check valve to ensure that no oil is sucked by the compressor in case of under-pressure in the discharge line. Subsequently, the pressurized oil tank is connected with the expander lubrication ports with a regulating oil valve. When the valve opens, the oil flows in the expander. It is remarked that the oil tank pressure is always higher than the pressure at the expander's distribution plates, shaft and pistons. The lubrication procedure involves a flash opening of this valve to allow the injection of a small amount of oil.

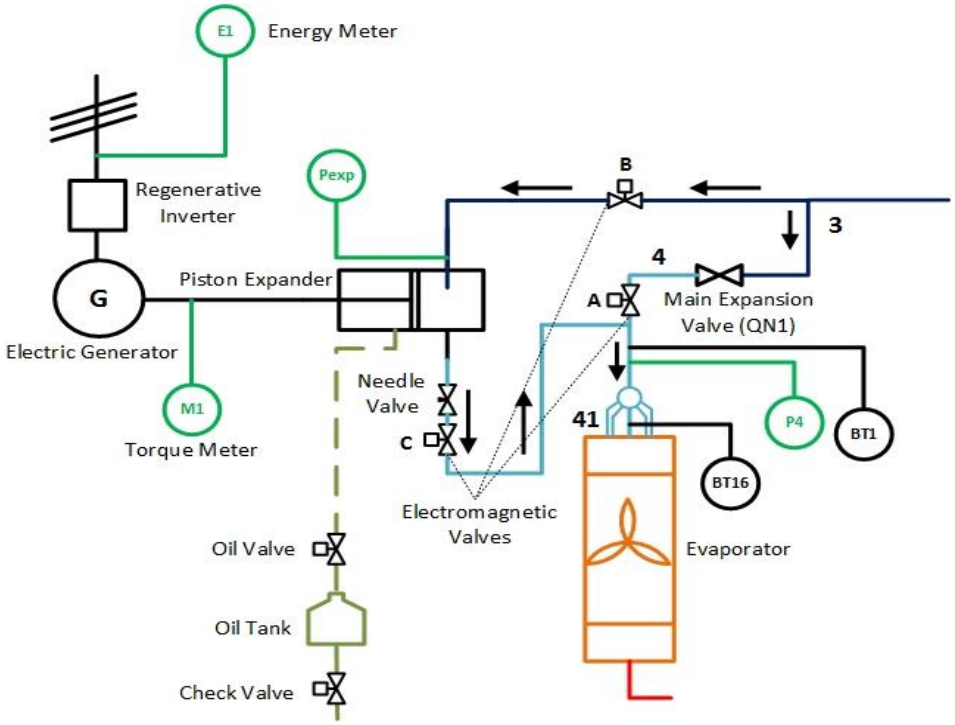

Figure 29 – Detail of the expander inlet/outlet piping system and electromagnetic control valves.

A complete list of the measuring sensors at each cycle point and other measuring and control equipment are depicted in Figure 31 and the table that is provided next:

Table 8. List of measuring sensors and other measuring and control equipment

Sensor Number	Measured Property	Cycle Point
P1	Pressure	1
BT17	Temperature	
P2	Pressure	2
BT14	Temperature	
P21	Pressure	21
BT15	Temperature	
T22	Temperature	22
T22'	Temperature	22'
P23	Pressure	23
T23	Temperature	
P3	Pressure	3
T3	Temperature	
P4	Pressure	4
BT16	Temperature	
BT3	Temperature	Supply water in
BT1	Temperature	41
BT12	Temperature	Hot water out
FM	Supply Water Flow meter	Supply water closed circuit
Pexp	Pressure	Expander inlet
E1	Energy-meter	Generator
E2	Energy-meter	Heat-Pump Consumption
M1	Torque-meter	Expander shaft
Regenerative Inverter	Frequency Drive Control of Generator/Expander speed	Generator-grid electric connection
Electromagnetic Valve A	by-pass valve	
Electromagnetic Valve B	expander liquid inlet valve	
Electromagnetic Valve C	expander outlet valve	

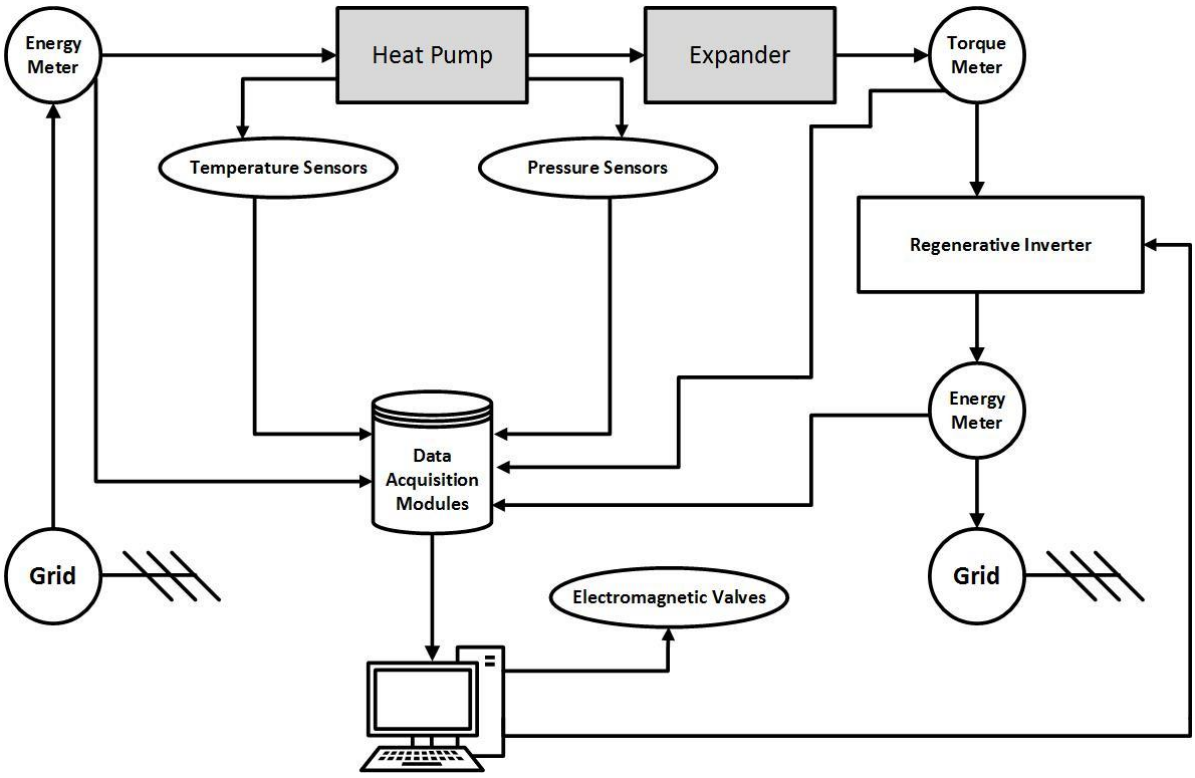

Figure 30 – Schematic overview of the data acquisition and control system.

The control system and data acquisition system was materialised with ADAM ADVANTECH input/output modules. The computer interface was done in DASYLAB software. The operation of the heat pump is controlled by its original control unit which has not been modified.

The main input variables are the values obtained by the measuring equipment:

- Temperature and pressure sensors
- Energy meters
- Torque meter
- Water flow meter

The main control (output) variables are:

- Electromagnetic valves
- Expander rotational speed (inverter output frequency)

Additional manually controlled variables are:

- Needle valve at the expander output (refrigerant mass flow regulation)
- Oil valve (ON/OFF)
- Hot water circuit adjustment valve (hot water mass flow regulation)

The interchange of information with the computer and the user are schematically depicted in Figure 30.

5.2 System Operation

Even though certain operational problems were expected especially during the expander start up, no particular issues were encountered during the operation of the unit. The start-up process was very smooth and did not indicate any malfunctions that should be resolved. The operation of the unit followed the procedure described in the following steps:

1. Start of the heat pump at normal mode with all the valves that lead to the expander closed. The unit is kept running until it gradually reaches its full output thermal load. The maximum flow in the hot water circuit is ensured so that the condensation temperature and thus pressure are as low as possible in order to achieve a smooth expander start-up. Once at full load operation, the heat pump is let running for several minutes in order to stabilize its operation.
2. After the heat pump's operation at full load is stabilized, the expander's outlet valve is opened (see valve C in Figure 31), while the inlet valve still remains closed. This allows the system to recover any remaining liquid refrigerant in the expander back to the heat pump's circuit. In that way, a smooth start-up of the expander is ensured, once it is connected to the rest of the system.
3. The expander's desired smooth start-up requires low rotating speeds. For that reason, the electric motor/generator coupled to the expander's shaft is set at a low rotational speed through the inverter drive.
4. After the expander's start-up, the inlet valve B (Figure 29 and Figure 31) is opened. As a result, a limited amount of refrigerant flows through the expander, while the majority of the flow continues to flow through the main expansion valve. It is intentional that the expander is not instantly driven into full load operation, as a rapid liquid refrigerant mass flow could cause a hydraulic pressure shock wave. Moreover, the needle valve (Figure 31) is kept half-opened to ensure a quite low mass flow rate at the first moments of the expander operation. The importance of the needle valve is further analyzed next.
5. After stability under these conditions is achieved, the electromagnetic valve A (Figure 31) is closed and the main expansion valve QN1 is isolated leading to full expander mode operation. At that point, all the circulating refrigerant mass flow passes through the

expander. Further adjustments to the mass flow rate can be done through the needle valve and the expander rotational speed, while the expander inlet pressure can be adjusted by the control of the flow in the hot water circuit.

An important point that needs to be highlighted and explains the importance of controlling the circulating refrigerant mixture mass flow rate is the superheating degree at the outlet of the evaporator, which is monitored by the Superheating Indicator (SHI - Figure 31). It is very important to maintain the superheating degree more than 2 K in order to prevent the suction of two phase refrigerant by the compressor that would eventual lead to its damage and failure. The superheating degree of the refrigerant is closely linked to the mass flow through the evaporator. In other words, it must be ensured that the evaporator can cope with the circulating mass flow, which can be adjusted either by the needle valve at the expander outlet (Figure 31) or by the expander rotational speed. Generally, it is preferred to operate the unit with the needle valve fully open so that no pressure losses are induced in the system. Indicatively, in the NTUA lab, stable conditions under low inlet pressure (13bar) are ensured at around 150rpm with the needle valve fully open. This value may vary according to the ambient conditions (due to the use of air to refrigerant evaporator) and the condensation temperature which affects both the high and the low pressure of the system. Most importantly, the adjustments ensure a sufficient superheating degree while at the same time the unit continued to deliver its nominal thermal power.

Overall, the retrofitted system at expander operation mode run in a very satisfying way without any major issues and its control proved quite easy.

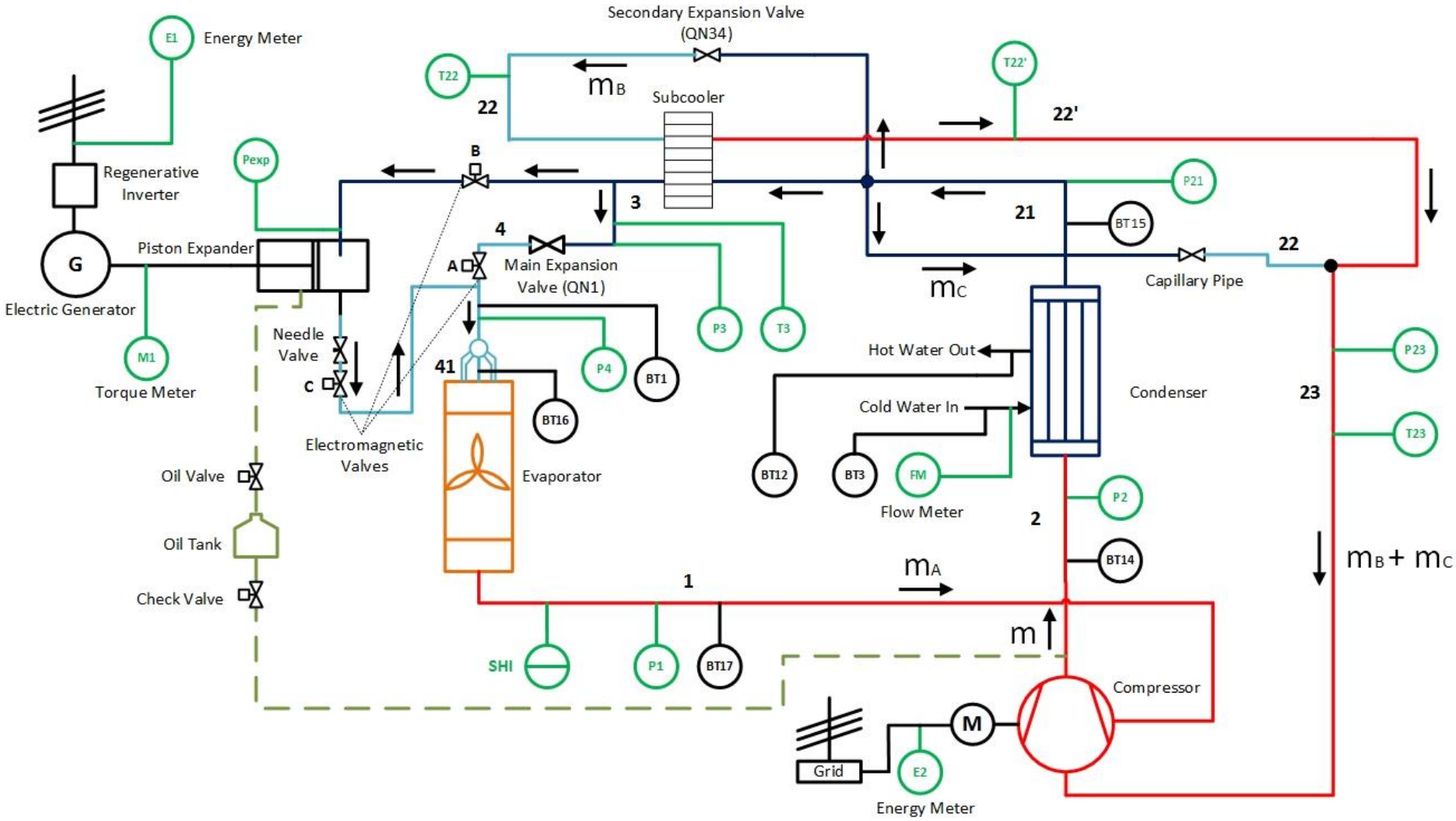

Figure 31 – Simplified Drawing of the experimental set up including the integrated expander prototype. Red colour refers to vapour state, blue to liquid state and light blue to a dual-phase state, with most of the mixture being liquid.

5.3 Photograph presentation of the experimental test rig in the NTUA lab

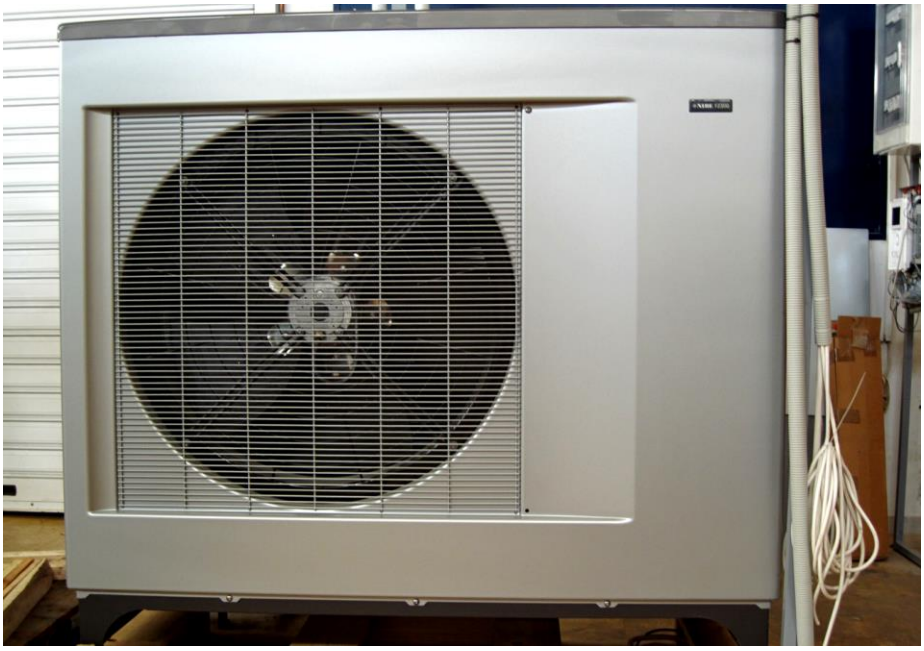

Figure 32 – Front view of the installed commercial heat pump before its retrofitting with the expander prototype.

Figure 33 – Side view of the installed commercial heat pump before its retrofitting with the expander prototype.

Figure 34 – Rear side view of the installed commercial heat pump before its retrofitting with the expander prototype. The closed water circuit and its heat exchanger can also be seen as well as the fins of the air/refrigerant evaporator heat exchanger can be clearly seen.

Figure 35 – Detail of the installed closed circuit supply water system – the plate heat exchanger, the circulation pump (black) and the manual adjustment valve (in blue) can be seen.

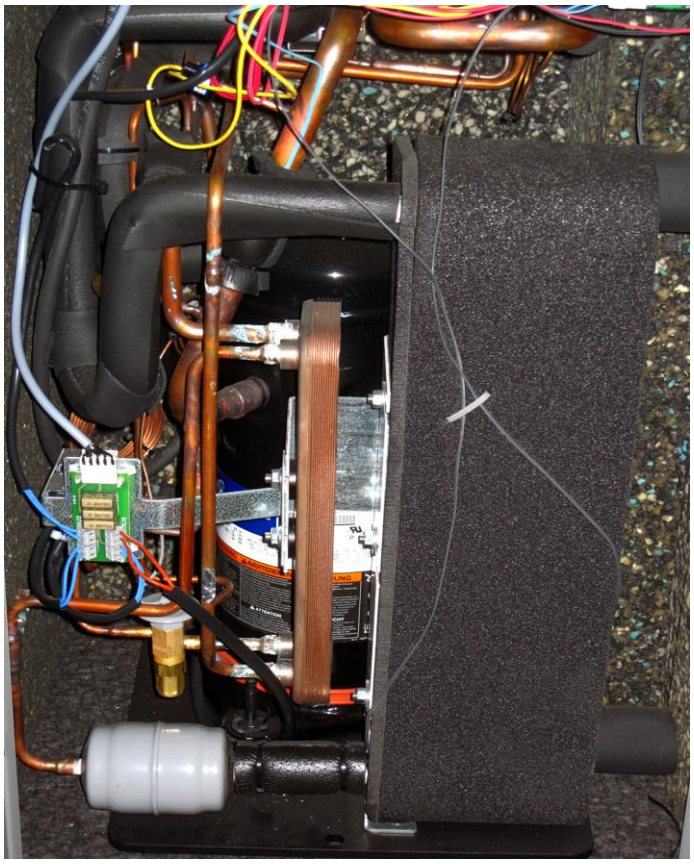

Figure 36 – Detail of the installed heat pump before its retrofitting with the expander hermetic scroll compressor, subcooler heat exchanger and condenser heat exchanger.

Figure 37 – Detail of the installed heat pump before its retrofitting with the expander The four-way valve QN2.

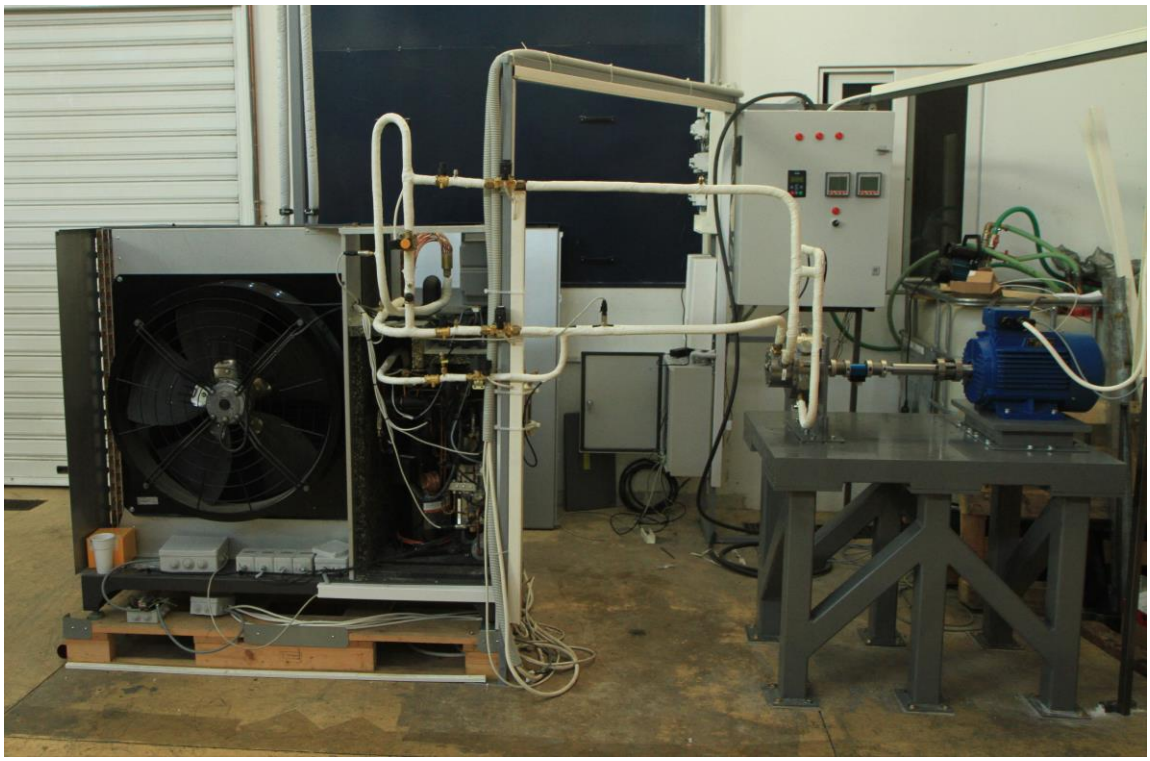

Figure 38 – The installed heat pump unit retrofitted with the expander prototype.

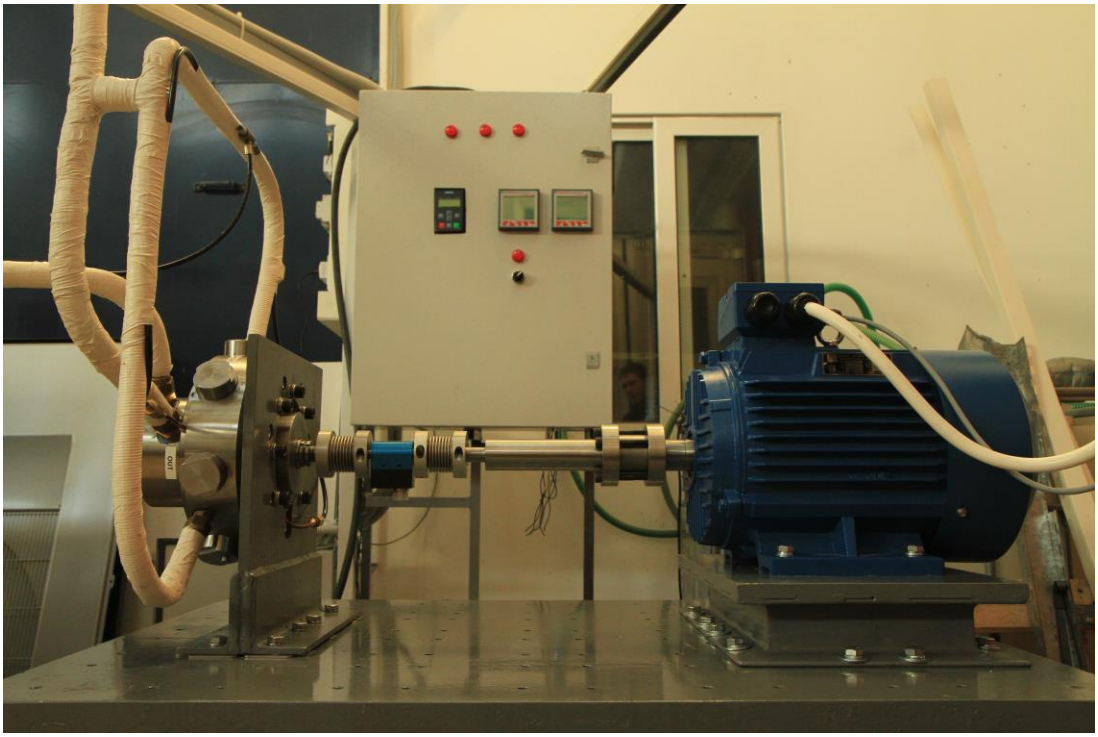

Figure 39 – The installed expander prototype coupled to the asynchronous generator. In the background the two energy-meters can be seen on the electric panel as well as the configuration board of the regenerative inverter.

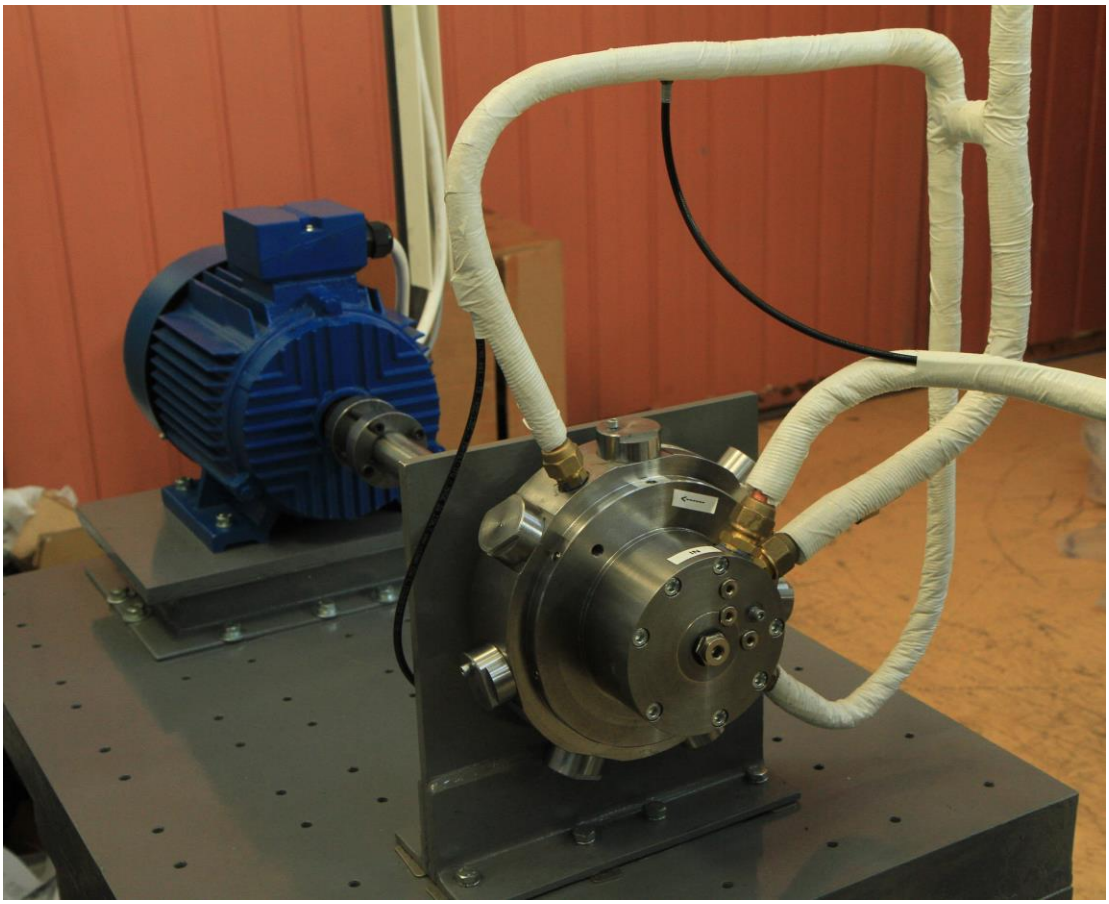

Figure 40 – The installed expander prototype and its refrigerant connection piping system.

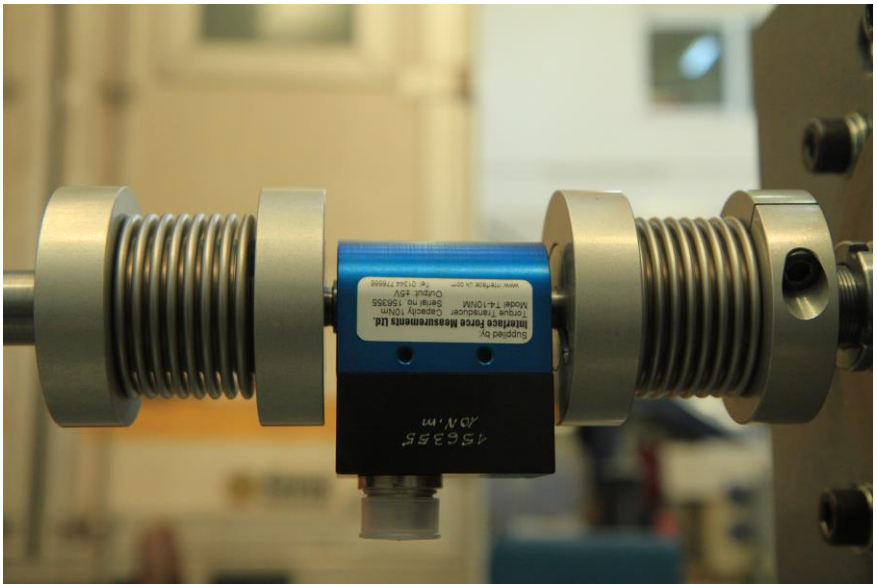

Figure 41 – The installed torque-meter on the expander's shaft.

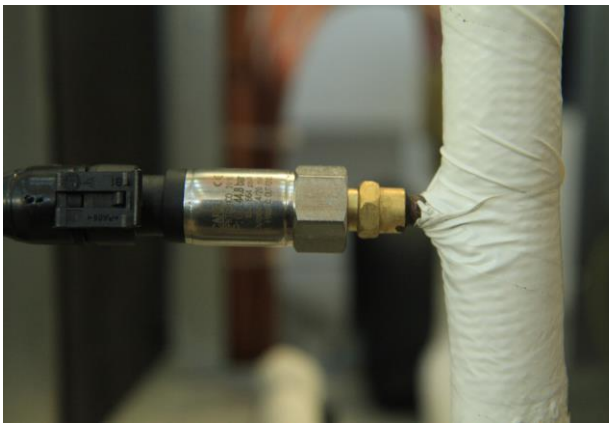

Figure 42 – Pressure transducer.

Figure 43 – Temperature sensors.

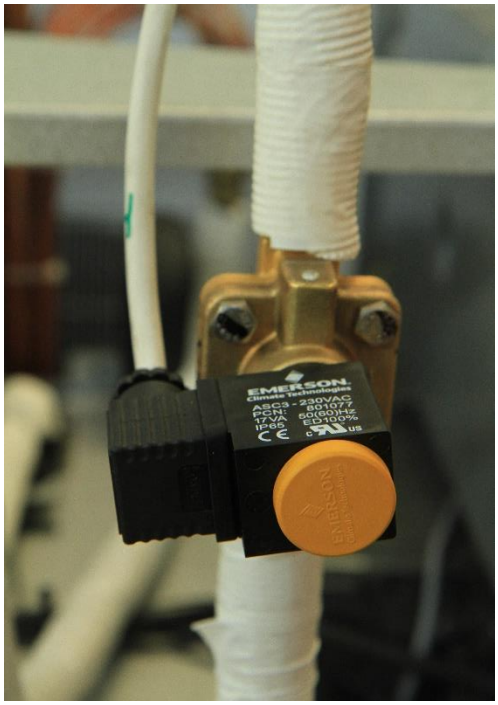

Figure 44 – Electromagnetic valve.

Figure 45 – Regenerative inverter.

Figure 46 – ADAM data acquisition and control modules.

Figure 47 – Supply water flow-meter.

Figure 48 – Heat pump information label.

Figure 49 – The dedicated test bench for the mounting of the expander and the generator.

Figure 50 – Expander Inlet/outlet piping system and respective control electromagnetic valves.

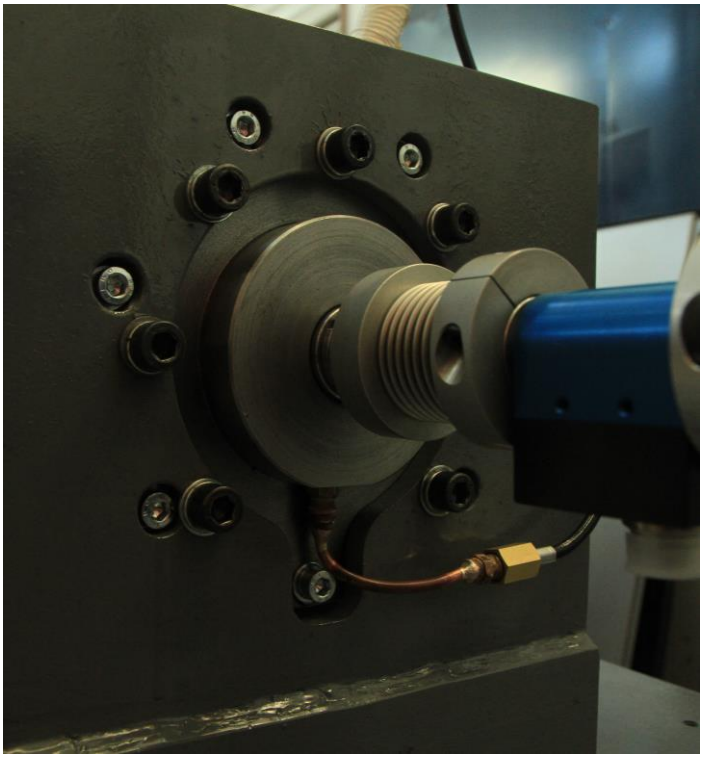

Figure 51 – The expander inlet lubrication port (rear side).

Figure 52 – The heart of expander lubrication system. The depicted oil container is connected with the high pressure circuit of the heat pump at the compressor outlet and this thus pressurized. When its outlet port is open through a dedicated valve the lubricant oil flows into the expander.

6 Tested Retrofitted System Performance

6.1 Experimental Data from Expander Mode Operation

The main goal of the experiment was to focus on the expander's performance and how it affected the whole unit. The mechanical power produced by the expander's shaft can be calculated as follows:

$$\boldsymbol{W_{expander} = T \cdot \omega} \quad (\mathbf{6.1})$$

where $\boldsymbol{T}$ is the shaft's torque (Nm) as measured by the data acquisition system. The shaft's rotational speed $\boldsymbol{\omega}$ (rad/s) can be calculated by the following equation:

$$\boldsymbol{\omega = \frac{2\pi \cdot N}{60}} \quad (\mathbf{6.2})$$

where $\boldsymbol{N}$ are the shaft's revolutions per minute (RPM), which are constantly maintained at a desired level by the frequency inverter that drives the motor/generator. The expander's performance was tested at various operating points, to gain a qualitative overview on its behavior under various inlet pressures, the shaft's rotational speed and finally the unit's thermal load. Therefore, the experiment was conducted in the way described next.

As it has already been mentioned, the hot water circuit is the means to control the high pressure of the refrigerant in the heat pump. As the supplied water's temperature increases, the refrigerant's pressure at the discharge line after the compressor also increases. Once a certain pressure level is established, the shaft's revolutions per minute are adjusted. As they are closely linked to the refrigerant mass flow through the expander and the shaft's torque, they are expected to have an impact on the produced mechanical power. The experimental data regarding the expander's power are presented in the following table. The additional properties that are being measured are the refrigerant's high pressure at the compressor exit (P2) and the pressure under which the liquid enters the expander ($P_{expander,in}$).

Table 9. Experimental data from the expander operation

P2 (bar)	RPM	ω (rad/s)	T (Nm)	$P_{expander,in}$ (bar)
13.6	50	5.235988	10.00235	12.24166667
13.37	75	7.853982	6.724343	11.47833333
13.4	100	10.47198	3.712841	11.18666667
13.45	125	13.08997	1.627606	10.995

13.48	150	15.70796	0.411338	10.80166667
13.5	175	18.32596	-0.41861	10.68166667
13.52	200	20.94395	-0.78441	10.685
14.84	50	5.235988	17.61859	12.92333333
14.98	75	7.853982	11.64906	13.29
14.98	100	10.47198	7.684297	12.74166667
14.99	125	13.08997	5.186104	12.335
14.98	150	15.70796	3.147864	12.02
14.98	175	18.32596	1.901741	11.67833333
15	200	20.94395	0.722982	11.645
16.95	50	5.235988	20.42012	15.18166667
16.98	75	7.853982	12.5973	14.72333333
17.12	100	10.47198	8.01756	14.41333333
16.9	125	13.08997	6.140048	13.88666667
16.95	150	15.70796	4.311151	13.56666667
17	175	18.32596	3.210393	12.8
17.05	200	20.94395	1.862113	13.21166667
19.2	200	20.94395	3.906174	15.10833333
19.23	175	18.32596	4.756104	15.26166667
19.3	150	15.70796	7.29101	15.835
19.01	125	13.08997	8.423546	15.665
19.08	100	10.47198	12.26235	16.53666667
19.04	75	7.853982	17.62735	17.266
19.12	50	5.235988	26.8066	17.41285714

The different colour groups represent the pressure levels that were achieved during the experiment. The expander was tested under 13.5, 15, 17 and finally 19 bar of high pressure refrigerant at the compressor's discharge line (P2). It must be mentioned that the above selection was based on the refrigerant vapour's temperature at the exit of the compressor. For safety reasons, this temperature was constantly being monitored during the experiment and its value never exceeded 103^{o}C in order to protect the compressor from any damage, as the manufacturer indicates. As a result, and combined with the fact that during the tests the ambient temperature was quite high (circa 24 ^{o}C) an upper limit to the high pressure side of the heat pump was inevitable.

Another point that needs to be highlighted is the pressure drop at the expander's inlet. A difference of about 2-4 bar between the vapour at the compressor exit and the liquid that enters the expander can be observed. The existence of the condenser between those two components cannot fully justify such a big pressure drop. It is assumed that this is caused due to the pipelines

that were retrofitted to the unit. They have a larger inner diameter with a ratio of 2 compared to the liquid pipeline between the condenser exit and main expansion valve, in order to match the expander inlet port, which causes the refrigerant to perform a certain kind of expansion as it flows through the connecting point between the pipe of the commercial heat pump and the pipe that was retrofitted to it. Taking that into account, along with the temperature restriction that has already been mentioned, the increase of the refrigerant's pressure at the expander inlet proved quite difficult. Even so, the experiment proceeded normally and certain conclusions on the expander's performance were made, as shown by the table below:

Table 10. Produced mechanical power at different operating points

		$P_{expander,in}$ (bar)			
		11.15	**12.38**	**13.97**	**16.16**
Points	RPM	$W_{expander}$ (W)			
1	50	**52.37**	**92.25**	**106.92**	**140.36**
2	75	**52.81**	**91.49**	**98.94**	**138.44**
3	100	**38.88**	**80.47**	**83.96**	**128.41**
4	125	**21.31**	**67.89**	**80.37**	**110.26**
5	150	**6.46**	**49.45**	**67.72**	**114.53**
6	175	**-7.67**	**34.85**	**58.83**	**87.16**
7	200	**-16.43**	**15.14**	**39.00**	**81.81**

A graphic overview of the expander's performance as far as its power is concerned is depicted in the following figures:

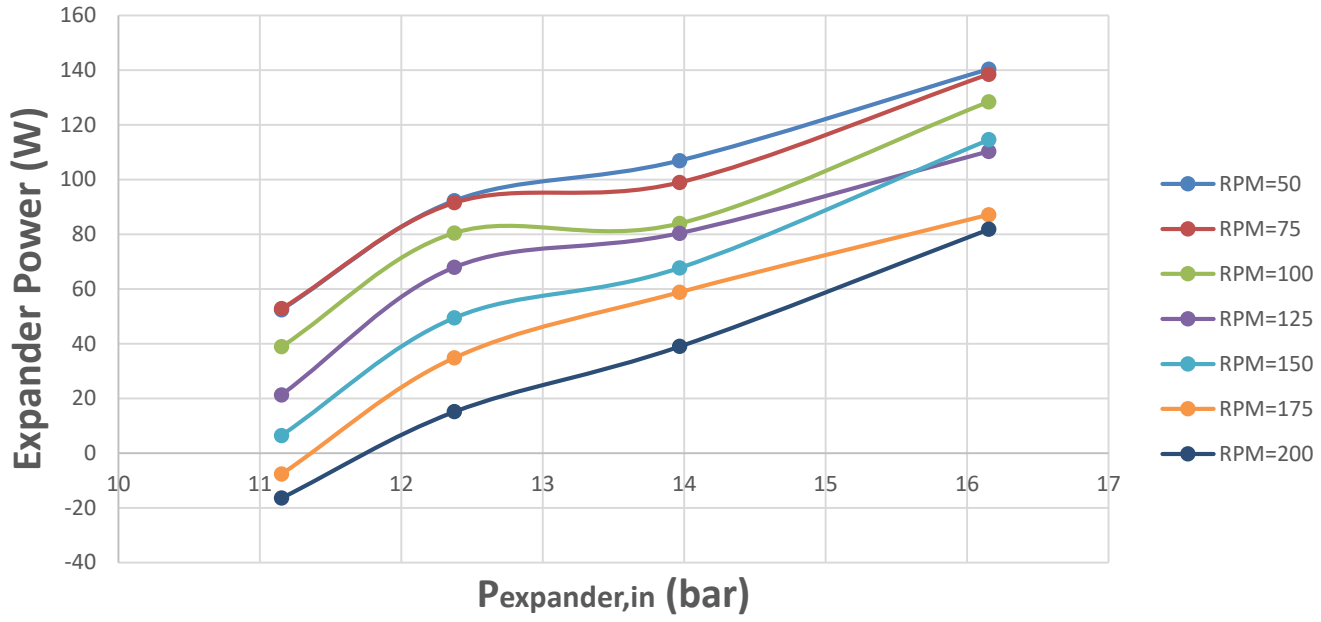

Figure 53 – Expander produced mechanical power vs refrigerant pressure at the expander's inlet for different RPM.

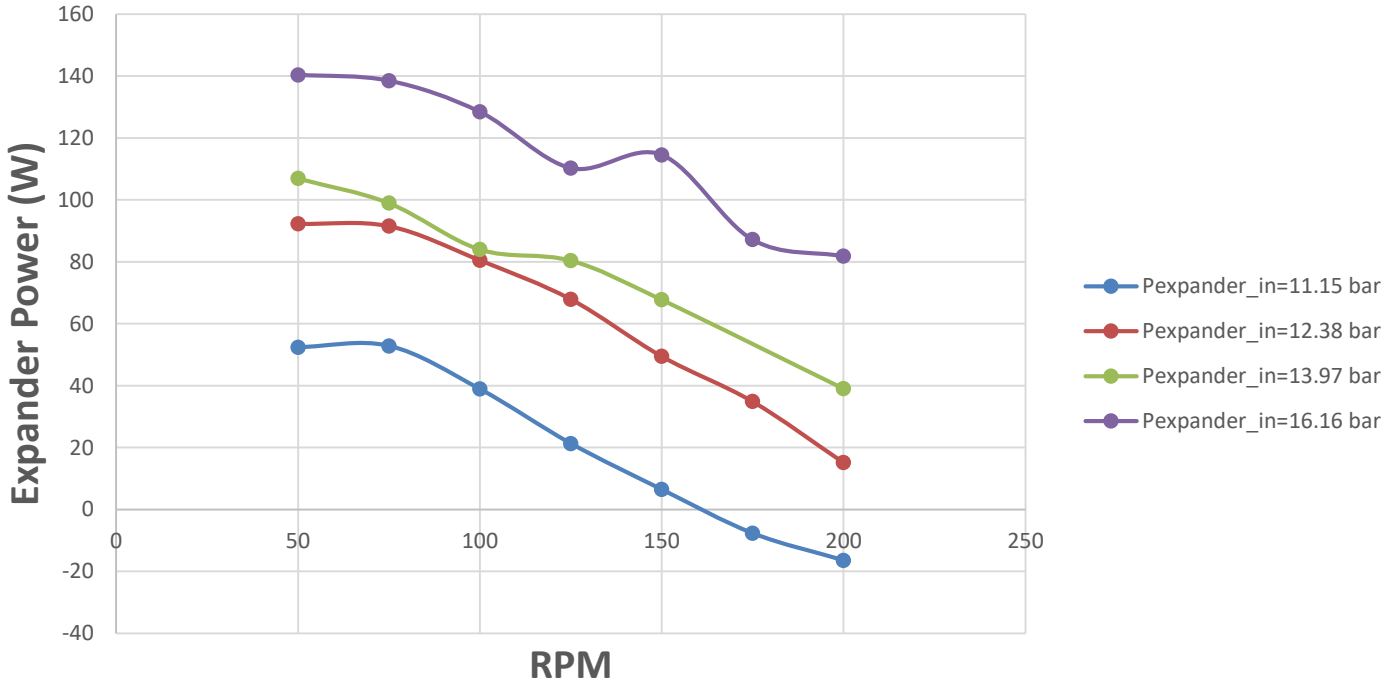

Figure 54 – Expander produced mechanical power vs revolutions per minute for different refrigerant pressure levels at the expander's inlet.

Under these operational conditions, a maximum output power of 140 W was achieved under 16.16 bar at the expander inlet. It must be mentioned that all figures are based on the pressure at the expander inlet and not the high pressure of the discharge line at the compressor exit. As it can be observed in Figure 54, there are two operating points that fail to produce any mechanical work since the expander power has a negative value. Further analysing that, the shaft's rotation is assisted by the motor/generator. Initially, the required torque for the rotation is provided by the motor. In that way, electrical power is supplied from the grid to the system. As the refrigerant expands in the pistons, the mechanical work produced by the expander tends to accelerate the shaft by also applying a torque. The frequency inverter maintains the revolutions per minute at a specific level. The equation that describes the shaft system is the following:

$$\boldsymbol{T_{motor} + T_{expander} = I \cdot \dot{\omega}} \quad \mathbf{(6.3)}$$

where $\mathbf{T_{motor}}$, $\mathbf{T_{expander}}$ are the motor's and the expander's torque

$\mathbf{I}$ is the system's moment of inertia and

$\dot{\boldsymbol{\omega}}$ is the shaft's radial acceleration.

As the expander's torque increases, the motor's torque must be reduced in order to keep $\dot{\boldsymbol{\omega}}$ constant, given that the moment of inertia remains the same. If reduced below zero, the motor's operation is reversed to an electric generator. As a result, any excessive power that would increase the rotational speed of the expander's shaft is converted into electricity that is fed to the grid.

Under low refrigerant pressures, the torque applied to the shaft by the expander fails to reach the required level for a constant rotational speed. In that case, the additional amount of power needed is supplied by the motor and the system recovers no energy. It is estimated that the low pressure values are not enough for power production. Apart from that, the relatively high rotational speeds (over 175 RPM) for the specific experiment and mass flow rates indicate that friction losses increase disproportionally leading to lower energy recovery.

Another crucial matter of the experiment is to measure the isentropic efficiency of the expander. Given that it is a piston-type machine, the isentropic efficiency is calculated using the following equation:

$$\boldsymbol{\eta_{is} = \frac{W_{expander}}{\dot{m}_A(h_3 - h_{4is})}} \quad \mathbf{(6.4)}$$

Where $\mathbf{W_{expander}}$ is the power produced at the shaft of the expander,

$\mathbf{\dot{m}_A}$ is the refrigerant mass flow that enters the expander (see Figure 31 – valve A closed)

$\mathbf{h_3}$ is the liquid refrigerant's enthalpy at the exit of the subcooler (see Figure 31)

$\mathbf{h_{4is}}$ is the refrigerant's enthalpy at the expander outlet if the process was isentropic.

The pressure at the expander inlet and outlet is measured. The temperature at cycle point 3 is also measured and as a result the enthalpy $\mathbf{h_3}$ and entropy $\mathbf{s_3}$ can be calculated using REFPROP. As the process is considered isentropic, the variables required to calculate $\mathbf{h_{4is}}$ are the pressure at the expander outlet and $\mathbf{s_3}$, which are both known. The calculation of the current $\mathbf{\dot{m}_A}$ has already been analyzed in the deliverable 6.1 and involves the calculation of the mass flows through the sub-cooling system. For this part, given that the mass flows $\mathbf{\dot{m}_B}$, $\mathbf{\dot{m}_C}$ have small values, they can be neglected as they have no serious impact on the isentropic efficiency value.

A certain operating point has been selected as a showcase example. At that point, the maximum value of the isentropic efficiency as described in equation 3.4 is achieved. The mass flow of the water in the hot water circuit can be calculated as the water's volume flow is measured. It is measured that:

$$\dot{V}_{water} = 0.863 \frac{lt}{s}$$

The temperature of the water that enters and leaves the heat pump's condenser is also measured:

$$T_{water,in} = 40.97\ °C \qquad T_{water,out} = 47.25\ °C$$

For the average water temperature ($\frac{T_{water,in}+T_{water,out}}{2}$), the water's density is calculated by REFPROP as:

$$\rho_{water} = 990.61\ \frac{kg}{m^3}$$

So the mass flow of the water is:

$$\dot{m}_{water} = \rho_{water} \cdot \dot{V}_{water} \cdot 10^{-3} = 0.855 \frac{kg}{s}$$

The heat pump's power can be calculated using the equation:

$$\boldsymbol{Q_{delivered} = \dot{m}_{water} \cdot C_{p,water}\left(T_{water,out} - T_{water,in}\right)} \quad \boldsymbol{(6.5)}$$

For this operating point: $\mathbf{Q_{delivered} = 22.48\ kW}$

It is important that the heat pump continues to deliver its nominal power that the manufacturer indicates, even after the retrofitting operations. The water's temperature increase is slightly lower than that of the normal operation (8.22 °C instead of 9.1 °C). As mentioned above, with the currents $\mathbf{\dot{m}_B}$, $\mathbf{\dot{m}_C}$ not playing an important role to the isentropic efficiency calculation, it can be considered that the mass flow of the refrigerant can be calculated by the following equation:

$$\boldsymbol{\dot{m} = \dot{m}_A = \frac{Q_{delivered}}{h_{21} - h_2}} \quad \boldsymbol{(6.6)}$$

The enthalpies at cycle points 21 and 2 are calculated by REFPROP, as the pressure and temperature at these points is measured (see Figure 31). Based on the experimental data:

T2 [C]	P2 [bar]	T21 [C]	P21 [bar]
102.45	19.12	43.25	19.11

for the specific operating point it is $\mathbf{h_{21} = 265.75\ kJ/kg}$ and $\mathbf{h_2 = 490.34\ kJ/kg}$

and $$\mathbf{\dot{m} = 0.1\ \frac{kg}{s}}$$

Knowing the temperature and pressure of cycle point 3 from the experimental data, its enthalpy and entropy can be calculated:

T3 [C]	P3 [bar]	h3 [kJ/kg]	S3 [kJ/kg K]
35.54	18.87	256.97	1.178

As the theoretical power considers the expansion process to be isentropic, the entropy at the exit of the expander will remain the same. The pressure is once again measured and so the enthalpy of the isentropic cycle point 4 (see Figure 31) can be calculated. Its value is represented bellow:

Pexpander,out [bar]	S4is [kJ/kg K]	h4is [kJ/kg]
5.66	1.178	248.76

The power of the expander has already been calculated and its value can be seen in

Table 10, at 50 RPM and under a expander inlet pressure of 16.16 bar, which are the conditions for this operating point, and has been found to be 140.36 W. For the calculation of the isentropic efficiency, the enthalpy of the refrigerant at the inlet of the expander was based on the experimental data from cycle point 3, as the pressure drop due to the expansion at the connecting point of the pipes is considered an isenthalpic process. As a result, using equation 3.4, the isentropic efficiency of the expander was found to be:

$$\boldsymbol{\eta_{is} = 17.05\%}$$

The expander's isentropic efficiency at the different operating points is shown in *Table 11*.

Table 11. Expander's isentropic efficiency at different operating points

		$P_{expander,in}$ (bar)			
		11.15	**12.38**	**13.97**	**16.16**
Points	RPM	Isentropic Efficiency			
1	50	**0.111**	**0.146**	**0.144**	**0.171**
2	75	**0.094**	**0.143**	**0.136**	**0.170**
3	100	**0.068**	**0.129**	**0.116**	**0.161**
4	125	**0.038**	**0.110**	**0.118**	**0.143**
5	150	**0.011**	**0.080**	**0.101**	**0.146**
6	175	N.A.	**0.058**	**0.097**	**0.113**
7	200	N.A.	**0.023**	**0.056**	**0.106**

N.A. stands for Not Available due to the negative expander power value at these specific points, where no isentropic efficiency can be defined.

A graphic overview of the expander's performance as far as its isentropic efficiency is concerned is depicted in the following figures:

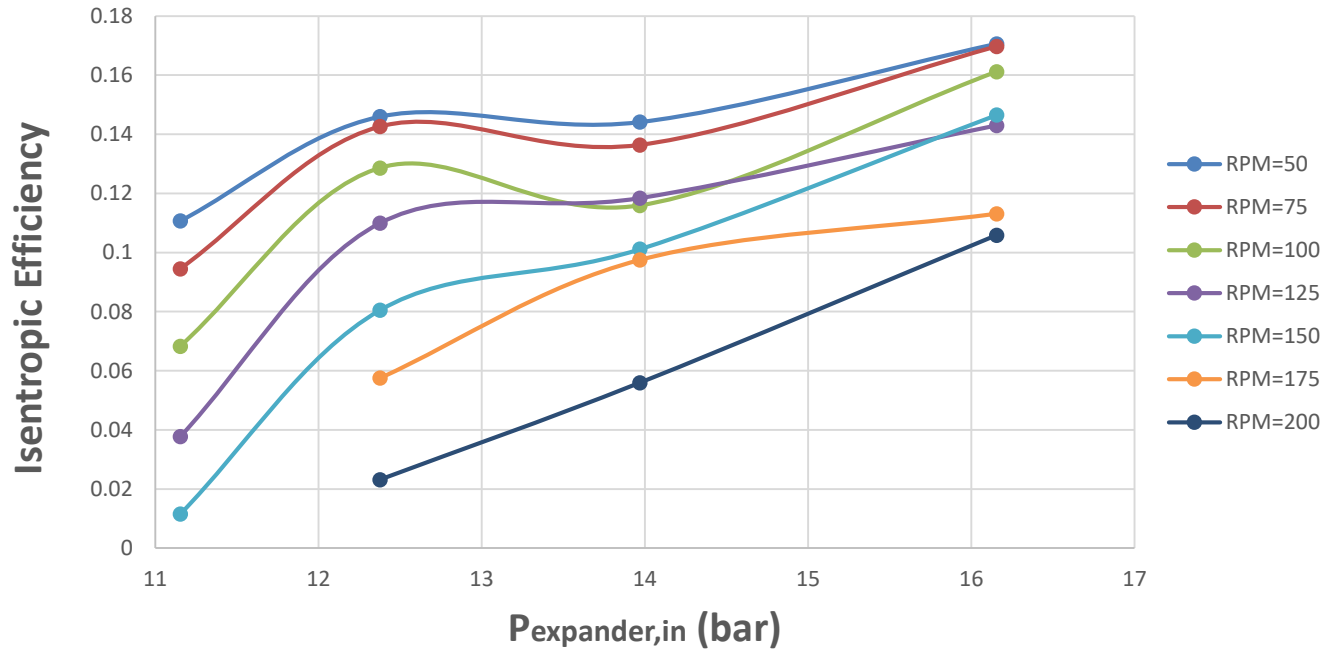

Figure 55 – Expander isentropic efficiency vs refrigerant pressure at the expander's inlet for different revolutions per minute.

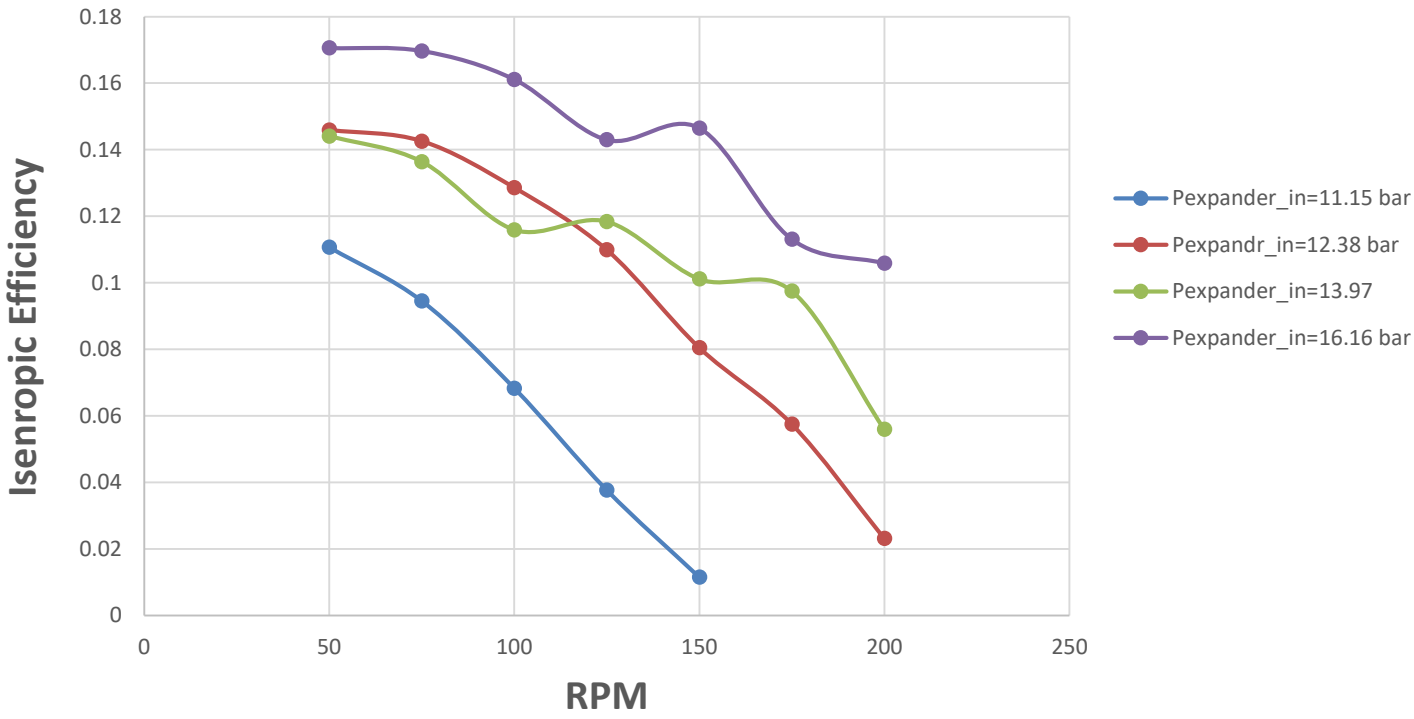

Figure 56 – Expander isentropic efficiency vs revolutions per minute for different refrigerant pressure levels at the expander's inlet.

The mechanical power produced by the expander can be compared to the work required by the compressor and the rest of the components for the heat pump's operation. As it has been mentioned above, **the performance of the expander reaches its peak at 50 RPM**. For the different pressure levels that were applied, the relationship between the required mechanical power and the one that is being recovered by the expander can be seen in Figure 57.

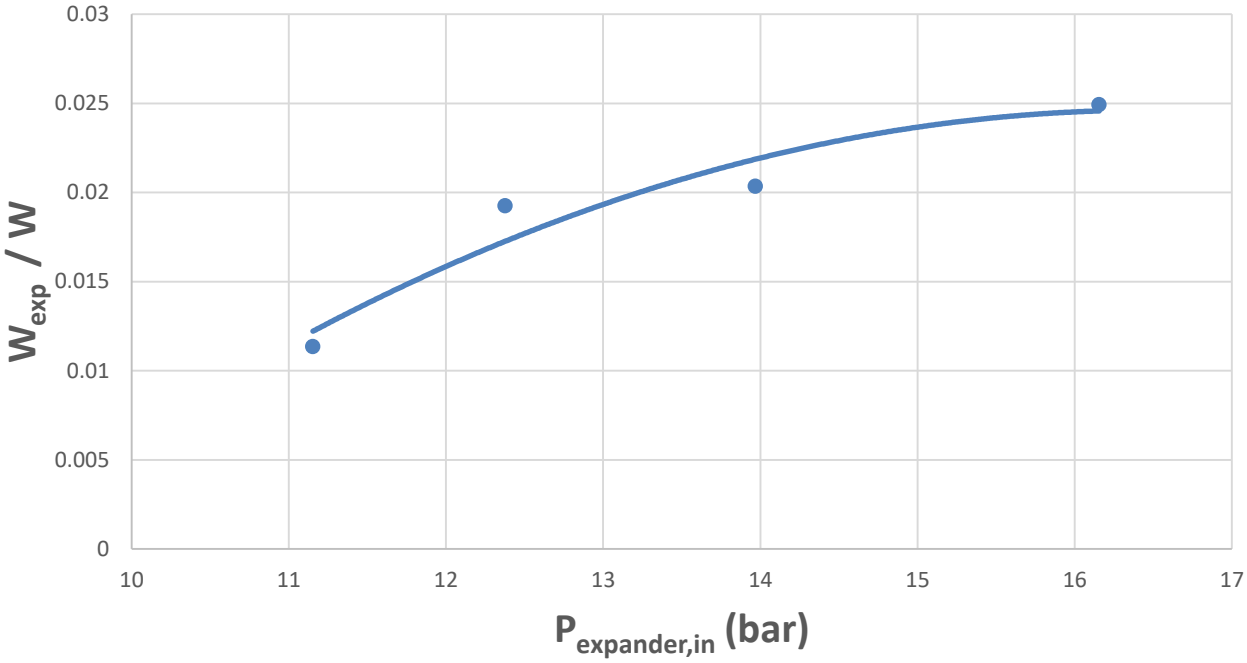

Figure 57 – Proportion of expander power ($W_{expander}$) to the power consumed by the heat pump vs refrigerant pressure at the expander's inlet ($N_{expander}$ = 50rpm).

Although a 2.5% of maximum contribution may seem a minor amount, the COP of the unit can increase by 1% to 2%, under certain experimental conditions.

If normal operation is considered, the heat pump's COP is calculated once again by using equation:

$$\boldsymbol{COP = \frac{Q_{delivered}}{W}} \quad (\mathbf{6.7})$$

Taking the useful power that the expander produces into account, the improved COP of the unit can be defined as:

$$\boldsymbol{COP' = \frac{Q_{delivered}}{W - W_{expander}}} \quad (\mathbf{6.8})$$

For the specific experiment, the average hot water output temperature and the average COP of the heat pump unit with and without the expander for the four different pressure levels are listed below:

$T_{water,out}$ [°C]	COP' (with expander)	COP (without expander)
32.9	**4.95**	**4.93**
37.2	**4.75**	**4.68**
42.3	**4.39**	**4.33**
47.1	**4.08**	**3.99**

A graphic overview of the COP's behaviour with increasing heat pump high pressure and hot water outlet temperature is represented in Figure 58.

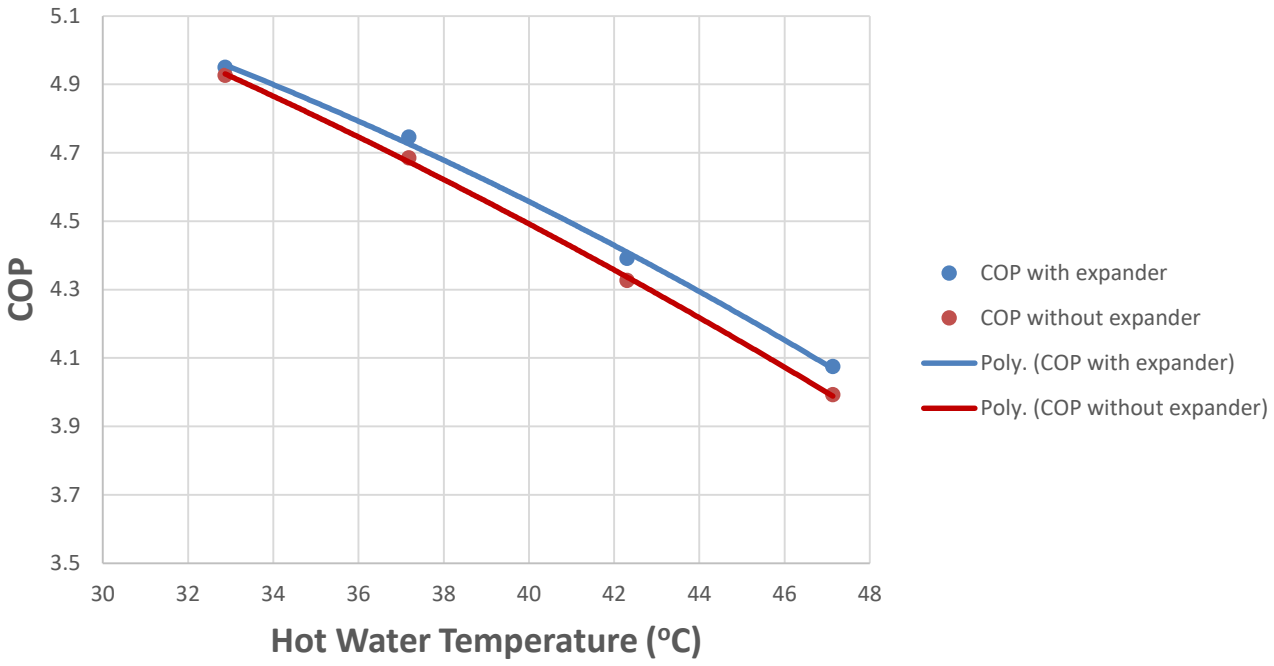

Figure 58 – The unit's COP with and without expander vs hot water temperature at the exit of the condenser (N_{exp}=50rpm).

It is clear that the expander operation is beneficial for the whole unit. As the high pressure increases, the COP at normal operation tends to decrease. The refrigerant pressure obtains higher values, so the expander is able to produce more power. Its contribution can be recognized in Figure 59, where the COP increase is represented in relationship with the refrigerant pressure at the expander's inlet. A COP increase of over 2% has been achieved at a maximum pressure of 16 bar.

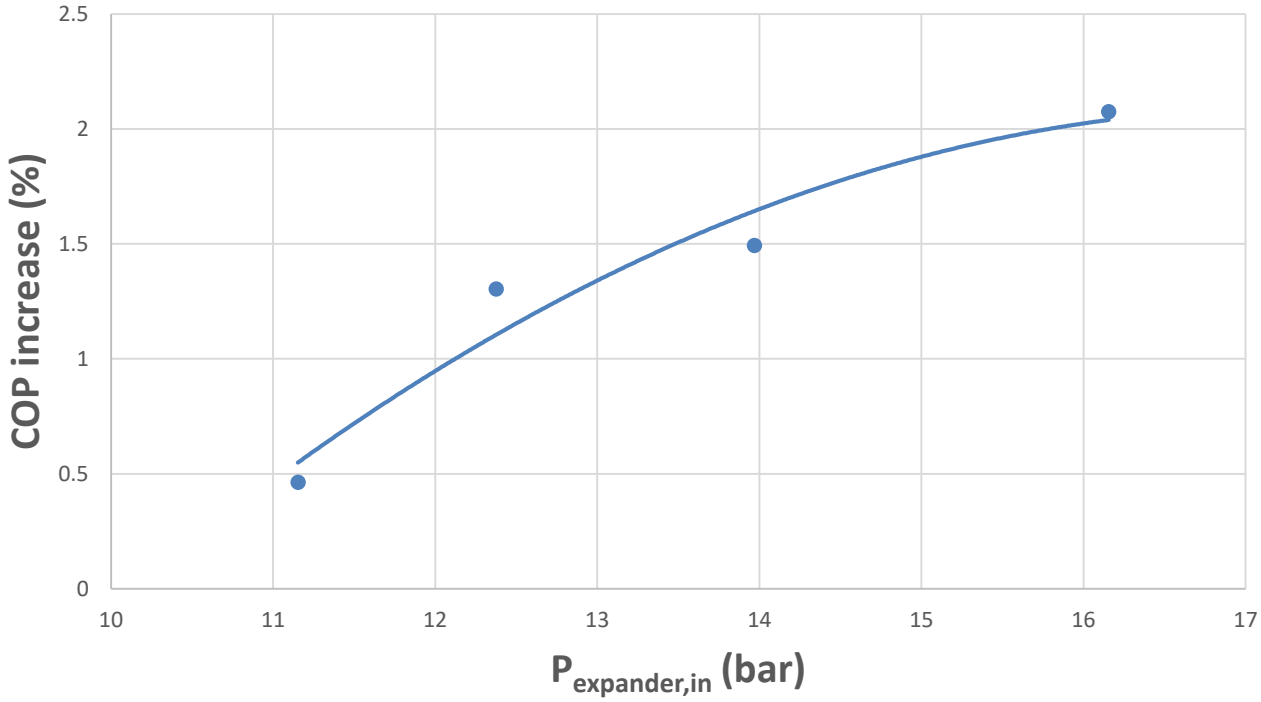

Figure 59 – COP increase (%) vs refrigerant pressure at the expander's inlet (Nexp=50rpm).

The refrigerant properties during the expander operation are represented in Figure 60. It is mentioned once again that the subcooling process is neglected, as it has no serious impact on the COP, the expander's efficiency and generally the thermodynamic cycle. The expansion curve (3➔4) now approaches an isentropic process. In fact, the refrigerant's entropy has a smaller increase than before, which means that the thermodynamic losses are reduced. The theoretical power that the expander would produce as the refrigerant expands per refrigerant mass flow unit is symbolized with $\mathbf{w_{expander}}$. Due to the friction losses and other factors that affect the expander's efficiency, a relatively smaller amount is finally the shaft's power output. The retrofitted heat pump is now operating at a high load as the increased temperature at the compressor exit (cycle point 2) strongly suggests.

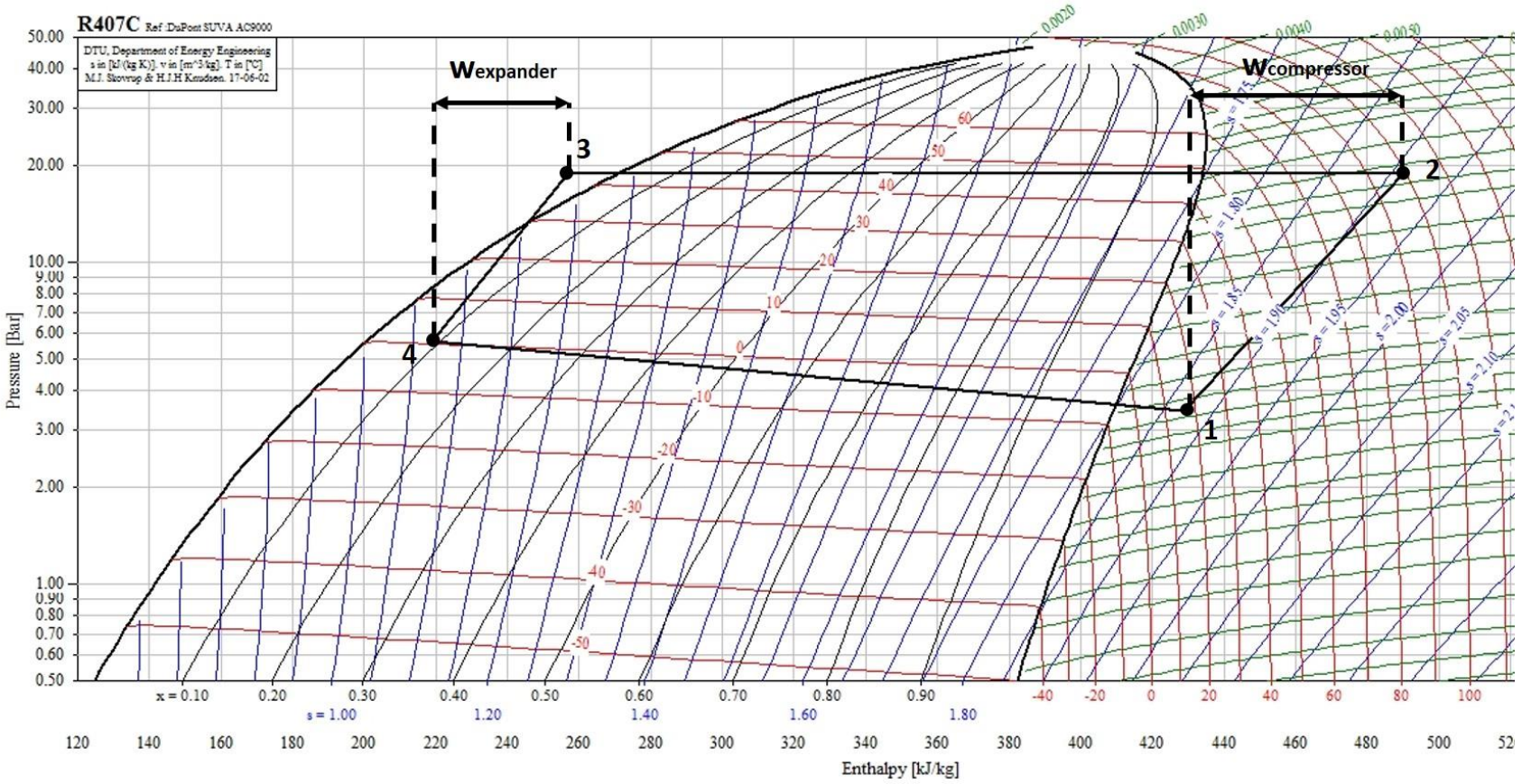

Figure 60 – Expander mode operation P-h diagram. The expansion curve (3 ➔ 4) now approaches an isentropic curve. In this way, thermodynamic losses are decreased compared to the standard expansion process through the heat pump's throttling valve.

6.2 Results Extrapolation

The optimal point of the expander's performance was found to be at 50 RPM and 16.16 bar as its inlet pressure. At that point, the expander produced 140.36 W with an isentropic efficiency of 17.05%. For safety reasons that have been analyzed in 6.1, the refrigerant's pressure did not exceed a certain limit. However, Figure 53 and Figure 55 suggest that both the expander power and its isentropic efficiency tend to increase as the refrigerant pressure obtains higher values. Assuming that there is a certain relationship between expander power and isentropic efficiency with the refrigerant pressure, as Figure 53 and Figure 55 strongly suggest, estimations about the expander's performance under higher refrigerant pressure are possible through the extrapolation of the obtained results. Taking into consideration that the higher power and efficiency values occur at low rotational speeds, the 50 RPM curve has been extrapolated for pressures over 16 bar and up to 25 bar (Figure 61) , assuming a linear relationship between expander power and inlet pressure. The estimated expander power can exceed 250 W if the inlet pressure increases to 25 bar.

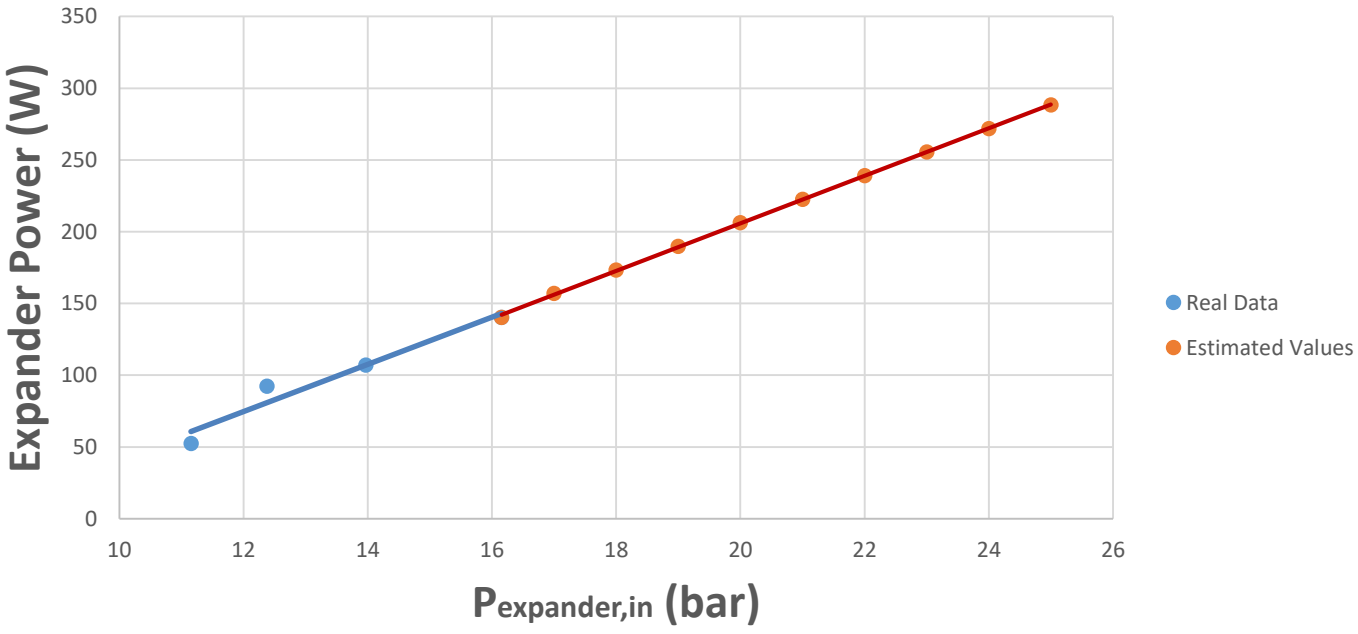

Figure 61 – Extrapolated curve of expander power vs refrigerant pressure for 50 RPM.

The isentropic efficiency of the expander on the other hand cannot increase infinitely. As a result, the 50 RPM curve has been extrapolated for pressures over 16 bar and up to 25 bar (Figure 62), assuming a logarithmic relationship between isentropic efficiency and inlet pressure.

A maximum value of 24% is possible if the inlet pressure increases to 25 bar and the unit's normal operation is ensured. Having in mind that the expander maximum efficiency of 26% was achieved with version 2.0 and R410A at 22 bar, along with the fact that R410A is more favorable compared to R407C used here, the results are well in consistence with previous tests.

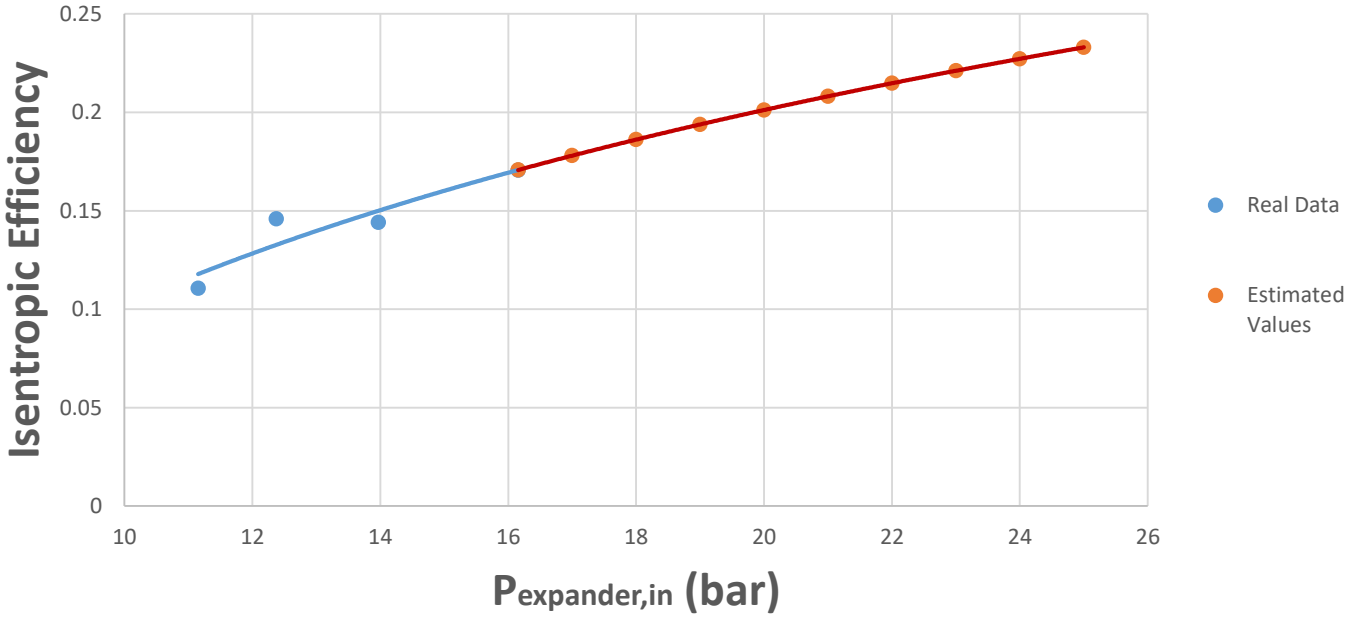

Figure 62 – Extrapolated curve of expander isentropic efficiency vs refrigerant pressure for 50 RPM.

The 50 RPM curve of the COP increase has finally been extrapolated for the same pressure levels (16-25bar), assuming once again a logarithmic relationship between COP increase and inlet pressure in order to rate the possible energetic benefits. The results are presented in Figure 63.

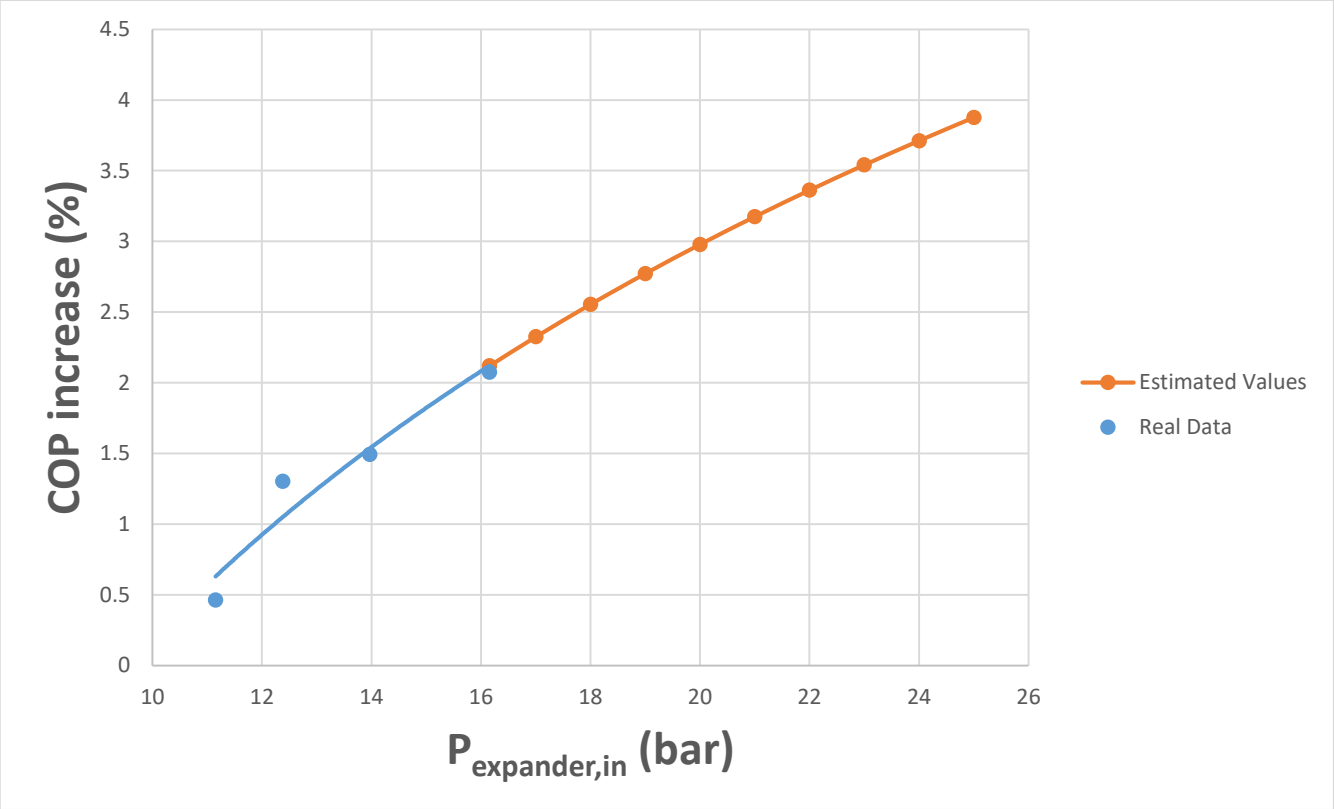

Figure 63 – Extrapolated curve of COP increase (%) vs refrigerant pressure for 50 RPM.

A maximum value of 3.8% is possible if the inlet pressure increases to 25 bar and the unit's normal operation is ensured. Having in mind that the project threshold target has been set to 3.5%, the obtained results are pretty encouraging.

7 Reliability, maintenance and final optimization issues

7.1 Control system optimization

The experience of the test campaign of the retrofitted commercial heat pump showed that the control procedures described above can be fully automated, which is an absolutely necessary step towards the development of a commercial retrofit kit product. Actually, in the final product, the expander/generator speed will not be controlled as there will be no frequency inverter. An optimal speed of the motor will be chosen according to the unit's refrigerant and nominal mass flow so that in full load the expander rotational speed ensures the nominal mass flow rate and the needle valve can remain fully open.

So the control of the unit mainly consists of the basic electromagnetic valves (Figure 31Figure 29), the oil electromagnetic valve and the needle valve. The control of the electromagnetic valves and the oil valve is basically the same as in the current experimental test bench. The needle valve on the other hand is currently manually controlled and needs to be fully automated. The superheating indicator is currently a sensor and a drive of an electronic expansion valve (EEV), it is programmable and can also drive the needle valve through its analogue outputs. The control with these drives is well proven and very widely used in all units equipped with EEVs. The desired superheating temperature can be set in the drive and with and internal PID controller the opening of the needle valve is defined and the respective command is sent to the valve via a 0-10V or 4-20mA signal. Should the superheating degree fall below a certain value, the drive can also activate a relay through a digital output signal and shut down the unit in order to protect the compressor. In normal operation mode the drive remains inactive and the needle valve remains fully open. As far as the automation of the lubrication system is concerned, it is analyzed in detail further on in this section.

Additional safety sensors will also need to be installed in order to ensure fully automated safety supervision of the system. Mainly, there are needed two over-pressure switches at the expander inlet and outlet and a speed sensor at the expander's shaft to monitor the rotational speed of the machine. In case of overpressure (e.g. due to a jammed expander outlet valve) or over-speed (e.g. in the case of a shaft or generator failure) the unit will be automatically shut down.

Regarding the original control unit of the heat pump unit it remains totally unmodified as the additional control procedures do not interfere with its operation. The new control unit can

be ideally materialized with an HMI screen that has an incorporated processor that gives the capability of data acquisition, control through analogue and digital outputs and real time overview of the unit's operation parameters. Other solutions can also be evaluated in order to find the most economical and reliable solution.

7.2 Reliability and maintenance

In order to further improve the expander reliability and performance, it is crucial to monitor the expander's operation in order to examine the proper functioning of certain key mechanical elements as described next. In this paragraph, different reliability and operational issues as well as technical solutions to deal with them will be discussed.

Although the data acquisition system provides a sufficient overview of the system's operation, a more detailed image of the expander's inside must be obtained by physical inspection. Actually, after several hours of operation, the whole system had to be shut down due to an oil leakage issue at the expander's shaft. The main goal was the identification of the leakage issue. A faulty O-ring was detected and the problem was solved. However, in the above described context the expander was fully dismantled for a complete inspection of its parts. In that way, interesting conclusions regarding different components have been made. Specifically:

The shaft's bearing as well the eccentrically positioned "crankshaft" bearing that is being driven by the piston rods had sustained serious damage (Figure 64). As a result, their rotation was no longer smooth increasing friction forces as well as destabilizing the expander's torque over a full rotation. The damage was attributed to iron debris (trims) which was found in the interior of the expander (Figure 65). The debris was also found between the bearing's cage, its steel barrels and the outer ring. Its presence within the bearing cause additional friction that incommodes the bearings' normal operation, leading eventually to their damage. The existing bearings were replaced with new, heavy-duty ones that are able to withstand higher loads and are generally much more robust and reliable. Every part of the expander was thoroughly cleaned so that any remaining debris would carefully be removed from the expander. However, in order to prevent the occurrence of this problem in the future is to ensure debris-free operation of the expander. Thus, the main issue that arose from the presence of debris is to identify and abolish the source of the debris.

Figure 64 – Damaged "crankshaft" bearing (foreground) and shaft bearing (background).

Figure 65 – Iron trims (debris) in the expander interior.

A meticulous inspection of the expander's interior led to the conclusion that the debris source is the piston rods, which were found to be damaged (Figure 66). The rods apply forces to

the inner bearing causing it to rotate. These forces become much more significant as the rotational speed increases, so the slightest misalignment or a rod's momentary detachment from the crankshaft bearing's outer ring (Figure 67) leads to impulse loads due to the collision of the rods with the expander case causing the creation of small debris. This fact is confirmed by the scratches on the surface of the crankshaft bearing as it can be seen in Figure 68. Another possibility is that the rods come in contact with the cylinder's edge if the piston overcomes its top dead centre, due to inertia phenomena. This was concluded after identifying damage to the piston rods and the surrounding area of the case (Figure 66). The reason for this detachment or misalignment has been mainly attributed to the following reasons:

- Insufficient spring force from the piston spring
- Viscosity action of excessive amount of lubrication oil between the sphere of the piston rod and the spherical contact surface of the piston blocking the free movement of the rod within this spherical surface
- radial forces cause the rod to lose its exact alignment with the crankshaft bearing surface and are repositioned by impulse forces causing damage to both the piston rods and the crankshaft bearing surface (Figure 66,Figure 68).

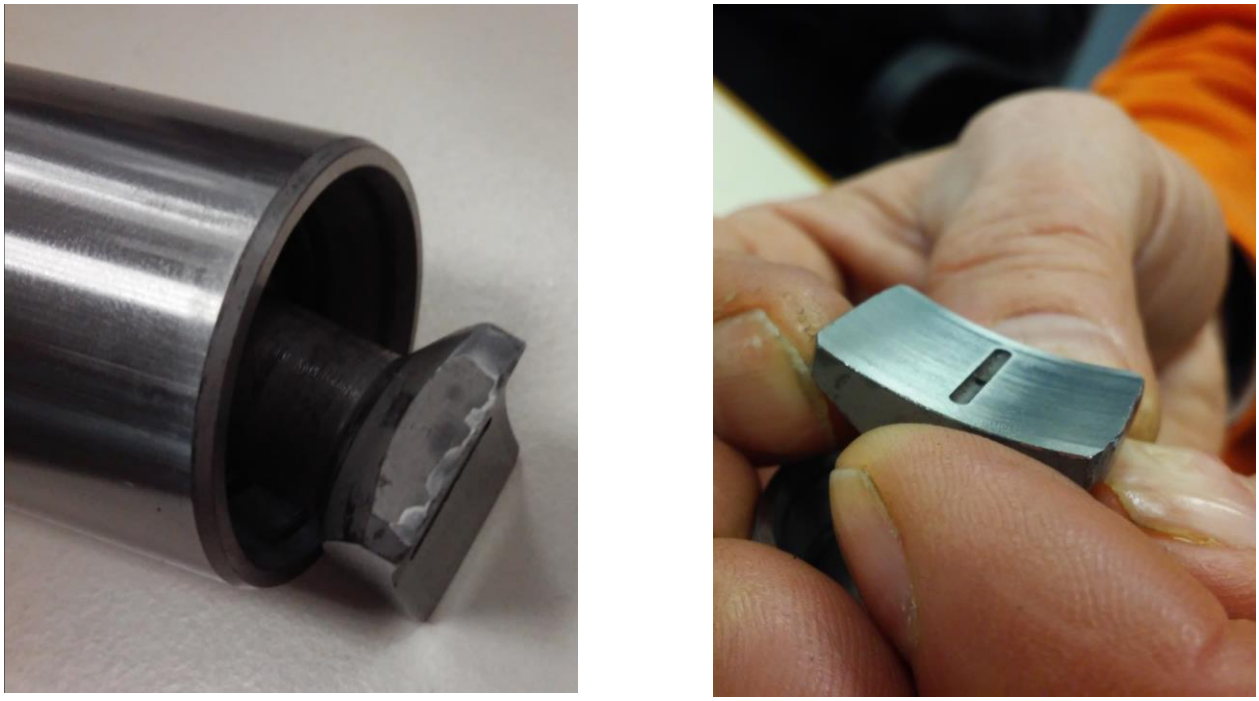

Figure 66 – Damaged piston rods.

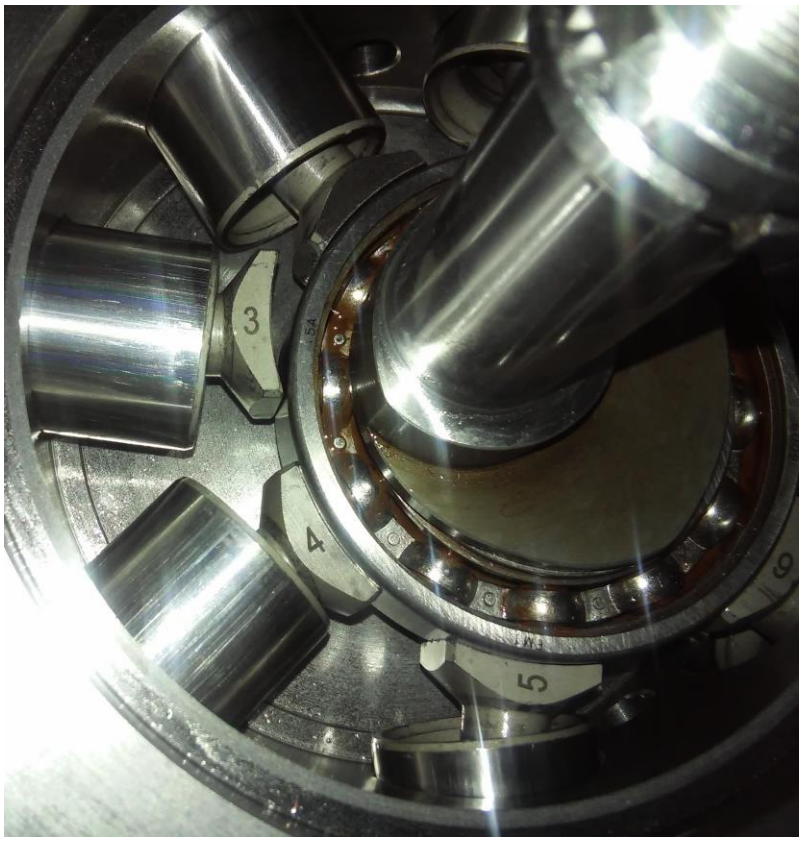

Figure 67 – Loss of contact between piston rod and bearing surface.

Figure 68 – Scratched surface of crankshaft bearing.

In cooperation with the laboratory personnel, the following technical solutions were concluded:

- use of stiffer springs between the piston and the piston head in order to ensure no movement beyond the top dead centre and as a result, no contact between the rod and the cylinder's edge. Moreoever, by applying that solution, it is ensured that the piston rods cannot lose contact with the crankshaft bearing surface.
- piston rods and piston spherical surface redesign in order to constrain the freedom of piston rods' movement.
- a guidance plate could be fixed on the sides of the crankshaft bearing so that the rods always remain vertical to the bearing's rotating axis and in full contact with the bearing's outer ring, preventing misalignents.
- the cylinders must be constantly supplied with refrigerant since any kind of expansion with different fluids such as the lubrication oil or air that is induced into the expander can cause displacement of the rods.

In addition to the damaged bearings and the debris, problems regarding the O-ring seals were also encountered. Some of the shaft O-rings were majorly deformed (Figure 69) causing the leakage problems mentioned above. This type of failure may have been caused by the shaft's marginal axial movement which was a result of the damaged bearings, leading to increased tension forces. However, it is estimated that the O-rings could have also sustained serious deformations during the expander's pressure test with nitrogen. The specific test was conducted under pressures that were much higher (50 bar) than the expander's designed conditions for standard operation (around 25 bar) due to the safety procedures followed in the NTUA lab. The purpose of that was to approach the expander's limits so that the absence of any type of significant failures could be guaranteed. In that way, safety during the experiments under various operating points can be assured, which is the main policy of the NTUA laboratory. Taking all the above mentioned parameters into account, new seals, suitable for higher temperature and pressure were installed on their respective components and no further problems were encountered.

Figure 69 – Deformed shaft O-ring.

Last but not least, as already discussed in a previous section, the lubrication of the whole expander was examined in detail. To begin with, the distribution plates were in perfect condition. All of their surfaces were oiled and no signs of wear were identified (Figure 70). Furthermore, no

debris was found between the plates, in the distribution holes or the inlet duct. The lubrication operated sufficiently for the pistons and the piston rods as well. As the piston rods were dismantled, wear was absent in contact surfaces and the metal parts of both the cylinder and the piston had maintained their colour, meaning that the friction was kept at normal levels and did not result in any temperature increase that could damage the material. Some light scratches that were observed in certain cylinders/pistons are attributed to the debris in the expanders' interior. As mentioned above, any iron dust and trims in the cylinders was removed before the expander was reassembled. No problems concerning the bearings' and the shaft's lubrication were detected.

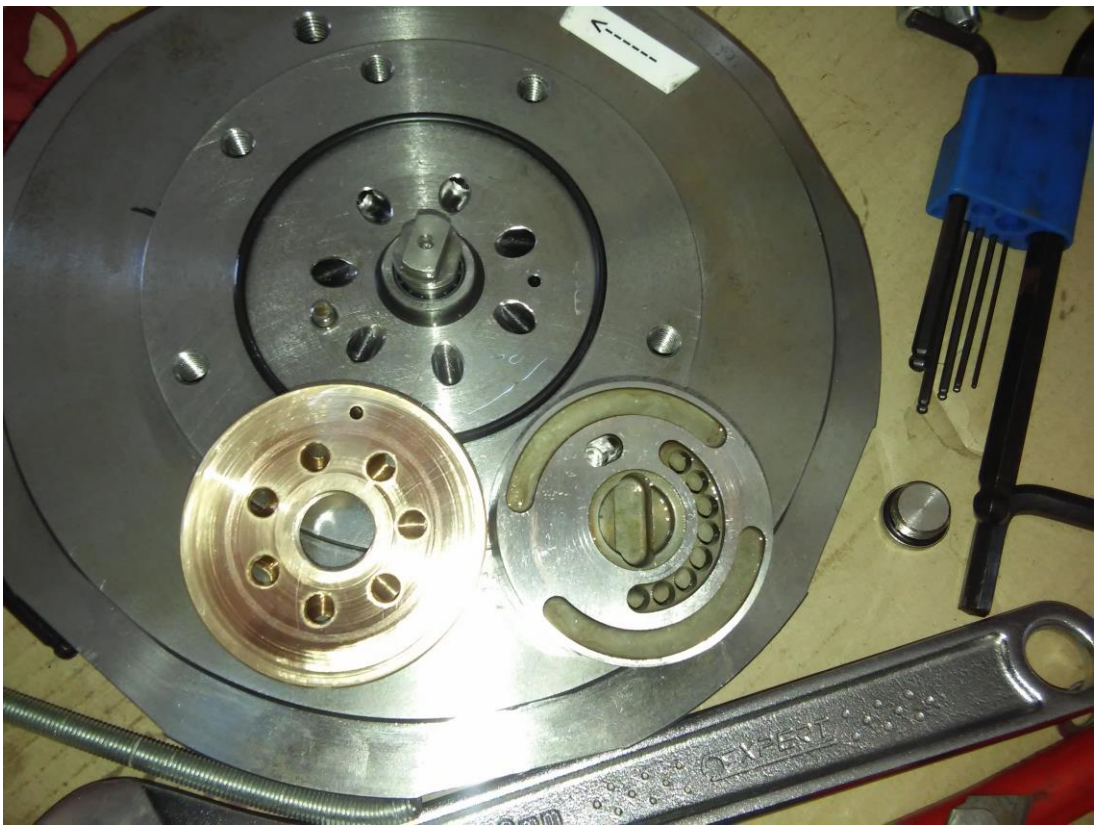

Figure 70 – Inspection of distributor rotating and stationary plates.

A last issue concerning the lubrication is the excessive oil that is gathered inside the piston rod spherical chamber, where the one edge of the rod is attached. Due to the high forces that develop, the formation of lubricant film between these two components is possible. As a result, the rod may stick in this position, being unable to move freely to reattach to the bearing's outer ring when the piston is at the bottom dead centre. In order to deal with this problem, it is important not to inject excessive oil to the expander through the lubrication system.

To conclude with the reliability and maintenance issues, some topics that refer to the whole operating system need to be mentioned. The debris from the expander that is led into the heat pump's circuit has caused no performance problems and is considered to be gathered at the compressor's sump guard and/or the heat pump's filter that is located after the condenser. Also, the only way to remove any excessive oil that the lubrication system supplies to the expander, is through the heat pump. A possible issue that could emerge is the sump guard's flooding or the blockage of the pump filter. If the former problem occurs, the return of the oil from the sump guard to the oil tank will be considered. For the latter issue, after several operating hours, the filter must be checked for excessive oil to ensure that the refrigerant continues to flow normally. If the oil quantity at the filter remains high, more drastic action is required. So, after evaluating the risk and taking financial parameters into consideration, an oil separator at the expander outlet is probably one of the most sustainable solutions.

8 Conclusions

The main concept of the Exp-Heat project was to replace the throttle/expansion valve used in common vapor-compression units with a hydraulic piston-type expander in order to investigate the possibility of energy recovery. Such an expander had already been developed within this project and its experimental evaluation as a heat pump component is the topic of this diploma thesis. In this context, the dedicated expander was retrofitted in an existing commercial heat pump unit in order to boost its performance. Also, a dedicated test rig was developed in the Laboratory of Steam Boilers and Thermal Plants in NTUA for the evaluation of the whole system's performance, focusing especially on the expander's effect on major parameters such as the combined unit's COP and the heat pump's normal operation.

Although the retrofitting of the expander in the commercial heat pump unit seemed to be a difficult task, no particular problems were encountered during the technical operations. Some existing pipelines were modified in order to connect the expander with the heat pump. Apart from that, some additional measuring sensors were placed in certain points to assist the experimental evaluation. During this procedure, the minor modifications that were made induced low costs and had no interference with the control unit, which continued to operate normally and according to the manufacturer's standards. After the retrofitting operations were finished, the heat pump's normal operation was once again tested to determine whether its performance had been affected. No issues emerged at that point. As a result, it can be concluded that the retrofitting process is quite easy to perform and a smooth operation of the heat pump is ensured. Apart from that, the low cost of the required operations is also a significant reason to further investigate the expander development for heat pump applications.

As far as the expander's performance in the retrofitted unit is concerned, a COP increase of over 2% was achieved under 16.16 bar of liquid refrigerant pressure at the expander inlet. The experimental data provided a certain relationship between the COP value and the inlet pressure which led to the extrapolation of the obtained results for higher operational pressures. An encouraging value of a theoretical 3.8% COP increase under a pressure of 25 bar was calculated. The expander's isentropic efficiency reached a maximum value of 17.1% that could theoretically exceed 24% if the inlet pressure is raised at 25 bar. To conclude with the expander's performance, the produced mechanical power by the expander's shaft reached 140.36 W, while through the extrapolation process of the obtained experimental data, an estimated value of over 250 W at 25 bar could be attained. The expander's performance reached its peak under shaft's rotational

speed of 50 RPM. Perhaps under lower rotational speeds, the results could be even more encouraging. A topic of further discuss is the increase of the pressure at the expander's inlet. For safety reasons that have been already explained in previous chapters of the thesis, its value could not overcome a certain limit. An interesting field of research would be the development of the suitable modifications that would allow the system to operate under a higher condensation pressure, which would consequently increase the expander's inlet pressure, allowing it to produce more power.

The maintenance of the expander was also an important issue that was investigated during this thesis. After the experiments were conducted, the expander was dismantled for a closer and more detailed inspection due to an oil leakage issue on the expander's shaft. The problem was linked with a faulty O-Ring and iron debris that caused damage to the expander's bearings. The physical inspection provided valuable data for identification of the debris source and how to resolve this issue. The expander's repair involved the replacement of the key components such as bearings and O-Ring seals with new, heavy-duty ones. After these actions, the expander's operation returned to normal and no further problems were encountered. The expander's lubrication is closely linked with the system's efficient overall performance. Specifically, the lubricant oil exits the expander and is mixed with the refrigerant in the heat pump circuit. A high amount of oil could block the heat pump's filter which would in turn decrease the refrigerant mass flow resulting in a decreased thermal power output. Two options have been discussed as a solution to this issue: an oil separator that would require no manual control or the regular cleaning of the heat pump's filter. Finally, after discussion, it was concluded that the development of a reliable fully automated retrofitted kit is quite possible by taking the right safety (e.g the superheating indicator) and operation parameters (e.g. the electromagnetic valve control) into consideration.

References

[1] Recent advances in vapor compression cycle technologies, Chasik Park, Hoseong Lee, Yunho Hwang, Reinhard Radermacher (2015)

[2] Hewitt NJ, Huang MJ, Anderson M, Quinn M. Advanced air source heat pumps for UK and European domestic buildings. Appl Thermal Engin (2011)

[3] Salehi Kouhestani M., Hewitt NJ., Huang MJ., Developing a combined compressor expander heat pump – experimental evaluation of the compressor & expander. 26th Int Congress of Refrigeration (August 21-26 2011, Prague, Czech Republic)

[4] Driver R., Hewitt NJ., Huang MJ., Anderson M, The testing of a rotary compressor heat pump with integrated expansion turbine. 22nd Int Congress of Refrigeration (Aug 21-26 2007 Beijing, P.R. China)

[5] Stosic N, Smith IK, Aldis CA. Development of the trilateral flash cycle system Part 3: the design of high efficiency two-phase screw expanders.

[6] Stosic N, Smith IK, Kovacevic A, Aldis CA. The design of a twin-screw compressor based on a new rotor profile. J of Engng Design (1997)

[7] Stosic N, Smith I K, Aldis CA, Brasz J, Sishtla V. Twin screw expanders in large chiller units. Proc of Int Conf on Industrial Compressors and their Systems, City University, London, (September 1999)

[8] Stosic N, Smith IK, Kovacevic A. Numerical simulation of combined screw compressor–expander machines for use in high pressure refrigeration systems. Simulation Modelling Practice and Theory (2006)

[9] Brasz JJ, Stosic N, Smith IK. Development of a twin screw expressor as a throttle valve replacement for water-cooled chillers. XV Int Compressor Engineering Conference at Purdue (2000)

[10] Wang M, Zhao Y, Cao F, Bu G, Wang Z. Simulation study on a novel vane-type expander with internal two-stage expansion process for R-410A refrigeration system. Int J of Refrigeration (2012)

[11] Li Zhao, Minxia Li, Yitai Ma, Zhongyan Liu, Zhenying Zhang. Simulation analysis of a two-rolling piston expander replacing a throttling valve in a refrigeration and heat pump system (2014)

[12] Mitsuhiro Fukuta, Fumiya Anzai, Masaaki Motozawa, Hiroyuki Terawaki, Tadashi Yanagisawa. Performance of radial piston type reciprocating expander for CO2 refrigeration cycle (2014)

[13] Giovanni Ferrara, Lorenzo Ferrari, Daniele Fiaschi, Giovanni Galoppi, Sotirios Karellas, Riccardo Secchi, Duccio Tempesti. Energy recovery by means of a radial piston expander in a CO2 refrigeration system (2016)

[14] She X., Yin Y., Zhang X. A proposed subcooling method for vapor compression refrigeration cycle based on expansion power recovery. Int. J. Refrigeration (2014)

[15] Heo Jeong, M.W. Baek C., Kim Y. Comparison of the heating performance of air-source heat pumps using various types of refrigerant injection. Int. J. Refrigeration (2011)

[16] Huff, Radermacher. CO_2 compressor expander analysis. (2003)

[17] Department of Energy. Buildings energy data book (2015)

[18] ANSI/ASHRAE standard 116. Methods of testing for rating seasonal efficiency of unitary air conditioners and heat pumps. (1995)

[19] Subiantoro, Ooi. Economic analysis of the application of expanders in medium scale air-conditioners with conventional refrigerants, R-1234yf and CO2. Int. J.Refrigeration (2013)

[20] Fukuta M., Yanagisawa T., Kosuda O., Ogi Y. Performance of scroll Expander for CO2 Refrigeration Cycle.Proceedings of the 18th International Compressor Engineering Conference at Purdue. (2006)

[21] McGovern, J.A., 1984. Analysis of a Refrigerant Compressor Load Stand Incorporating Hot Gas Bypass and a Single Full Condensation Heat Exchangers. Proceedings of International Compressor Engineering Conference at Purdue, West Lafayette, IN.

[22] Bell, I.H, Groll, E.A., Braun, J.E., Horton, W.T., 2013. Experimental testing of an oil-flooded hermetic scroll compressor. Int. J. Refrigeration 36, 1866-1873.

[23] Gessler, P.D., Mathison, M.M., Bowman, A.J., 2014. Modeling of a Hot Gas Bypass Test Block for Centrifugal Compressors. Proceedings of International Compressor Engineering Conference at Purdue, West Lafayette, IN.

[24] Bradshaw, C., 2014. Hot-Gas Bypass Load Stands. Compressor Engineering Conference at Purdue, West Lafayette, IN.

[25] Baek J.S., Groll E.A., Lawless P.B. Piston-cylinder work producing expansion device in a transcritical carbon dioxide cycle. Part I: experimental investigation. Int. J. Refrigeration (2005)

[26] Subiantoro A., Ooi K.T. Analysis of the revolving vane (RV-0) expander, part 1: experimental investigations. Int. J. Refrigeration (2012)

[27] Subiantoro A., Ooi K.T., 2012b. Analysis of the revolving vane (RV-0) expander, part 2: verifications of theoretical models. Int. J. Refrigeration (2012)

[28] Karellas, S., A.D. Leontaritis, K. Braimakis, Energetic Investigation of Heat Pumps Efficiency Improvement with the Implementation of an Expansion Machine (2014)

[29] http://www.expheat.eu/.

[30] http://ec.europa.eu/eurostat/statistics-explained/index.php/Consumption_of_energy

[31] http://www.nibe.eu/Products/AirWater-heat-pumps/